Experimental investigation on dynamic responses of a spar-type offshore floating wind turbine and its mooring system behaviour

Xue Xu[*], *Sandy Day*

Department of Naval Architecture, Ocean and Marine Engineering, Henry Dyer Building, University of Strathclyde, 100 Montrose Street, Glasgow, G4 0LZ, UK

[*]*corresponding author;* e-mail: xue.xu@strath.ac.uk

ABSTRACT

This study investigated the dynamic behaviour of a spar-type OFWT analysed under various wave loads by conducting an experiment campaign. Both the characteristic of the spar platform itself and the spar with realistic moorings have been investigated. A particular focus of the study was the motions of the mooring lines, which were measured at a series of discrete points along one line using an underwater motion capture system, in parallel with tension measurement at the anchor points. The main objective of this study is to provide experimental measured data to validate numerical software on the research of mooring line motions.

A free decay test has been carried out to confirm the spar platform motions natural frequencies and damping characteristics. The platform was then subjected to a range of regular and irregular waves to obtain the motion characteristics of the platform and the mooring lines. For the mooring line motions, which has rarely been discussed in published research, a non-linear snatching phenomenon has been observed at the tank for some wave frequencies. This non-linear behaviour shows that snatching leads to the high instantaneous mooring line tensions and platform accelerations could cause the failure of the mooring lines in the real structure.

***Keywords*:** offshore floating wind turbines, spar platform, mooring motion, tank tests

1 Introduction

With the burning of fossil fuel such as coal, natural gas and oil, a huge amount of greenhouse gas has been emitted to the environment and has caused severe pollution problems. Also, the fossil fuel is not sustainable. Thus, developing clean and renewable energy is becoming an urgent priority; one of the potential resources for large-scale renewables is wind energy. People mainly use two types of wind turbines – onshore and offshore, to harvest the wind energy while offshore wind resources allow more reliable generation of electricity. According to the water depth of the offshore environment, two types of foundation systems for offshore wind turbines have been proposed -- fixed foundations and floating platforms with mooring systems. For water depth between 20 to 50 m, fixed foundations would be the preferred choice due to the lesser cost. However, for sites further away from the coast where the wind resources are greater than near shore, the water depth can be up to hundreds of metres on sites and floating systems must be used.

The spar platform is a ballast-stabilized substructure for OFWTs. It normally consists of a spar buoy and catenary mooring lines. The long cylindrical spar platform achieves stability

by using ballast to lower the centre of mass far below the centre of buoyancy, which creates righting moment and high inertial resistance in pitch (Proskovics, 2015). It is one favoured solution for deep water sites because of its simplicity in design, modelling and commercialization (Shin, 2011). Thus, in this study, a spar type OFWT model which is known as the OC3-Hywind installed with the NREL 5 MW benchmark wind turbine, as proposed by Jason Jonkman based on the Statoil Hywind model (Jonkman, 2010), will be employed.

The earliest tank test of a 5 MW spar type OFWT (the Hywind model) was conducted by Skaare et al. (2007), at a linear scale of 1:47 using Froude scaling. Both the irregular waves and wave loads were investigated, but the focus was on the comparison with a numerical software code (SIMO/REFLEX) and the platform dynamic characteristic was not presented. This, however, still provides a reference scaling ratio model tests on the Hywind model. Utsunomiya et al. (2009) have conducted an experiment for a spar-type floating platform with 60 m draft and a 2MW wind turbine under both regular/ irregular waves and steady wind load (scale factor 1:22.5). The experimental results were compared with their numerical simulations to verify the numerical codes (mainly based on Morison's Equation). Reasonable agreement was achieved but the damping force evaluations needed further improvement. They then developed a 2 MW wind turbine with 70 m draft spar platform and a 1:10 model has been made, to conduct at-sea experiment, where the wind speed/ direction, tidal height, wave height, motion of the spar platform, mooring tension and strains in the tower/spar platform have been measured. Their platform is designed as a hybrid structure, where the upper part is constructed of steel and the lower part is pre-stressed concrete. This provides a good preliminary concept model for further design of offshore wind turbines (Utsunomiya et al., 2013a). This hybrid-spar had also survived during Typhoon Sanba, where the average wind speed at the hub height was 48.3 m/s, which verifies the safety of the structure (Ishida et al., 2013). The author also developed numerical tools to compare the simulation results with the at-sea measurement. Their dynamic mass-spring model for mooring lines show better agreement with the experimental measured values than the quasi-static catenary mooring model. The standard deviations of yaw responses were overestimated by the numerical tools but the mean values agreed well (Utsunomiya et al., 2013b). In the at-sea experiment, the group used a 100 kW wind turbine on top of the hybrid-spar. The platform responses were investigated when the turbine was operating, where they found the mean pitch responses was not very large, but the standard deviation of the roll/pitch responses was significant (Utsunomiya et al., 2014). In 2015, they published the design methodology for hybrid spar which includes the environmental design conditions, design load cases, dynamic and fatigue analysis; the installation procedure was also presented, where they consider the spar as a simple one-dimensional structure. However, they also pointed out that further studies are needed to reduce the cost for commercial application (Utsunomiya et al., 2015).

The most recent open-sea experiments on a spar type OFWT is conducted by Ruzzo et al. (2018), and they used a 1:30 scale model of the OC3-Hywind. The experiments site is located in the sea front of Reggio Calabria (Italy). The intermediate-scale, open-sea experiment can help to overcome some limitations of small-scale models, such as the limitation of experiment durations and the scale effects. However, the open-sea wave frequencies may not able to cover the complete frequency range of the platform motions, but, in their studies, the roll/heave/pitch motions can be captured.

The research group in the University of Ulsan have also done experiment studies on the OC3-Hywind model, with scaling factor 1:128. In 2011, Shin conducted a model tests to investigate the OC3-Hywind platform motion characteristics (Shin, 2011). They then developed three new spar platforms with the same mass and volume of the OC3-Hywind but different body shapes and carried out the model tests still with the scale 1:128. Both the wave and wind (with operating turbine) were tested, and the platform motion RAOs and maximum motion were presented. By adding the ring cylinders on the spar platform, they found that the added mass and damping has increased which resulted in an increase of the motion period and decrease in platform motion amplitude. However, their rotor was scaled with the Froude method, which means the aerodynamic characteristics may not be captured accurately and thus the platform responses presented may not be precisely represented. The 1:128 OC3-Hywind tank test model has also been used to validate their in-house code and an open-source numerical software – FAST v8. The platform six degrees of freedom and the mooring tensions for one mooring line were presented under both regular and irregular wave with wind load. They suggested that for a coupled wind and wave tank test for floating wind turbines, when Froude scaling method were used, the blade geometry should be designed for a low Reynolds number environment. In sea state 7 (Tp=13.6, Hs=9.14), a strong nonlinearity in surge have been noticed in experiment (Ahn and Shin, 2019). The tank tests of Shin's group had inspired this study, and most of the wave profile in their papers have been included in this study.

The research group in Shanghai Jiaotong University - Duan et al. (2015) have investigated the isolated wind/wave effects and the integrated wave-wind effects on the OC3-Hywind floating systems by conducting the model test (scale factor 1:50). They then (Duan et al., 2016a) conducted a model test on the OC3-Hywind spar type floating platform, using two different rotor systems under both wind and wave load conditions to investigate the floating system response behaviours. The gyroscopic effects from the rotor rotation resulted in yaw decays and strong coupling effect between surge and pitch, and the heave motions were quite independent. In addition, they found that the wind load could reduce platform motions at natural frequencies. The mooring tensions were also measured. Duan et al. (2016b) have conducted another model test for the OC3-Hywind model to check the floating system dynamic responses. The calibration tests included the characterized stiffness of the delta type mooring system and free decay responses. It is found that the wind loads have obvious influence on surge, heave and pitch motions of the spar type floating wind turbine. Similarly, to their previous study, the mooring tensions measured from the experiment were found to be affected by either the wave or wind-wave excited surge/pitch and heave coupling and it was found that the wind loads can have a clear influence on the dynamic responses of the mooring system. It is also found that the aerodynamic loads can somewhat reduce the floating system peak response amplitudes, which could be beneficial for extending the fatigue life of the mooring system.

Tomasicchio et al. (2018) have used a Froude scaled model to conduct tank tests of an OFWT. They presented a very detailed literature review about the experiment on OFWT, and they have pointed out the major difficulties on conducting wave-basin experiments of OFWTs. They had also investigated the hydrodynamic and dynamic behaviour of the platform and the interactions with the mooring system.

It is seen that many experiments have been conducted by researchers in the past decades to investigate the characteristics of spar type OFWT platforms and the scaling ratio ranged from 1:128 up to 1:10, while the largest model of the OC3-Hywind platform is at 1:30 scale.

Most of the studies are focused on the platform motions or the mooring tensions, but there has been little research on the detailed mooring line motion dynamics. The mooring line motion, is coupled with platform motion, and thus can also show the coupling effect with the operating turbines, so it is very important to understand the mooring line motion behaviour. Consequently, in this study, the motions of one of the mooring lines will be investigated in the tank tests. In this paper, the detailed experiment set-up to measure the platform dynamic responses, mooring motions & tensions are presented, and key experiment results will be discussed.

2 Experiment Design

To investigate the OFWT spar platform and its mooring systems hydrodynamics behaviour thoroughly, it is necessary to carry out experimental measurements. This section will give the details in the preparation stage of the experiment been carried out at the Kelvin Hydrodynamics Laboratory (KHL). A brief introduction of the KHL facilities are presented first. The layout of the tank for both spar-only and spar with realistic mooring lines are given. The design and limitations of the experiment are discussed. The parameters scaling, such as the scaling methodology and the scaled model dimensions are given. The set-up of the instrument been used in the experiment are presented in detail.

2.1 Kelvin Hydrodynamics Laboratory

The Kelvin Hydrodynamics Laboratory (KHL), at the University of Strathclyde, has dimensions of 76 m×4.6 m×2.5 m. It is equipped with a variable-water-depth computer-controlled four-flap absorbing wave maker, which can generate both regular and irregular waves over 0.5 m height (subject to the water depth), as shown in Figure 1. At the back of the tank, there has a high quality variable-water-depth sloping beach, with reflection coefficient typically less than 5% over the frequency range of interest. A state-of-the-art, real-time, non-contact infrared motion capture system has been installed in the tank to measure the motions of floating vessels and structures. For this experiment, five motion capture cameras have been installed above the tank. Two at the left side and the other three are above the tank, as shown in Figure 2. To capture the mooring line motions, three underwater cameras have also been installed in the tank.

Figure 1 Four Flap Wave Maker at KHL

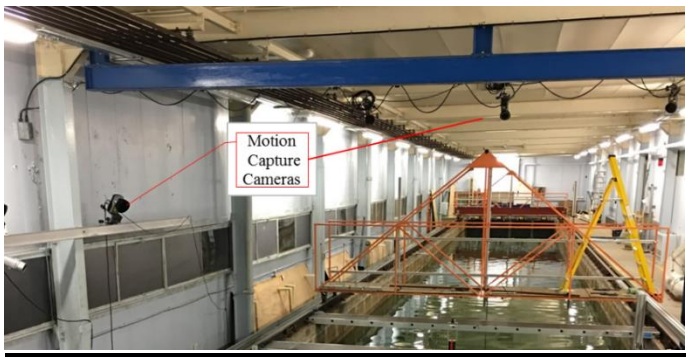

Figure 2 Structure Motion Capture Cameras at KHL

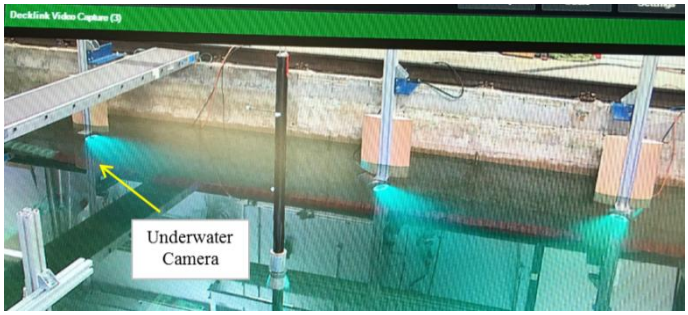

Figure 3 Underwater cameras in the tank

2.2 Brief Model Description

There are many factors that can affect the experiment outcome and need be assured before the start of an experiment, such as the water depth, the scaling factor/methods, the mooring design, the wave frequencies selected, tests running time, the sampling frequency and the effect of using the 2-D flume assumption.

The effect of wind loading is not included in the tank tests reported here, as the intention is to provide a set of baseline data for validation of numerical simulation. Since the focus of this study is on the hydrodynamic response of the spar platform and dynamic behaviour of the mooring lines, and it is expected that wind induced loads have relatively little effect on the wave frequency responses of the platform (Yu et al., 2015), it was decided to focus on the mooring line dynamics under purely hydrodynamic loading as a base case. It would be of interest in the future to carry out further tests with steady or unsteady wind loading which will add further complexity to the system dynamics.

2.2.1 Water Depth

The water depth in the tank is chosen as 2.0 m, according to the wave conditions during tests, and the wave maker capability. The beach at the back of the tank has been adjusted in height to maximise absorption over the frequency range of interest, as some long duration runs of waves will be generated during the test.

2.2.2 Scaling Methods and Factor

It is important to scale the model and environmental conditions as reliably as possible, such that the result is meaningful and helpful for real design and further research. Both Reynolds number and Froude number are important non-dimensional scaling parameters for fluids. However, Reynolds number is normally used to scale flows around models in unbounded fluids dominated by viscous effects, which is not the case in the present experiment. Froude number describes the relationship between inertial and gravitational forces. It forms the basis

of a scaling method for physical experiments in water waves in which viscous forces are of lesser importance, as maintaining Froude similarity (i.e. keeping the correct model scale Froude number) will scale the waves and the dynamic behaviour of structures correctly (Chakrabarti, 1994). Thus, Froude scaling is used to conduct the experiment campaign in this study.

For a scaling factor - λ, to satisfy both the geometric similarity and the Froude similarity, an established scaling factor table for OFWT model test is presented in Table 1.

Table 1 Established Scaling Factors for OFWT model test (Rolo, 2014)

Parameter	Unit	Scale Factor
Length (e.g. displacement, wave height and length)	L	λ
Area	L^2	λ^2
Volume	L^3	λ^3
Density	M/L^3	1
Mass	M	λ^3
Time (e.g. wave period)	T	$\lambda^{0.5}$
Frequency (e.g. rotor rotational speed)	T^{-1}	$\lambda^{-0.5}$
Velocity (e.g. wind speed)	LT^{-1}	$\lambda^{0.5}$
Acceleration	LT^{-2}	1
Force	MLT^{-2}	λ^3
Moment (e.g. rotor torque)	ML^2T^{-2}	λ^4
Power	ML^2T^{-3}	$\lambda^{3.5}$
Stress	$ML^{-1}T^{-2}$	λ
Mass moment of inertia	ML^2	λ^5
Area moment of inertia	L^4	λ^4

Considering the 2.0 m water depth at the KHL, the scaling factor has been chosen as 1:74 (Santos-Herrán, 2016), which gives the spar platform model draft at 1.621 m. For the Hywind Scotland Pilot Park, the water depth on site is 105m and the draft of the spar platform is 78 m (Equinor, 2019). Its ratio between water depth and platform draft is about 0.743 and 0.810 in this study, which shows the scaling factor -- 1:74 is reasonable.

2.2.3 Mooring Design

Two sets of tests were carried out in this study. In the first the spar was moored with “soft” elastic mooring lines; in the second set of tests, realistic mooring lines were utilised. Figure 4 (a) presents the layout of the tank for spar-only tests. The soft elastic lines are used to prevent the model from drifting down wave and the stiffness is chosen to minimise the interaction of mooring lines with the system dynamics.

For spar with realistic mooring lines tests, compared with the OC3-Hywind model, the water depth in full scale has decreased from 320 m to 148 m. Although the platform draft can work well in this depth, the mooring length and anchor position need to be adjusted. This has been done by using the Principle of Similarity based on the geometry, and the static balance has been checked in numerical model before conducting experiment, which shows the current design is reasonable. For the mooring stiffness, it has been scaled (using the scaling factor) down from the OC3-Hywind mooring system. As the transverse fluid forces on the mooring lines are dominated by viscous effects, ideally the Reynolds scaling method should be used.

However, since this study focuses on the platform dynamic responses, which are dominated by Froude scaling it is accepted that the tests could not capture all aspects of the mooring responses correctly. The mooring line length, diameters and weight distribution are therefore chosen to be close to the target values based on Froude scaling.

Due to the width limitation of the tank, the mooring configuration has been slightly re-designed from the original layout. For the NREL OC3-Hywind model, the angle between each mooring line is 120°. In this tank test, to make the mooring system as similar as possible to the NREL model, Mooring Line 1, as shown in Figure 4 (b), is aligned with the wave direction, i.e., positive of X-axis but the angle between the other two mooring lines is reduced to 60°, with the lines placed symmetrically about the centreline of the tank.

2.2.4 Wave Frequencies

The wave frequencies were chosen to lie in the range from 0.253 Hz to 1.229 Hz (at model scale), which covers the predicted platform heave and pitch natural frequencies, and also covers the range over which the wave maker (and the beach absorption) work efficiently.

2.2.5 Test Running Time and Sampling Rate

For free decay tests, the test duration varies substantially with the degree of freedom, since for example the heave motion is damped much more slowly than the yaw motion. In most cases, at least 10 to 15 motion cycles have been recorded and usually 10 motion cycles were used for the natural frequency and damping ratio calculations (only about 5 cycles for yaw motion).

For regular wave tests, the recorded running time is about 120 s at tank test scale, which is enough for the platform to respond for at least 10 stable periodic motion cycles. The data used for the analysis is started when the platform motion becomes stable, as it can take about 10 s for the generated wave to reach the model. In addition, when the wave has just reached the model, it can cause some transient splash effects and the first few cycles of platform motion show transient response under regular waves.

For irregular wave tests, a 3 hour duration at full scale is typically adopted to model a full storm in offshore engineering tests as recommended by the ITTC (Stansberg et al., 2002). In the present tests, the test duration was chosen to be 1200 s at model scale – which corresponds to about 2 hr 40 mins (9600 s) in full scale, which is hence considered reasonable to capture the key phenomena associated with the sea states encountered in a real sea site.

The sampling frequency is set at 137 Hz during the tank tests, which means the highest recorded frequency which can be identified without aliasing is 68.5 Hz (the Nyquist frequency)(Landau, 1967). The choice of a prime number reduces the risk of harmonics, while the value chosen is large enough to cover all the possible wave frequencies. A further consideration is possible noise from the AC mains electricity with frequency 50 Hz in UK. Thus, if the mains noise (could from the data recording and transferring equipment) appears during the data recording process, it can be identified from the spectrum analysis and can be eliminated from the predicted response spectrum of the floating systems. In this study, mains frequency noise was not found to be an issue through all the tank tests.

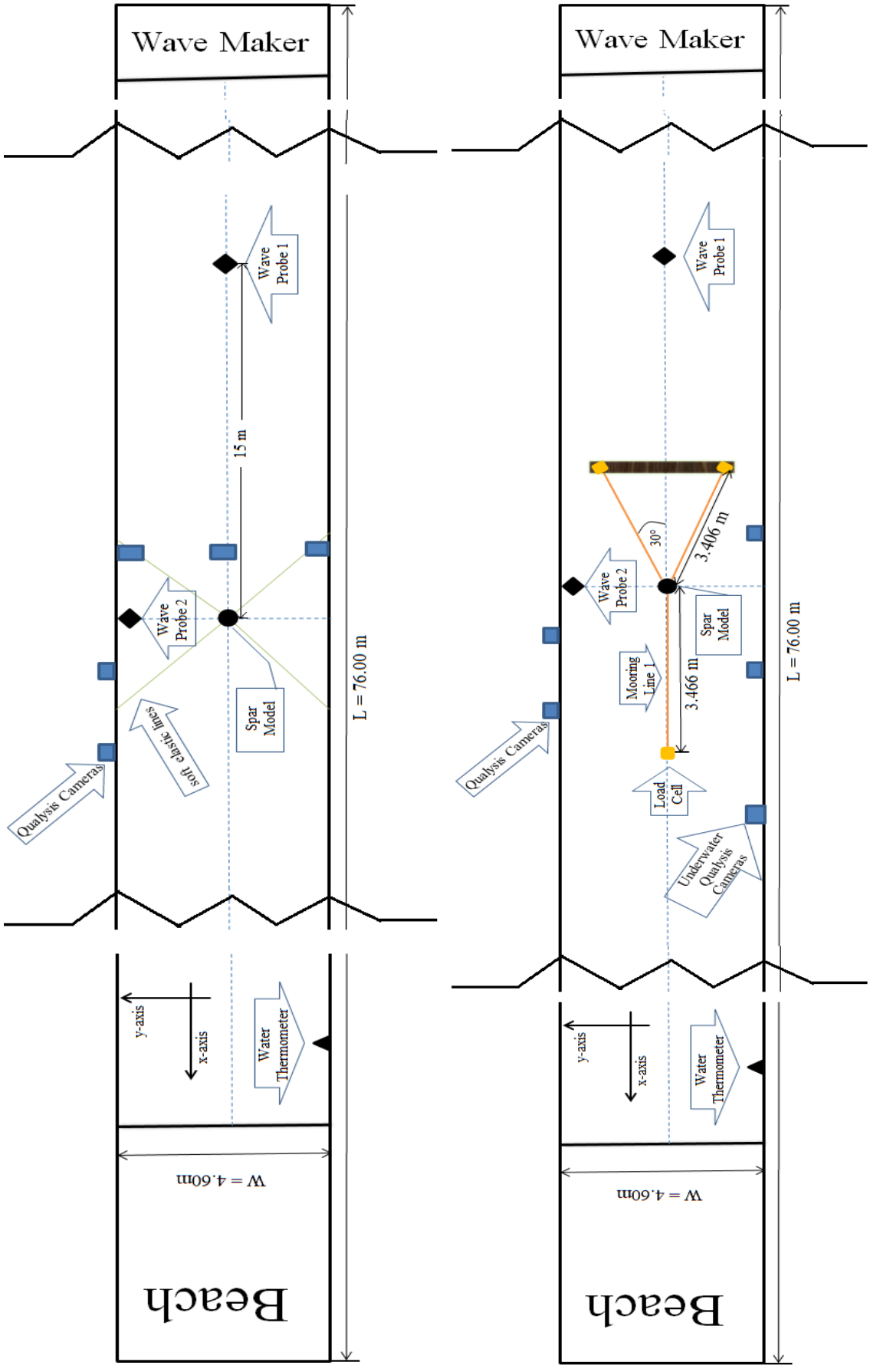

(a) Spar-only (b) Spar with realistic mooring lines

Figure 4 Tank layout

During the regular wave tests with realistic moorings, a non-linear snatching behaviour was discovered at some frequencies in the floating systems. In this phenomenon, one mooring line becomes very tight and then goes slack within a very short time period. In order to confirm that the sampling rate was adequate to capture this phenomenon, the time histories of the mooring tension data have been checked, as shown in Figure 5. There are about 160 points recorded in the 10 seconds during the period in which the snatching is happening. Examination of the curve peak in detail shows that there are about 5 points defining the peak; hence, it is unlikely any higher points have been missed. Hence, it can be seen that the sampling frequency at 137 Hz is a reasonable recording frequency capturing the featured changes in the floating system.

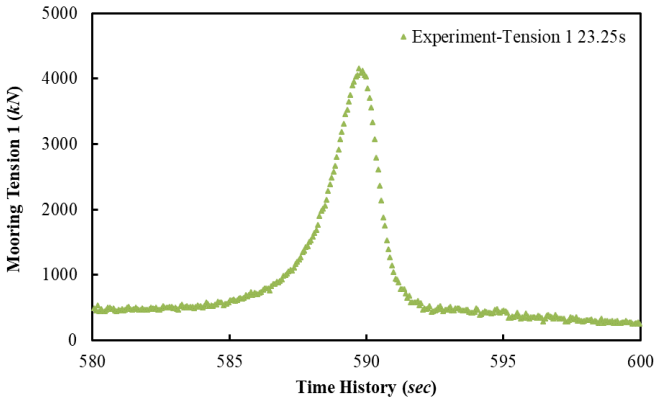

Figure 5 Recorded time steps of mooring tension in experiment

2.2.6 2-D Flume

The wave generated at KHL is considered as a long-crested, which means that there are no directional waves as in realistic open seas. However, compared with the platform motion in real sea site, the motion can be larger in the tank tests than would be the case in the real sea, as the wave energy are all in one direction, instead of spreading to other directions. The results may be seen as a limiting case of zero spreading, and will be used later to compare with the numerical simulations, where the 2-D flume assumption is also employed.

2.2.7 Blockage and Wall Effects

When conducting the tank tests, *"the model should be small enough to avoid noticeable effects of restricted water in the towing tank"(Zürcher, 2016).* Thus, the blockage and wall effects of the tank, due to the radiated and diffracted waves should be considered. The blockage means the effects of finite width due to tank walls on the flow around a body and also the wall effect on reflected waves. In this study, the blockage ratio, i.e. the ratio between the model's cross sectional area and the cross-section area of the tank is 2.24%, which is very small.

In addition, as shown in the heave free decay test figures (Figure 16 and Figure 18), no motions due to the reflections of radiated waves have been observed. Thus, the blockage and wall effects are neglected in this tank test study.

2.2.8 Brief Test Description

A spar-only model and a spar with three scaled realistic mooring lines will both be tested in free decay, a range of regular waves and four sea states. A simplified tower has been installed upon the spar platform in order to allow correct ballasting. The tank tests will involve no

wind flow. The spar model is placed at the middle of the tank both longitudinally and transversely and a wave probe has been placed centrally between the spar model and the wave maker, as shown in Figure 4.

For spar-only tests, four very soft elastic moorings were applied to the platform to keep it on station. The stiffness of the lines are chosen so that they do not affect the first order (wave-frequency) motions of the platform.

For the test of the spar with scaled realistic mooring lines, a frame was installed at the bottom of the tank to attach the load cell and the mooring lines. Through all the tests, the spar motions in six degrees of freedom were measured. The three mooring line tensions and the motions of Mooring Line 1 (which is the mooring line downstream of the wave maker aligned with the X-axis) will be recorded as well.

2.3 Tank Test Model's Pitch/Roll Inertia

Since the spar platform is a perfect axis-symmetric cylinder, the pitch and roll inertia can be assumed the same.

The model is weighed to determine the mass. Then the CG is measured by placing the model on a knife-edge, adjusting its position until the model reached a balance position and then measuring the distance from the platform base to that point, as shown in Figure 6. Finally, the whole system pitch/roll inertia about its CG is measured by conducting a Bifilar Suspension test. In this test, the model is suspended on two wires with the CG of the structure located at the mid position of the wires, as shown in Figure 7. The model is then perturbed around a vertical axis, and the natural period is measured, allowing calculation of the moment of inertia.

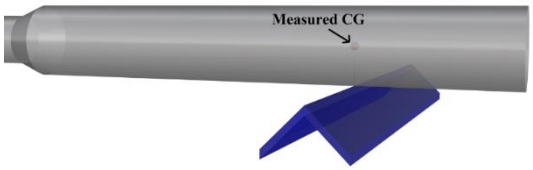

Figure 6 Measure the CG of the whole model

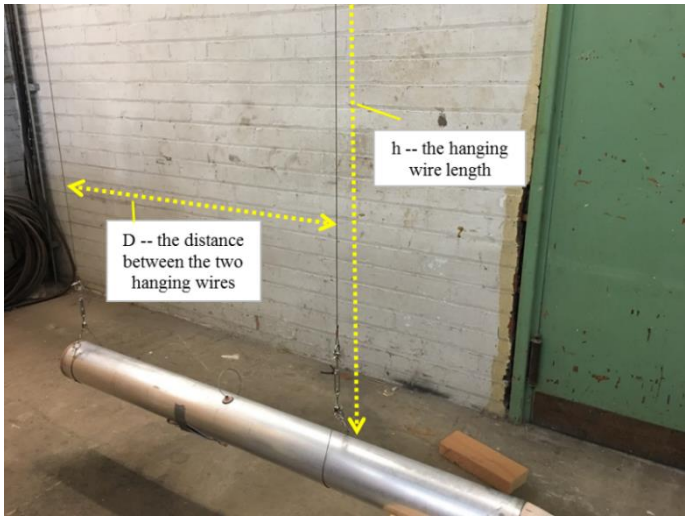

Figure 7 Conducting the Bifilar Suspension test

In this test, the measured D = 0.960 m and h = 4.816 m. Three 10 cycles of the harmonic motion are measured as t_1 = 63.030s, t_2 = 62.670s and t_3 = 62.990s. Thus the pitch/roll inertia of the whole structure will be I = 9.303 kgm^2. The pitch/roll inertia of the NREL model after scaling is I_{NREL} = 8.883 kgm^2. Thus, the difference between the NREL model and the designed tank test model of the whole structure pitch/roll inertia is less than 5%, which means the ballast arrangement of the tank test model is considered acceptable.

2.4 Equivalent Mooring Line Extensional Stiffness

The wire (Figure 8) been used in the experiment to represent realistic mooring line is the code number 603.000.018 from the TecniCable company (Tecni-Cable, 2016). Its E is 116,739 N/mm^2 (1.16739*10^{-5} N/m^2) and the diameter is 1.8mm.

$$\text{equivalent mooring line extensional stiffness} = E \times a \tag{1}$$

where a is the equivalent cross sectional area is about 55% of the whole area. I.e. a = 55%$\times$ $\pi \times (1.8/2)^2$ = 1.4 mm^2. Thus, the equivalent mooring line extensional stiffness is 163,268 N/m of the tank test model.

Figure 8 Schematic plot of the mooring line's cross sectional area

2.5 Tank Test Model Parameters

To keep the same draft with the OC3-Hywind model, the platform mass need to be re-calculated, instead of simply scaled down, to account for the use of fresh water in the tank tests rather than seawater. Then, according to Table 1, the parameters of tank test model and full scale model, compared with full scale NREL OC3-Hywind model, are shown in Table 2. It is clear that the geometric parameters of platform are well matched with the designed model (the NREL OC3-Hywind model). For the mooring lines, the diameter scaled up from the tank test model matches well with the NREL full scale model, while the equivalent mooring line weight is slightly lighter than the target value – about 8%. A significant difference between the target value and the model is noticed in the equivalent mooring line extensional stiffness, due to it is very hard to find the exact same properties of the small scale wires. However, the tank test model stiffness was adopted in the numerical model in this study, so the results from the two approaches should be comparable. Figure 9 shows the geometry scope of the tank test model.

Table 2 Tank test model properties and parameters

Final Model Properties	Tank Test Model	Full scale Model	NREL full scale model
Water Depth (*m*)	2.0	148.0	320.0
Depth to Platform Base Below SWL (Total Draft) (*m*)	1.6	120.0	120.0
Depth to Top of Taper Below SWL (*m*)	0.054	4.0	4.0
Depth to Bottom of Taper Below SWL (*m*)	0.162	12.0	12.0
Platform Diameter Above Taper (*m*)	0.088	6.5	6.5
Platform Diameter Below Taper (*m*)	0.127	9.4	9.4
Platform Mass, Including Ballast (*kg*)	18.5	7.5E+06	7.5E+06
CM Location of the Whole Structure Below SWL Along Platform Centreline (*m*)	1.1	80.7	79.9
Pitch/Roll Inertia of the Whole Structure about CG ($kg \times m^2$)	9.3	2.1E+10	2.0E+10
Number of Mooring Lines	3	3	3
Angle Between Adjacent Lines (*deg*)	0/150/210	0/150/210	120
Depth to Fairleads Below SWL (*m*)	0.9	70.1	70.0
Unstretched Mooring Line Length (*m*)	3.6	263.1	902.2
Mooring Line Diameter (*m*)	0.002	0.1	0.1
Equivalent Mooring Line Weight (see section 2.4) (*kg/m*)	0.013	71.2	77.7
Equivalent Mooring Line Extensional Stiffness (*N/m*)	1.6E+05	8.9E+08	3.8E+08
Radius to Anchors from Platform Centreline (*m*)	3.5/ 3.4	256.4/252.1	853.9
Anchor Depth (*m*)	1.9/ 1.8	139.9/135.3	316.7
Radius to Fairleads from Platform Centreline (*m*)	0.074	5.5	5.2
Tower Height (*m*)	1.2	89.5	90.0
Tower Total Mass (*kg*)	1.3	5.2E+05	6.0E+05

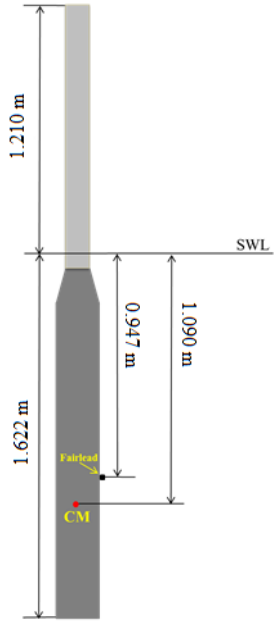

Figure 9 Tank scale model

2.6 Qualysis System and the Cameras, and the Load Cells

The platform 6 DOF motions – surge, sway, heave, roll, pitch and yaw, and the underwater mooring line motions (X, Y and Z) were recorded using a Qualysis motion capture system. The cameras (as shown in Figure 2 & Figure 3) detect the model's motion by tracking the movement of the reflective targets, which have been installed on the model. To make sure all 6 DOF motions of the platform can be captured, four reflective targets have been installed on the tower part of the model. The weight of these reflective targets has been accounted for in the tower model ballast. Figure 10 presents the arrangement of these reflective targets on the tower. For the underwater mooring line motion capturing, seven reflective targets were used, as shown in Figure 11. The density of each reflection target is 991.260 kg/m^3, which is very near the fresh water density, so they are considered neutrally buoyant and the flow effect been generated by these reflection targets have been neglected in this research. The first reflective target – named as Rear in the Qualysis software, has been installed on the load cell for Mooring Line 1 (as shown in Figure 12). This rear reflective target is being used as a reference point, since it is "anchored" and should not move during all the tests, which can help in generating a reference point for the Qualysis system. Another reflective target has been attached on the spar platform at the fairlead position of Mooring Line 1; this target's motion allows comparison with the platform's motion measured from the above-water system to double check if the underwater camera system is correctly synchronised with the above water system. The other five reflective targets are attached along Mooring Line 1. Details of these targets position on Mooring Line 1 are presented in Table 3. The uneven arrangement of the reflection targets can help to reduce the possibility of mis-identification of the targets by the Qualysis system.

The three mooring line tensions are measured by underwater load cells. These three load cells were placed at the anchor points on the bottom of the tank, rather than at the fairlead position. The maximum tension at the anchor points will typically be less than at the fairlead; however determining the maximum tension was not the focus in the context of the present study. Locating load cells on the model leads to concerns regarding the interference with the flow around the model, the effect of the cabling on the platform dynamics, and the instantaneous angles of the devices as the platform moves; so it was considered that the

effect of these issues could be reduced by measuring the tensions far from the model on the tank floor. The load cells measure loads from 0 to 100 N very accurately, which lies in the range of the expected measured mooring tensions. The calibration results show that the error is less than 1%. The height of the load cells has been considered as this will affect the mooring line anchorage height and position, details of the anchor depth have been shown in Table 2. The depth of the anchors are slightly different between the rear anchor and the other two, due to the different methods used to locate the anchors. This difference is only around 3% and it is considered reasonable to ignore this effect.

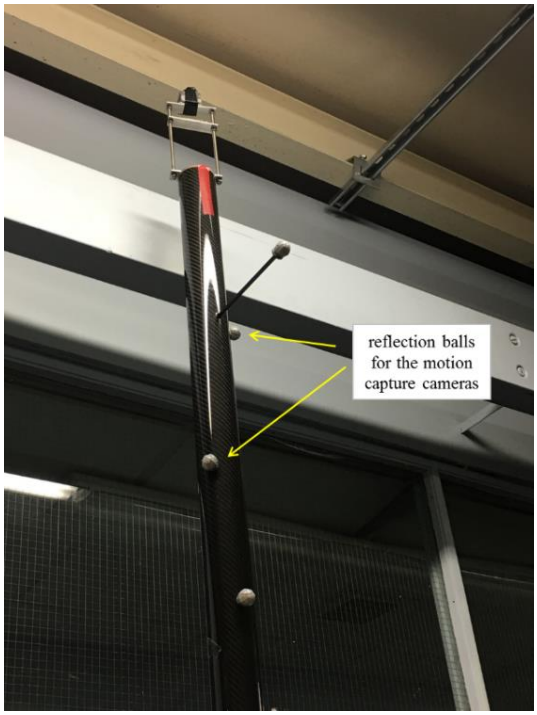

Figure 10 Qualysis reflection balls arrangement on the tower model

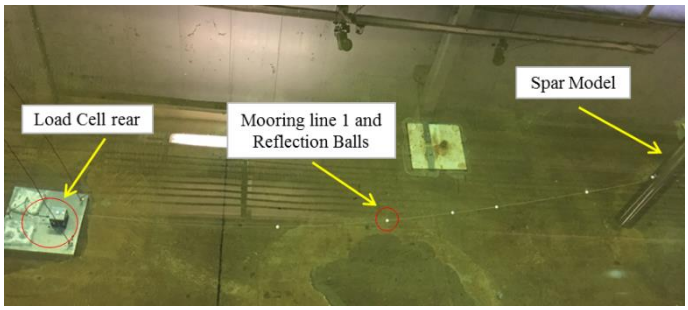

Figure 11 Mooring line with underwater reflection balls in the tank

Table 3 Reflection balls position on the Mooring Line 1

Arc Length	Model Scale	Full Scale
Reflection Ball Number	(*mm*)	(*m*)
1	2321.150	172.007
2	1638.460	121.417
3	1228.850	91.063
4	955.770	70.827
5	409.620	30.354
Spar (at fairlead)	0	0

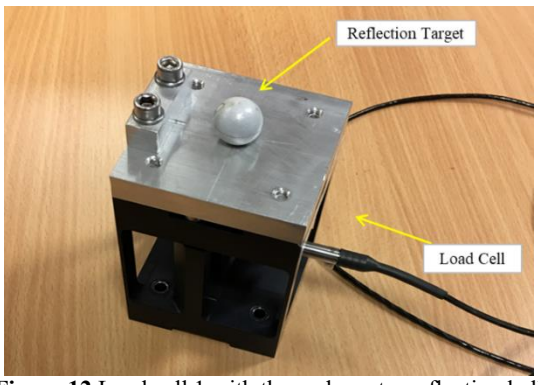

Figure 12 Load cell 1 with the underwater reflection ball

2.7 Wave Probes

Two wave probes are being applied in the tank to measure the wave passing the model. One resistance-type probe was installed upstream of the model – to measure the (regular) wave height passing through the model without any diffraction effects from the model. A second ultrasonic probe is installed adjacent to the model and near the wall of the tank to allow the phase of motions relative to the wave surface to be established. The irregular waves used were calibrated prior to model installation by measured the water surface elevation at the model position using the same wavemaker time history, and adjusting the significant wave height to meet the target values The wave height of the regular waves is 2.52m at full scale; frequencies ranged from 0.029 Hz to 0.143 Hz. This range was chosen to covers the natural frequencies of the platform DOFs, apart from surge, which is too small to be checked at model scale. The irregular wave parameters are shown in Table 4; it can be seen that the measured significant wave heights are matching quite well with the target significant wave heights in each sea state (Shin, 2011), which shows satisfactory calibration of the sea states.

Figure 13 and Figure 14 show calibrated results for Sea State 1. The fitted curve shows that it is generally fits the Rayleigh distribution, although there are some unexpected points at the peak. The wave spectrum shows close match between the measured wave from Wave Probe 1 (located where the model was installed) and the calculated target wave spectrum. The target wave spectrum is calculated by using the JONSWAP equation and the shape parameter is 3.3.

Table 4 Wave parameters for the four sea states

	Target Full Scale		Target Tank Scale		Measured Tank Scale	
Sea State	Tp (s)	Hs (m)	Tp (s)	Hs (m)	Tp (s)	Hs (m)
1	9.700	3.660	1.128	0.050	1.093	0.050
2	11.300	5.490	1.314	0.074	1.302	0.075
3	13.600	9.140	1.581	0.124	1.569	0.124
4	17.000	15.240	1.976	0.206	1.883	0.205

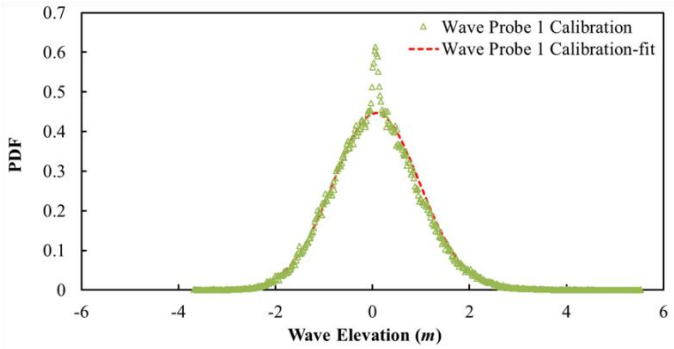

Figure 13 Wave amplitude distribution, measured by Wave Probe 1 for Sea State 1 (full scale)

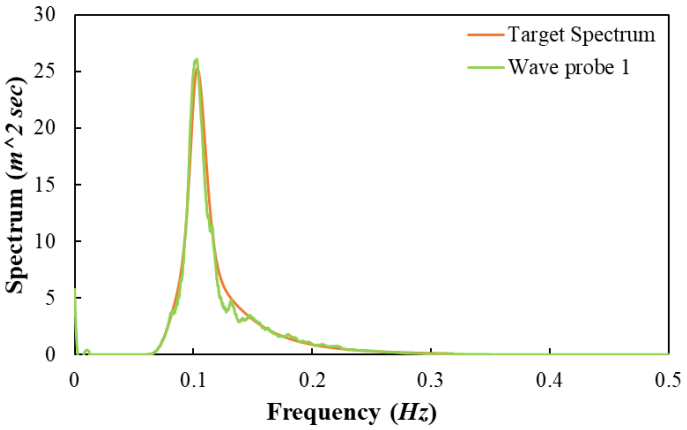

Figure 14 Wave spectrum, measured by Wave Probe 1 compared with the target wave spectrum, for Sea State 1 (full scale)

2.8 Mooring Set-up

Before the tank test start, the mooring's pre-tension of the three mooring lines have been measured, as shown in Table 5. As shown in the table, the tension on Mooring Line 2 and 3 are slightly different. This is assumed to be caused by the small magnitude of the forces and small inaccuracies in locating the model in the tank. It was found to be very hard to adjust the position of the anchor frame on the bottom of the tank extremely precisely, and the measured load on the transducers were found to be very sensitive to small movements. Thus, the pre-tension shown in Table 5 were the best results achievable at the tank.

Table 5 Pre-tensions of the three mooring lines

	Experiment test scale (*N*)	Experiment full scale (*kN*)
Tension 1	0.938	380.041
Tension 2	0.655	265.405
Tension 3	0.732	296.567

To ensure that the platform was not leaking and to double check that the anchor position does not change during the tests, a repeatable static check was conducted both before and after all wave tests. When the water surface and the model are still, three masses – 100g, 200g, 300g were added on top of the model tower. The platform positions and mooring tensions were then recorded during this process to check how the tension changes. During this process, the X-position of the model (along the tank) changes due to the asymmetry of the mooring system. The still-water platform Z-position does not change between the start and the end of experiment campaign, which confirms that the model did not take on any water. During the free decay tests, the regular wave tests, and the first three irregular wave

tests, the still-water X position did not change between the value before and after each test. However, after the last irregular wave tests – Sea State 4, it was discovered that the platform X-position has changed by about 2.4 mm (0.178 m in full scale) which indicates that the anchor position might have changed during the test. After checking all the tank test data for the anchor position, the results show that the anchor position for Mooring Line 1 changed by about 50 mm (3.7 m in full scale) in the very last tank test-which was Sea State 4 (the largest sea-state). However, it was confirmed that for all the free decay tests, regular waves and Sea State 1 to 3, the anchor position did not change and therefore the test results obtained were unaffected by this. It may be assumed that the anchor position changed during Sea State 4 due to the greater loads caused by the larger waves and this group of data is not used in this study.

The absolute value of three mooring tensions showed a difference between the results before and after the tank tests. This is assumed to be due to the amplifier zero value drifting during the tank tests. However, the tension values were seen to reduce linearly with the same gradient before and after the tests. This means that the dynamic changes in mooring tensions in the measured time histories, for example, due to wave loads or platform motions, are still correct. Thus, the recorded data may be corrected with an offset value representing the estimated drift. The baseline tension values are taken from the case measured with no added mass before the experiment started, which was recorded just after the load cell/amplifier system had been calibrated and the model been put into the tank, and the mooring anchors adjusted to match the target values as closely as possible. As the amplifiers may be expected to drift slightly during the tank tests, the zero offset values may be variable. However, if the anchors have not moved, and the model draft has not changed, it is reasonable to assume that the tension will not in fact have varied. Thus, before running each test, when the model is still and balanced, the tensions were modified with an offset value to adjust the measured pre-tension in each test match with the values in Table 5. By adopting this process, the modified data will represent the real tensions on each mooring line. The same process was also conducted when dealing with the mooring tensions in irregular waves.

3 Results and Discussions

3.1 Free Decay Tests

As the main parameters which can affect the platform's dynamic behaviour, the natural frequencies and damping ratios can be obtained by analysis of the free decay test.

3.1.1 Spar-only

As the spar model is a perfect symmetrical cylinder, the pitch and roll, and the surge and sway will be the same. In addition, although there has no realistic scaled mooring line for the spar-only test, four elastic mooring lines have been used to prevent the model drifting away, which are sufficiently soft to make sure that the motion response for the heave and pitch were not affected by the presence of the lines. The sway is not considered as the wave propagates only in one direction – along the X-axis. Therefore, only the surge, heave, pitch and yaw data will be analysed.

It is typically noticed that in the tank test, the damping ratio is more variable than the natural frequencies among each mode of the free decay test, so the free decay tests were repeated 10 times for surge, heave and pitch, and 5 times for yaw. For each mode of motion in each

free decay test, 5-10 cycles are selected. Data is analysed by fitting the response of a linearised spring-mass-damper system to the time histories of the motion as shown in Eq (2):

$$F(t) = A \times e^{-\zeta * \omega_n * t} \times cos\left(\sqrt{1-\zeta^2} \times \omega_n \times t - \varphi\right) + B \qquad (2)$$

where *F(t)* is fitted value after calculation – ideally this should be the same as the experimental data; t is the time history; A is the amplitude of the fitted function; ζ is the damping ratio; ω_n is the undamped natural frequency; φ is the phase angle and B is the offset.

In the case without realistic moorings, the free decay test in surge and yaw is carried out to confirm that the natural frequency is sufficiently far from the values for heave and pitch that the heave and pitch are unaffected by the moorings. Since the soft moorings lead to a very low natural frequency, the surge decays in a small number of cycles; hence only two cycles were selected. Figure 15 shows an example of the surge free decay and its fit curve. The small variations are assumed to relate to the coupling effect from the pitch motions. It can be seen that the surge natural frequencies are far away from both heave and pitch natural frequencies, which suggests that the four station-keeping lines will not affect the heave/pitch natural frequencies.

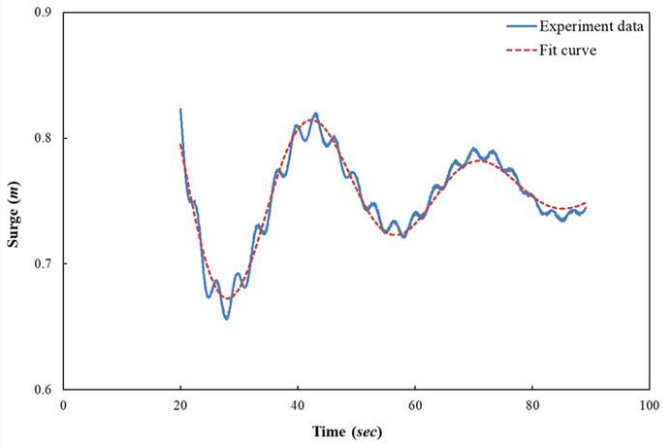

Figure 15 Surge free decay in experiment, spar-only

Figure 16 and Figure 17 show the heave and pitch free decay with the fitting curves, respectively.

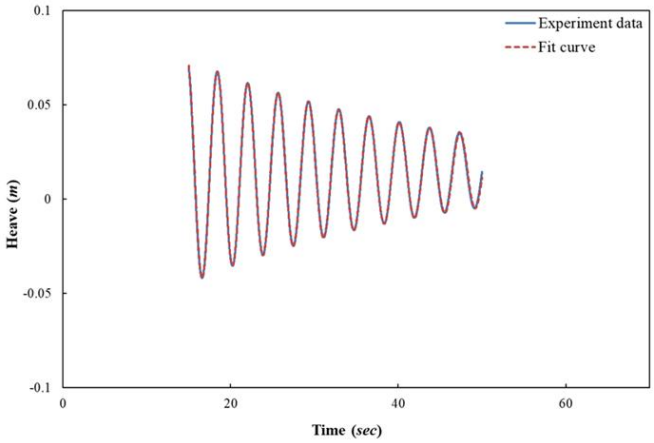

Figure 16 Heave free decay in experiment, spar-only

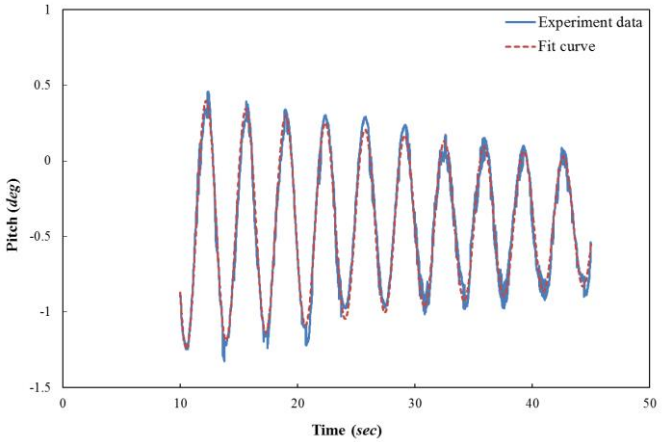

Figure 17 Pitch free decay in experiment, spar-only

Table 6 presents the mean value of measured natural frequencies of the spar-only and the NREL OC3-Hywind model. The pitch and heave natural frequency are matching very well with the NREL model.

Table 7 presents the mean value and the standard deviation (STD) of the damping ratio for heave and pitch. The difference between each of the tests are below 2%. The small value of the STD shows that the damping although may change from each test but it is still stable.

Table 6 Natural frequencies for spar-only compared with the NREL OC3-Hywind (Ramachandran et al., 2013)

	Experiment Scale	Full Scale	NREL
Pitch Frequency (Hz)	0.292	0.034	0.034
Heave Frequency (Hz)	0.275	0.032	0.032

Table 7 Mean value and STD of damping ratio, for spar-only

	Mean Damping Ratio	STD
Heave	0.014	0.004
Pitch	0.023	0.013

3.1.2 Spar with Realistic Mooring Lines

Similar with the process described in Section 3.1.1, Table 8 and Table 9 show the natural frequencies and damping ratios for the spar with realistic mooring lines, compared with the NREL OC3-Hywind model. It can be seen that only the yaw natural frequency does not match with the NREL model. This is assumed to be due to the slightly different mooring configuration from the NREL results and in particular the lack of the delta connection (which can restrict the yaw motion of the spar platform) (Jonkman, 2010) in the present experiment. Compared with the spar-only tank tests, the pitch and heave natural frequencies did not change significantly, but the surge and yaw motion's natural frequencies have increased as expected. The standard deviations of the damping ratio are all very small, and the damping behaviour are much more repeatable than the spar-only tests, especially in surge and yaw and thus the tank tests results would be considered acceptable.

It is noticed that the pitch damping ratio estimated from these tests appeared to reduce from 0.023 to 0.007 when the spar with realistic mooring lines. This result is counter-intuitive, as it can be expected that adding the mooring lines should increase damping. This test was investigated in some depth. A study of the time histories of the motions suggested that while the fit to the data appeared good, the simple approach adopted for conducting the free decay tests in pitch was flawed once the moorings were present. The free decay tests were

conducted both with and without moorings by displacing and then releasing the tower. For the tests without moorings, the resulting motion was close to pure pitch; however, with the realistic moorings present, the restoring force from the moorings contributed to a coupled oscillatory pitch-surge response, which had not been present in tests without the moorings. This combination of response had the result of reducing the apparent rate of decay of the pitch motion in this test. Ideally, a pure angular displacement in pitch would be imposed so that no surge resulted; however, this could be hard to achieve in practice. As discussed later, tests in waves show that the introduction of the realistic mooring lines does reduce the pitch motions compared to the spar only case, reinforcing the conclusion that the pitch damping coefficient estimated from these free decay tests with the mooring lines is not valid.

Table 8 Natural frequencies for spar with realistic mooring lines compared with NREL OC3-Hywind (Ramachandran et al., 2013)

Platform DOFs	Experiment Scale	Full Scale	NREL
Pitch Frequency (*Hz*)	0.292	0.034	0.034
Heave Frequency (*Hz*)	0.275	0.032	0.032
Yaw Frequency (*Hz*)	0.292	0.034	0.121
Surge Frequency (*Hz*)	0.069	0.008	0.008
Roll Frequency (*Hz*)	0.292	0.034	0.034

Table 9 Estimated Mean value and STD of damping ratio for spar with realistic mooring (*Note: this value is regarded as unreliable for reasons discussed in text)

	Mean Damping Ratio	STD
Heave	0.028	0.004
Pitch	0.007*	0.001
Surge	0.017	0.009
Yaw	0.084	0.003
Roll	0.011	0.001

Figure 18 shows the fairlead motion (after removing the offset between the two recording points) compared with the platform heave when conducting the heave free decay test. This shows that the two results match perfectly and thus demonstrates that the underwater Qualysis system data matches the data from the above water system.

For the surge free decay test with the realistic moorings (see Figure 19), the natural frequency is predicted well by the linearized Fit Function, but the plot shows some non-linear damping behaviour only been observed in the surge decays. The rate of decay of the measured data is greater than that for the fitted data, which is typically the case when non-linear viscous damping is affecting the motions. It can thus be concluded that viscous damping has more effect in surge than the other degrees of freedom.

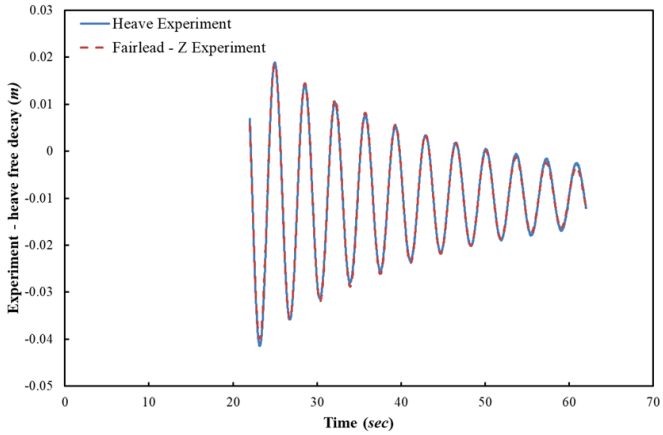

Figure 18 Fairlead-Z and platform heave free decay motion in experiment, spar with realistic mooring lines

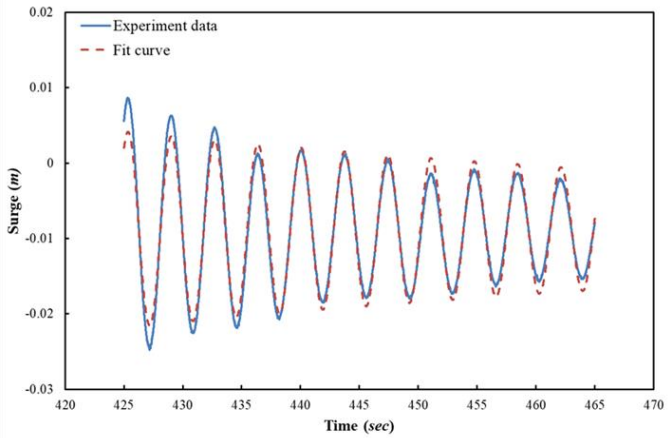

Figure 19 Surge free decay in experiment, spar with realistic mooring lines

3.2 Regular Waves

3.2.1 Repeatability Check

To make sure that the tank test results are reliable, it is necessary to repeat a test more than once. In this experiment, a wave frequency (f = 0.269 Hz for spar-only and f = 0.287 Hz for spar with realistic mooring lines, wave amplitude = 0.017m) has been selected to be applied to the spar platform model three times. In this process, other wave frequencies will be run by the wave maker between each of the repeat test, which can make sure that the results are more accurate. Table 10 presents the results for spar-only and Table 11 presents the results for spar with realistic mooring lines. It can be seen from the table that the experiment results are very stable.

Table 10 Repeatable check test results, spar-only

	Data20	Data22	Data24	MEAN
Input frequency (*Hz*)	0.269	0.269	0.269	0.269
Measured Wave Amplitude (*mm*)	15.2	15.2	15.4	15.3
Heave Amplitude (*mm*)	107.6	106.2	106.4	106.8
Pitch Amplitude (*deg*)	2.84	2.83	2.85	2.84

Table 11 Repeatable check test results, spar with realistic mooring lines

	Data019	Data023	Data025	MEAN
Input frequency (*Hz*)	0.287	0.287	0.287	0.287
Measured Wave Amplitude (*mm*)	16.7	16.7	16.8	16.7
Heave Amplitude (*mm*)	61.2	61.3	61.2	61.2
Pitch Amplitude (*deg*)	4.98	4.96	5.00	4.98
Surge Amplitude (*mm*)	76.5	76.5	77.0	76.7
Yaw Amplitude (*deg*)	1.44	1.41	1.44	1.43

3.2.2 Platform Responses

A range of regular waves has been applied to the platform (both with and without realistic mooring lines) to obtain the platform motion RAOs (response amplitude operator) – which can be used to predict the platform dynamic responses under other wave conditions. As a fully non-dimensional parameter, the definition of the RAO for surge/sway/heave is shown in Eq (3) and for roll/pitch/yaw is shown in Eq (4). The equation to calculate the maximum wave slope shown in Eq (5).

$$RAO\ \ (m/m) = \frac{motion\ amplitude}{wave\ amplitude} \tag{3}$$

$$RAO\ \ (deg/deg) = \frac{motion\ amplitude}{maximum\ wave\ slope} \tag{4}$$

$$maximum\ wave\ slope = \arctan\left(\frac{2 \times \pi \times wave\ amplitude}{wave\ length}\right) \times \frac{180°}{\pi} \tag{5}$$

3.2.2.1 Spar-only

Figure 20 and Figure 21 present the heave and pitch RAO of the spar platform itself, respectively. As shown in the figures, the heave and pitch peak responses are at 0.032 Hz and 0.034 Hz, which are well matched with the natural frequencies measured from the free decay tests. For the heave RAO, the peak value is around 8; this relatively high value is due to the absence of realistic mooring lines and their associated damping for these tests.

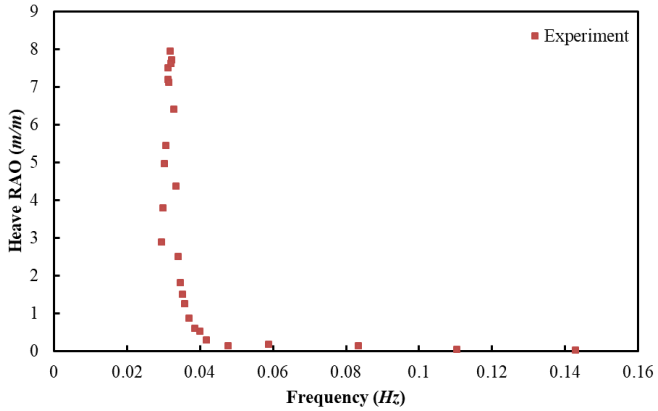

Figure 20 Heave RAO for spar-only (full scale)

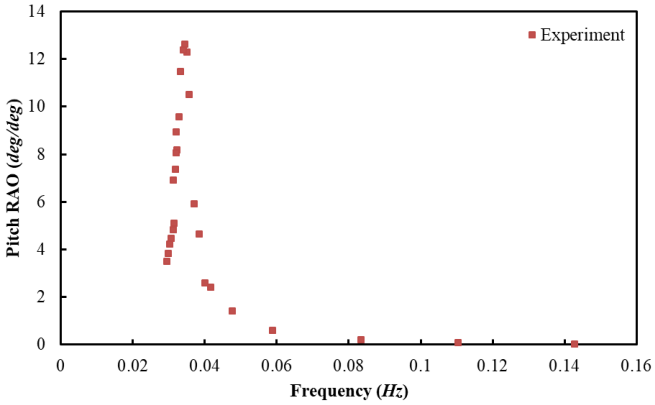

Figure 21 Pitch RAO for spar-only (full scale)

3.2.2.2 Spar with Realistic Mooring Lines RMS

Since non-linear behaviour has been observed at some wave frequencies (see details in Section 3.2.3.1), for the spar with realistic mooring lines, the motion response is not sinusoidal in some cases, and hence the root-mean-square motion (RMS) will be used to represent platform hydrodynamic responses rather than the amplitude of a sinusoidal motion

Due to the wave only propagating towards the positive X-axis and the lack of wind, no sway and roll will be expected and the yaw would be expected to be very small. Thus, only the surge, heave, and pitch RMS values will be presented here, as shown in Figure 22, Figure 23 and Figure 24. The RMS values are calculated from sections of the data when the platform is showing stable periodic motion curves in both experiment and numerical models. The equation is:

$$X_{rms} = \sqrt{\frac{x_1^2 + x_2^2 + \cdots + x_n^2}{n}} \tag{6}$$

As shown in Table 8, the full-scale surge natural frequency obtained from free decay tests is about 0.008 Hz. This is well outside the capability of the wave maker to generate waves and can happen only very rarely in real ocean environment. However, it is seen in Figure 22 that the surge RMS has a peak frequency similar to the peak frequency in pitch. This is presumed to be due to a coupling effect between surge and pitch.

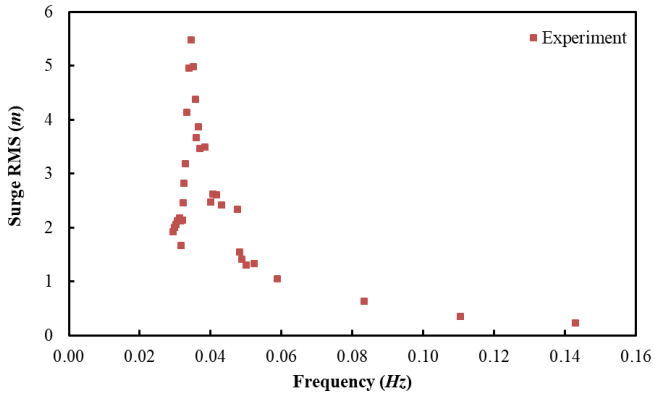

Figure 22 Surge RMS, spar with realistic mooring lines (full scale)

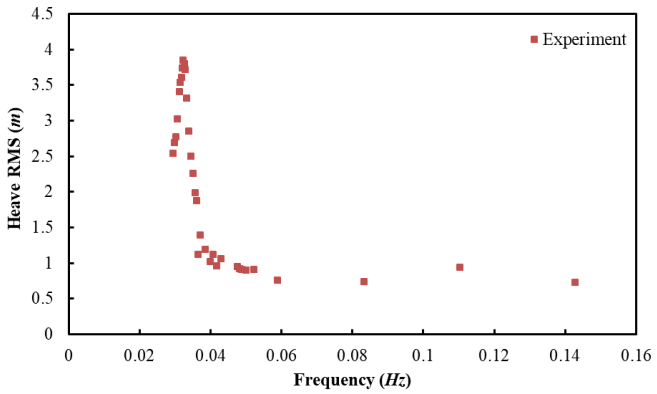

Figure 23 Heave RMS, spar with realistic mooring lines (full scale)

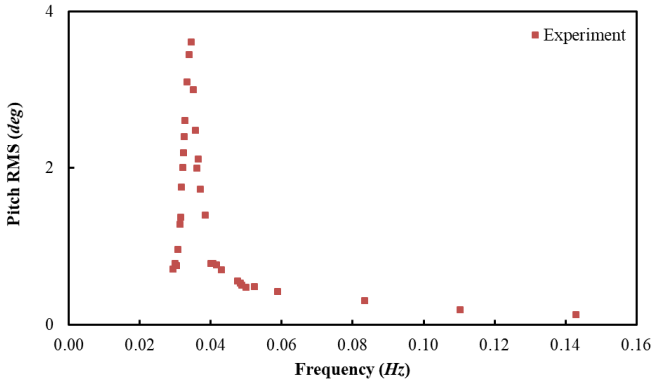

Figure 24 Pitch RMS, spar with realistic mooring lines (full scale)

It can be seen in Figure 23 that the peak heave RMS occurs at a frequency around 0.032 Hz with the RMS value close to 4. This corresponds to a heave amplitude at full-scale of 5.94m, compared to the equivalent value of 10.08m heave amplitude for the spar-only model. This reduction in amplitude is presumed to be caused by the additional damping introduced by the moorings.

The surge/pitch peak RMS occurs at around 0.034 Hz, which is similar to the spar-only tank tests. The peak RMS value of pitch is found to be 3.61 deg, which corresponds to a pitch amplitude of 5.64 deg. This can be compared with the equivalent pitch amplitude of 5.85 deg for the spar only tests, which suggests that the damping from the mooring also reduces the pitch motion. This reduction in pitch motion compared to the spar-only case reinforces the suggestion discussed in Section 3.1.2 that the pitch damping coefficient estimated from the free decay tests for the spar with realistic mooring lines is not accurate, and that the value of the pitch damping coefficient should be larger than that shown in Table 9.

3.2.3 Mooring Line Tensions and Motions

3.2.3.1 Non-linear Snatching Phenomenon

During the experiment, when monitoring the time history output curves, it is interesting to notice at some frequencies a “snatching” like behaviour is seen in which the mooring lines went slack and then suddenly went tight, yielding a substantial effect on platform motions and mooring line tension, as shown in Figure 25. Surprisingly, when the wave frequency was near the platform’s heave/pitch natural frequency, the snatching disappeared and the motion reverted back to quite sinusoidal behaviour, as shown in Figure 26, where the motion

reverts to sinusoidal when the wave frequency co-incides with the heave natural frequency. In Hsu et al. (2017)'s study, they have also found this snatching behaviour, which they names "snap" loads, on a semi-submersible OFWT. However, in their study, only the mooring tensions under extreme environmental loads were investigated.

The snatching could result due to a variety of reasons, such as the drag coefficient of the mooring lines, the mooring line weight or mooring configurations. In addition, increasing the mooring line pre-tension might be able to help to eliminate the snatching. This should be studied in detail in the future, as this non-linear motion in the platform could potentially be quite harmful for the wind turbine, due to the potential for rapid accelerations on top of the tower along the surge direction. However, there is no suggestion of strongly non-linear behaviour in surge at the tower top, as shown in Figure 27.

Figure 28 shows the tension time history in the Mooring Line 1 when the snatching happens. It can be seen that the full-scale mooring tensions can increase dramatically from about 200 kN (the pre-tension) up to more than 4,000 kN, which is very harmful to the mooring lines and could cause the mooring line to fail.

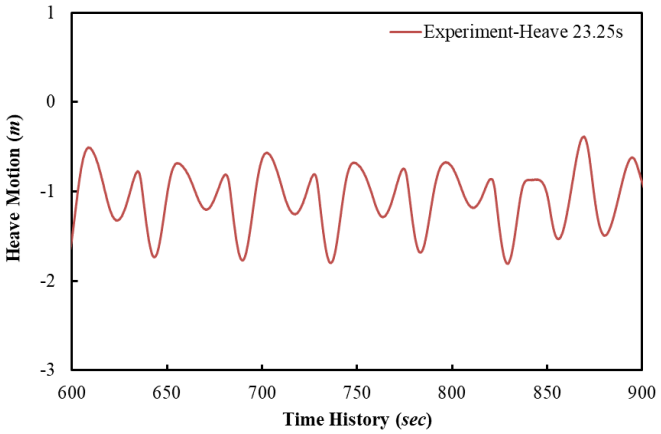

Figure 25 Non-linear heave motion in experiment, 23.25s (full scale)

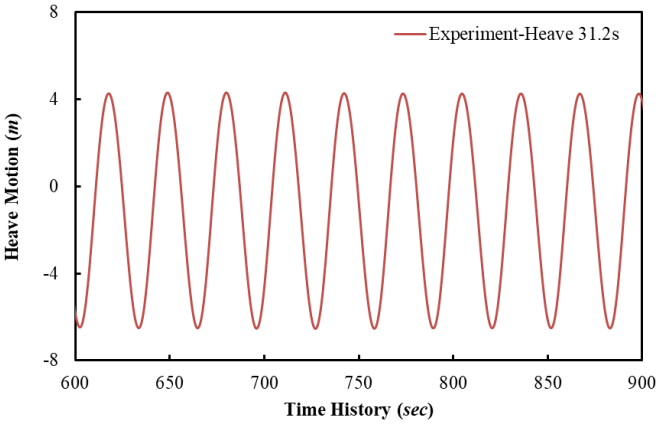

Figure 26 Heave motion in experiment, 31.20s (full scale)

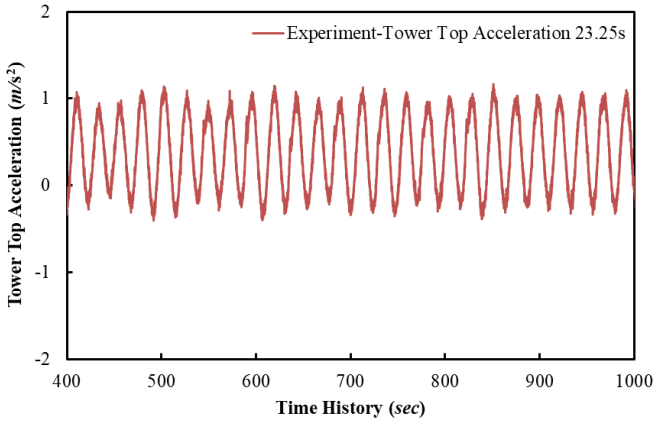

Figure 27 Tower top acceleration in experiment along X-axis, 23.25s (full scale)

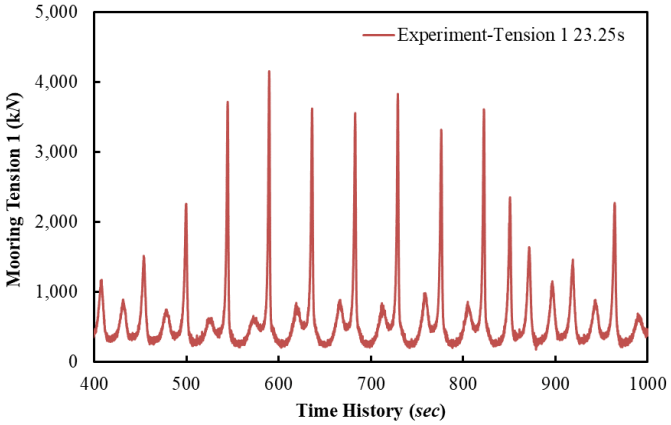

Figure 28 Mooring Tension 1 in experiment, 23.25s (full scale)

3.2.3.2 Mooring Tensions

As the snatching was seen at some regular wave frequencies, thus, as for the platform motions, it is no longer appropriate to present the results as RAOs based on the amplitudes of sinusoidal signals. Instead, the RMS mooring tension values, and the maximum and minimum tensions found will be presented. Figure 29 presents the RMS values of the three mooring line tensions with the various regular wave frequencies. It is seen that the average tension in the experiment could reach up to nearly 1,400 kN on Mooring Line 1 and 1,100 kN on Mooring Line 2 and 3. The small difference between Mooring Line 2 and 3 is due to the adjustment of the anchor frames, as mentioned in Section 2.8.

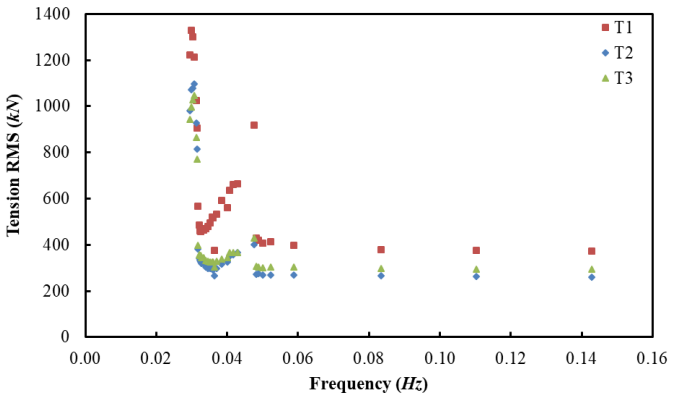

Figure 29 RMS of the mooring tensions (full scale)

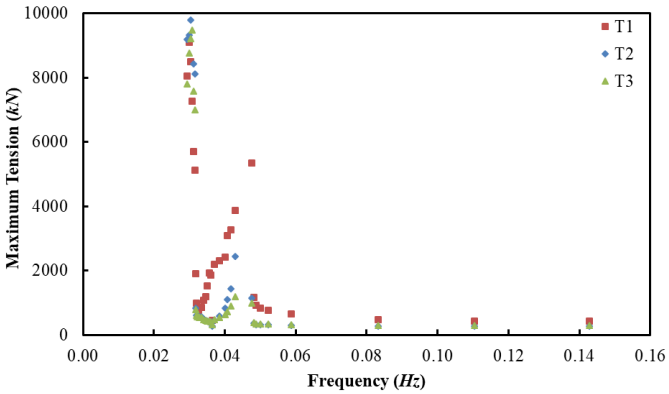

Figure 30 Maximum mooring tensions (full scale)

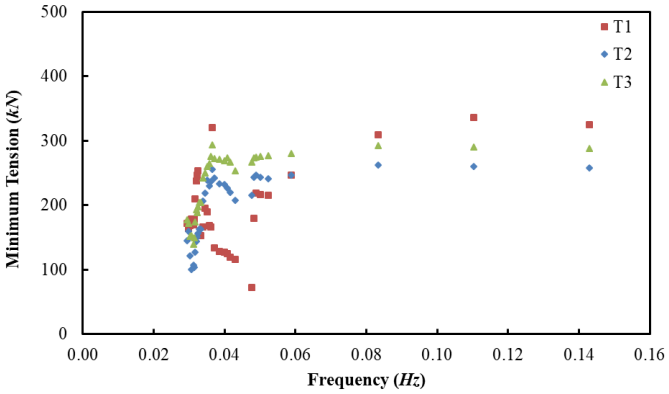

Figure 31 Minimum mooring tensions (full scale)

Figure 30 and Figure 31 present the maximum and the minimum values on each mooring line. For the maximum mooring tensions, it can be seen that the maximum mooring tensions could reach up to 10,000 kN. The suddenly sharp increase in mooring tensions during the snatching clearly has the potential to be very dangerous for the structure and could cause failure in the mooring lines. For the minimum mooring tensions, it is seen that when the snatching happens and the mooring line are close to becoming slack, the minimum tension could be as low as 100 kN for Mooring Line 2 and 3, and about 60 kN for Mooring Line 1.

3.2.3.3 Mooring Motions

The motion of Mooring Line 1 (along with the X-axis) has been recorded by the underwater cameras. The position of the seven reflective targets on Mooring Line 1 is shown in Table 3. In this section, the Mooring Line 1 RMS motion amplitudes along the X-axis and Z-axis (surge and heave) are presented. As the wave only propagates towards the positive X-axis, motions in the y-direction can be ignored. Due to the limit of the length, only the data for the representative Points 1, & 4 and the fairlead are presented, as shown from Figure 32 to Figure 34. The RMS amplitude is calculated in terms of the motion amplitude of each point relative to its initial static position. The experiment results have been converted into full scale before plotting. Along the Z-axis, a peak frequency can be seen which co-incides with the heave natural frequency, while Figure 34(b) shows that the platform fairlead motion, measured by the underwater Qualysis gives almost the same results as the platform heave RMS, measured by the above-water Qualysis system.

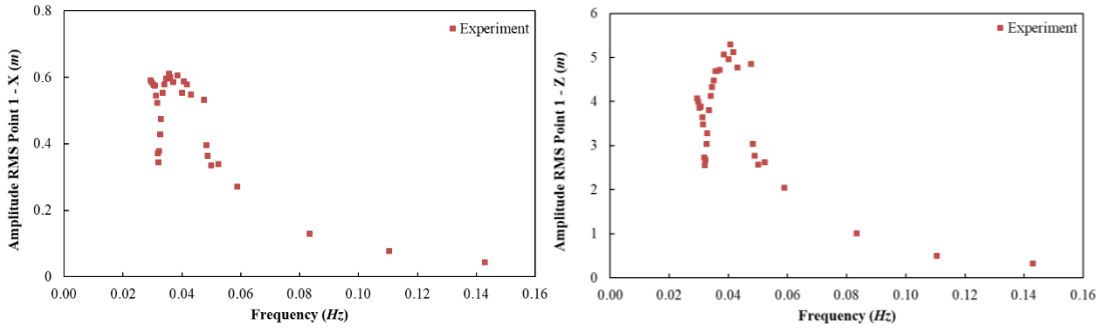

(a) X- axis (b) Z-axis

Figure 32 Amplitude RMS for Point-1 (full scale)

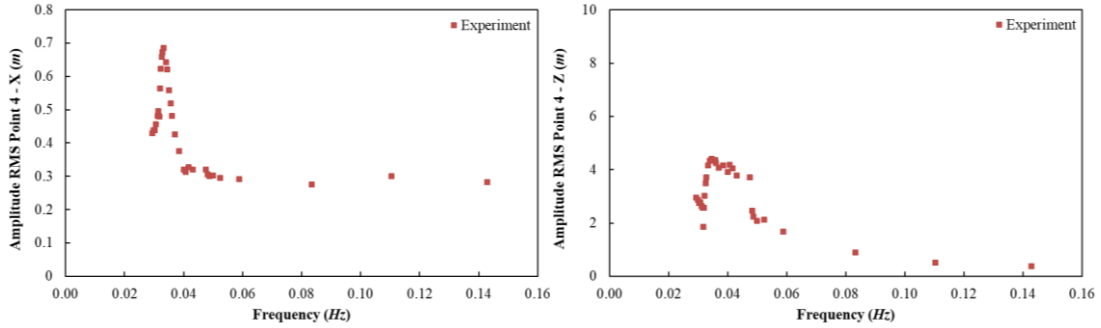

(a) X- axis (b) Z-axis

Figure 33 Amplitude RMS for Point-4 (full scale)

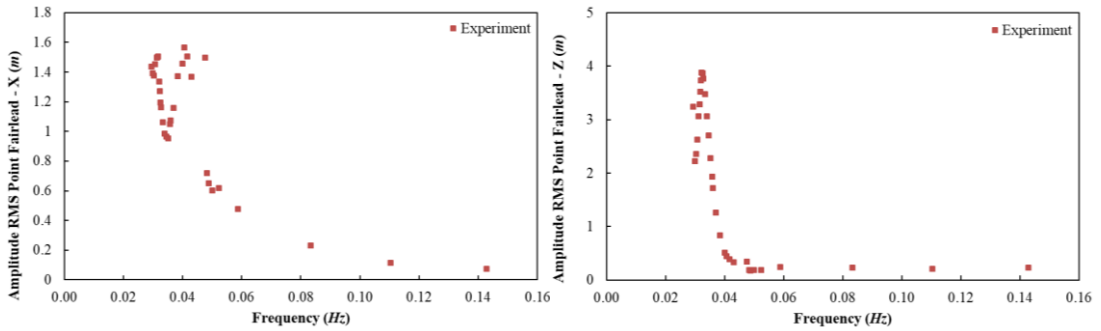

(a) X- axis (b) Z-axis

Figure 34 Amplitude RMS for point at the spar Fairlead position (full scale)

3.2.4 Linearity Test

Linearity tests have been conducted for both heave and pitch, at their peak RAO frequencies. The purpose of the linearity test is to check how linear is the experimental results. A range of wave amplitude from 0.004 m to 0.018 m has been applied to the spar model. The wave frequencies are at the peak RAO frequency of heave and pitch, respectively. With the linear increasing of the wave amplitude, at the set wave frequency, the resulted platform RAO is expected to decrease which is due to the increasing of viscous damping. Figure 35 and Figure 36. present the heave/pitch linearity tank test results for spar-only. Since the snatching has disappeared when the wave frequency nears the platform heave/pitch motion natural frequency, as discussed in Section 3.2.3.1. Thus, the platform heave/pitch time history show a sinusoidal curve in this part and the RAO can be found in a meaningful manner. Figure 37 and Figure 38presents the heave/pitch linearity tank test results of the spar with realistic mooring lines, both of the heave and pitch RAO decreasing with the increasing wave height, as expected.

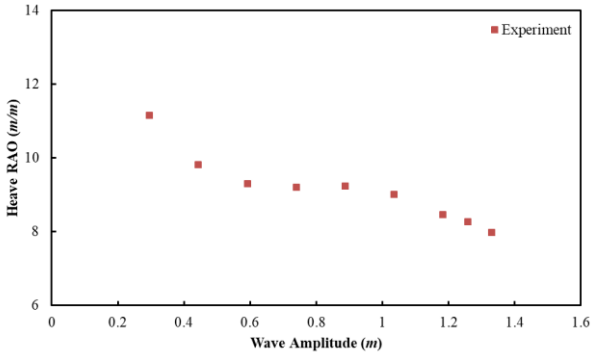

Figure 35 Heave linearity test, spar-only (full scale)

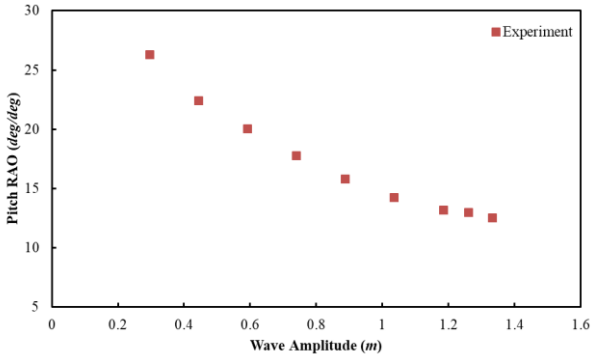

Figure 36 Pitch linearity test, spar-only (full scale)

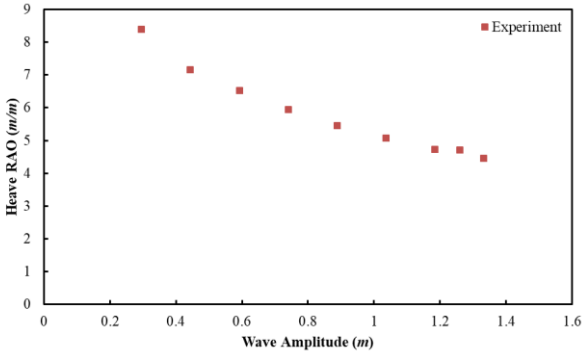

Figure 37 Heave linearity test, spar with realistic mooring lines (full scale)

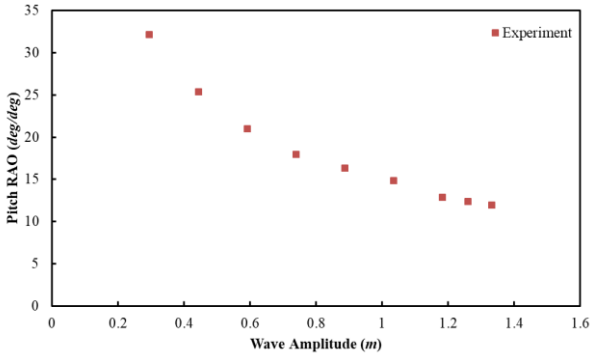

Figure 38 Pitch linearity test, spar with realistic mooring lines (full scale)

3.3 Irregular Waves

3.3.1 Platform Motions Probability Density Function (PDF) and Spectrum

The platform responses (both with and without mooring lines) under the four sea states (Table 4) are been tested. Selected sea state results are presented here.

3.3.1.1 Spar-Only

Due to the lack of realistic moorings, only the heave and pitch motion's PDF and motion spectrum are presented. The experimental measured data have been calculated into full scale before calculating its PDF and spectrum. For experimental heave spectrum, as presented in Figure 40, the first and major peak is happening at its natural frequency and the other peak is at the peak wave frequency – around 0.070 Hz. For the pitch motion spectrum, the major peak is at the peak wave frequency, while a very small peak is seen at the pitch natural frequency. Figure 39 and Figure 41 show the heave and pitch motion amplitude are mainly within 1m and 2°, in Sea State 3.

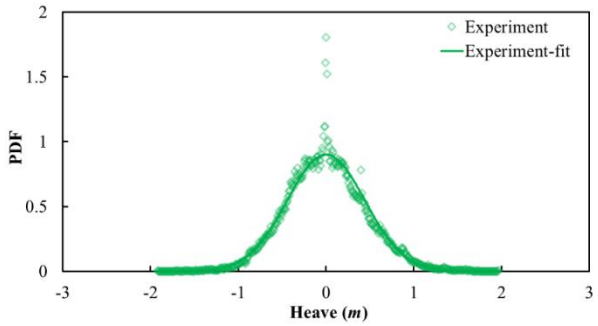

Figure 39 Heave motion amplitude PDF for Sea State 3, spar-only (full scale)

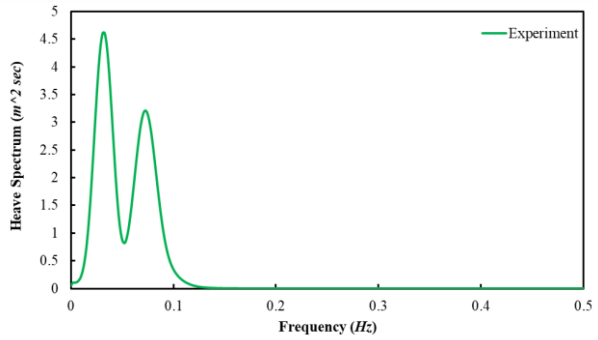

Figure 40 Heave motion spectrum for Sea State 3, spar-only (full scale)

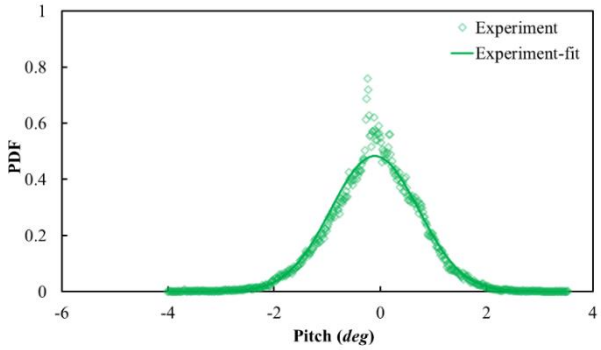

Figure 41 Pitch motion amplitude PDF for Sea State 3, spar-only (full scale)

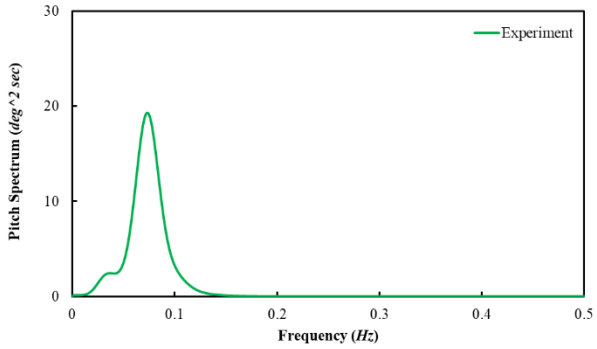

Figure 42 Pitch motion spectrum for Sea State 3, spar-only (full scale)

3.3.1.2 Spar with Realistic Mooring Lines

The heave, pitch and surge motion's PDF and spectrum from Sea State 2 are shown from Figure 43 to Figure 48. The experimental measured data have been calculated into full scale before calculating its PDF and spectrum.

Figure 43 shows the heave motion amplitude probability density function (PDF) are mainly within 0.5 m. When looking at the heave motion spectrum, in Figure 44, one peak has been found at the wave spectrum peak frequency (about 0.089 Hz) while another one is seen at the heave motion natural frequency (about 0.032 Hz). Figure 45 shows the pitch amplitude mainly lies below 1°. For the pitch motion spectrum, as shown in Figure 46, the two peaks occur around the peak wave frequency, and the pitch natural frequency (around 0.034 Hz). As mentioned in Section 3.2.2.2, the pitch motions do not appear to be substantially affected by the presence of the mooring line, so the mooring system seems cannot affect the pitch motion behaviour. In surge motion PDF, it is seen that the surge motion amplitude can range from 0 to 2m, as shown in Figure 47. For the surge motion spectrum, see Figure 48, two peaks are observed – one is at the peak wave spectrum frequency and the other one is around the pitch natural frequency (0.034 Hz), which shows the prediction of the coupling effect between the surge and pitch motion.

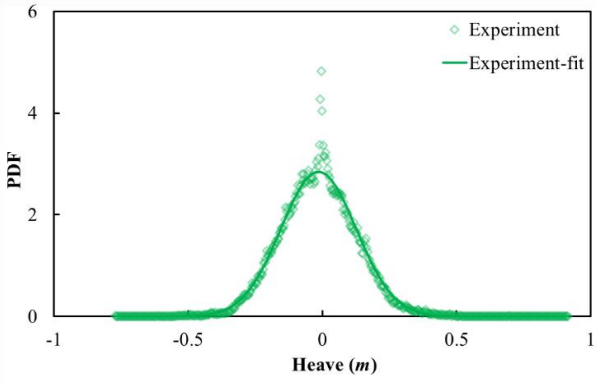

Figure 43 Heave PDF for Sea State 2, spar with realistic mooring (full scale)

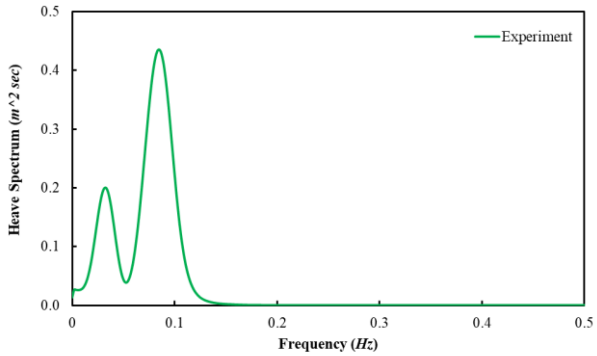

Figure 44 Heave motion spectrum for Sea State 2, spar with realistic mooring (full scale)

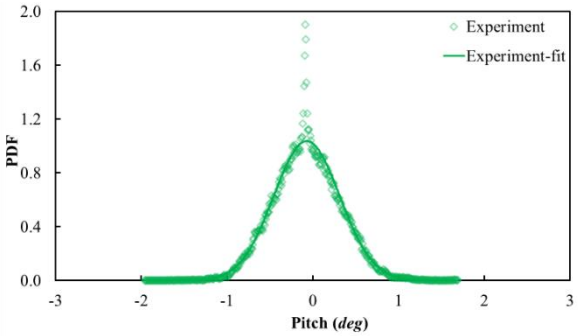

Figure 45 Pitch PDF for Sea State 2, spar with realistic mooring (full scale)

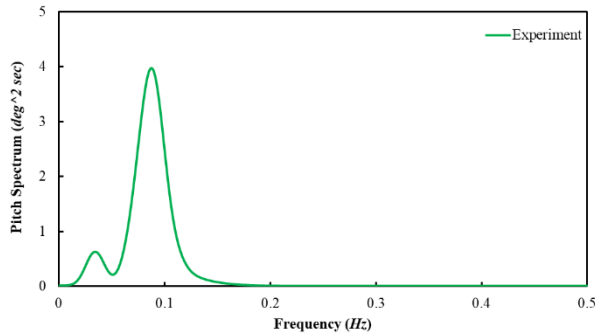

Figure 46 Pitch motion spectrum for Sea State 2, spar with realistic mooring (full scale)

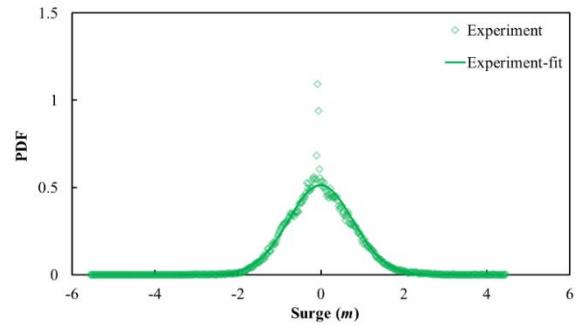

Figure 47 Surge PDF for Sea State 2, spar with realistic mooring (full scale)

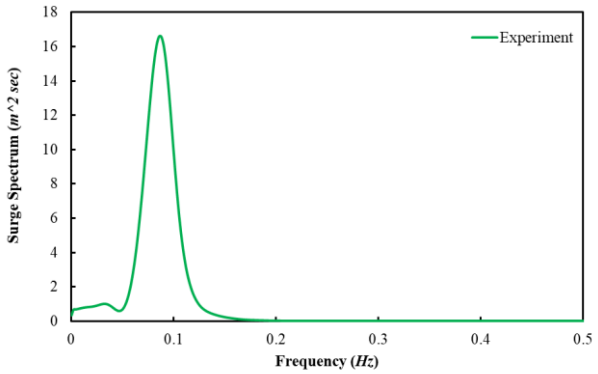

Figure 48 Surge motion spectrum for Sea State 2, spar with realistic mooring (full scale)

When checking the heave motion spectrum in Sea State 3, a very low frequency behaviour – 0.002 Hz – has been discovered, as shown in Figure 49, and this low frequency shows quite high energy. The spectrum of heave, pitch and surge motion in the heave free decay test were first checked to make sure that this small frequency is not related to any coupling effect, but no evidence of behaviour at this frequency was found. The tank test time history (scaled into full scale) in Sea State 3 and the recorded video were then examined.

The time history of the heave motion in Sea State 3 is shown in Figure 50. A few quite large motions can be seen from around 1500s to 4000s and from 5350s to 6100s; these large motions were also observed in the video, especially for the time from 5350s to 6100s.
In particular, it can be seen that the mean vertical location of the platform is depressed for an extended period from 5350 to 6100s. At the same time, large values of tension can be seen in the tension time history, which suggests that the quite large heave energy is caused by a series of large waves. Large motions can be seen in sway and yaw at the same time. This suggests that this large slowly-varying vertical motion is not due to the model taking on water. A truncated time history has been produced to exclude these large motions, and the response spectrum recalculated are shown in Figure 51, where the large energy at 0.002 Hz has disappeared. Thus, it can be concluded that the large energy apparent at 0.002 Hz is caused by the slowly varying large vertical motion of the platform in the tank. The same small frequency (0.002 Hz) can also be seen in the mooring line motions along X-axis in Sea State 3 and it is assumed that this could be related to the large heave motion as well.

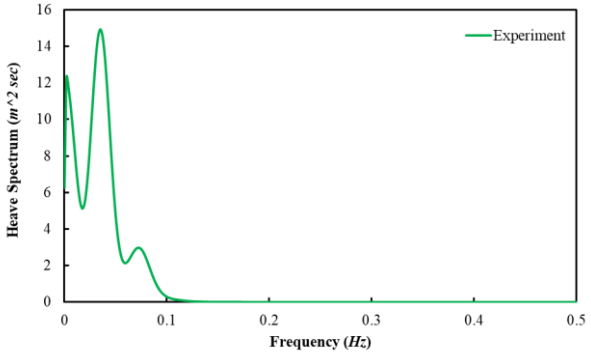

Figure 49 Heave motion spectrum for Sea State 3, spar with realistic mooring (full scale)

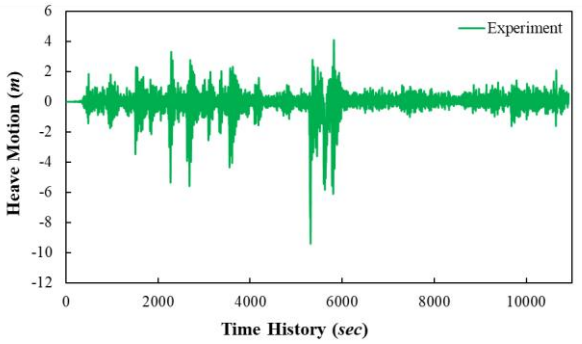

Figure 50 Heave motion time history in experiment, Sea State 3, spar with realistic mooring (full scale)

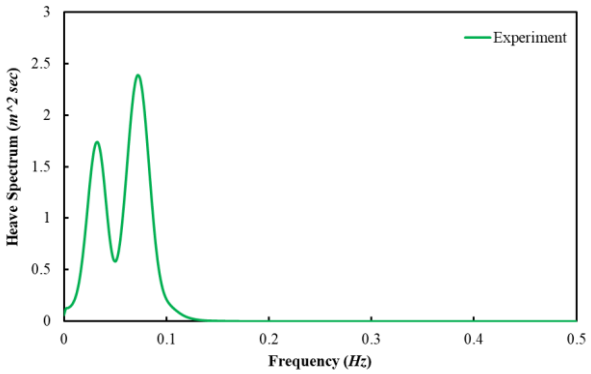

Figure 51 Heave motion spectrum from truncated time history in experiment, Sea State 3, spar with realistic mooring (full scale)

3.3.2 Mooring Line Motions and Tensions

Similar to the regular wave results presented, only three selected points' data in Sea State 2 are discussed in this part. Figure 52 to Figure 54 show the motions of Point 1 (the point furthest from the spar platform apart from the anchor), Point 4 (point near the middle of the line) and the Fairlead position motion (as a reference point compared with the platform motion), along both X-axis and Z-axis. An obvious peak has been observed at the peak wave frequency (0.089 Hz) and the other peak occurs at about 0.025 Hz for motion along X-axis and 0.023 Hz in Z-axis. These peaks could indicate the mooring line motion natural frequencies along the two directions; similar peaks are also found in the other three sea states. It seems that with the position changing from the anchor to the platform fairlead position, the mooring motions in both X-axis and Z-axis are increasing till the middle of the mooring line and then decreasing to the fairlead position in all of the four sea states. The experiment generally shows a higher peak spectrum at the peak wave frequency and a smaller peak spectrum at its natural frequencies. Comparing all the points for motion along X-axis, reveals a tendency that the motion energy gets higher for the points near the platform, and weaker in the middle floating part of the mooring. Near the anchor position, the motion energy is still higher than the floating part but smaller than points near the platform, which could indicate the damping effect is the main factor in the middle parts. The motion along Z-axis shows an opposite behaviour than with the X-axis. At the fairlead position, it can be seen that the motion along the Z-axis matches perfectly with the platform heave spectrum which gives re-assurance that the underwater and above-water motion capture systems are working correctly. In contrast, the X-axis, motion at the fairlead position shows smaller energy than platform surge motion, but the curve shape is quite similar. This difference is believed to be due to the effect of platform pitch on the X-axis motion of the centre of gravity of the platform.

The three mooring line tension spectrum from Sea State 2 are shown in Figure 55. The tension spectrum of Mooring Line 1 shows two peaks – the main peak occurs at around 0.089 Hz, which is the peak wave frequency, while the other one occurs at around 0.025 Hz – which is similar to the mooring line motion spectrum along X-axis, which indicates that the mooring line motion can indicate its tension behaviour. For the mooring tension in Mooring Lines 2 and 3, as shown in Figure 55(b), the experimental spectrum exhibits two peaks – one is still at the peak wave frequency, and the major one is at a quite low frequency, about 0.002 Hz, which corresponds to the frequency observed in the heave motion in Sea State 3. This indicates there should exist some non-linear dynamic behaviour or the effect from difference frequency waves at this small frequency, which could usefully be investigated with further studies.

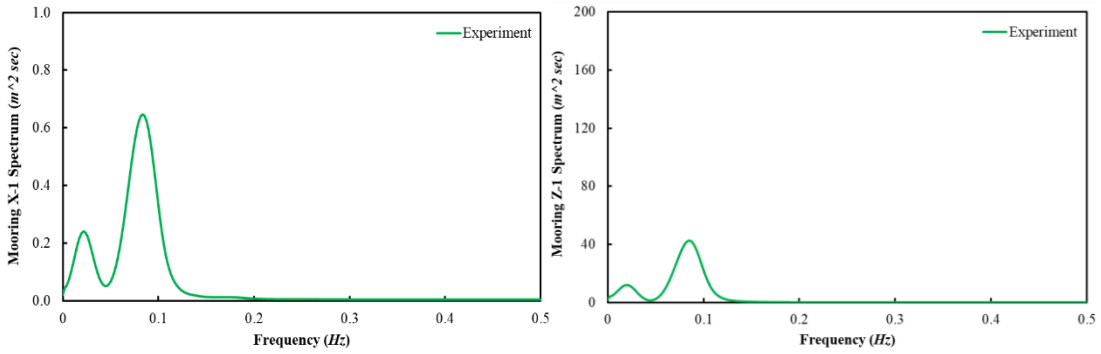

(a) X- axis (b) Z-axis

Figure 52 Point-1 motion spectrum, on Mooring Line 1 in Sea State 2 (full scale)

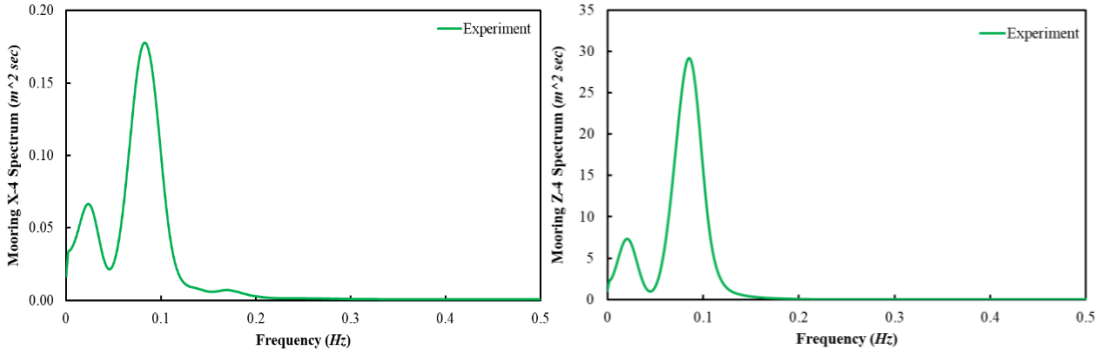

(a) X- axis (b) Z-axis

Figure 53 Point-4 motion spectrum, on Mooring Line 1 in Sea State 2 (full scale)

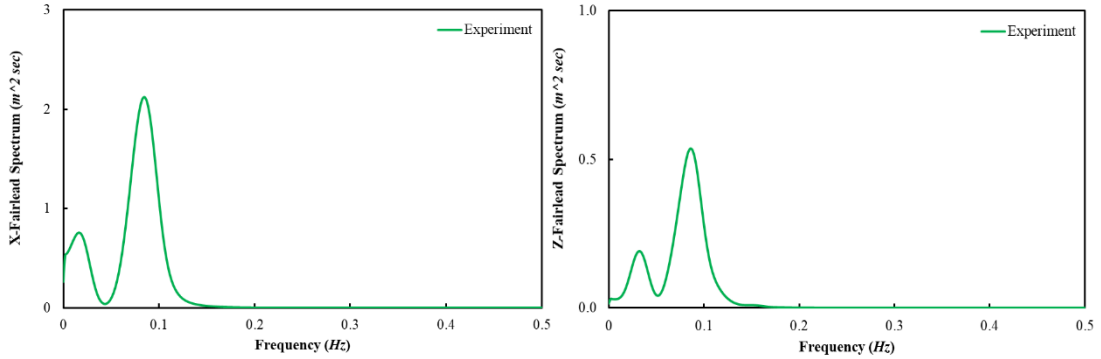

(a) X- axis (b) Z-axis

Figure 54 Fairlead motion spectrum, on Mooring Line 1 in Sea State 2 (full scale)

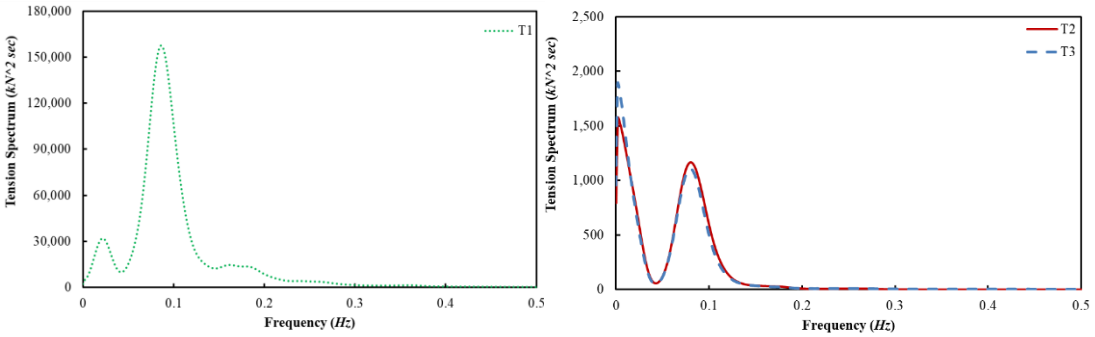

(a) Mooring Line 1 Tension (b) Mooring Line 2/3 Tension

Figure 55 Mooring tension spectrums, Sea State 2 (full scale)

4 Conclusion

This study conducted the tank test for a spar type OFWT (both with and without realistic mooring lines). Detailed process of experiment set-up and the limitations of the experiment have been discussed and they are all felt to be acceptable in this study scope. The platform 6 DOF motions and the mooring line tensions/motions were captured by the Qualysis camera both above the tank and under the water line of the tank. The mooring line tensions are measured by high accuracy underwater load cells.

The spar platform (both with and without realistic mooring lines) natural frequencies are obtained through the free decay tests. The heave, pitch and surge (spar with realistic mooring lines) natural frequencies can match perfectly with the NREL OC3-Hywind model, while the yaw cannot match due to different mooring configurations and the lack of the delta connection. The damping ratios have also been obtained which can be used to set-up numerical models for future study.

The spar platform RAO (spar-only) and RMS (spar with realistic mooring lines) are obtained through the regular wave tests, which show the peak responses for heave and pitch are matching perfectly with the results from free decay tests. The coupling motion between surge and pitch have been observed. A non-linear snatching phenomenon has been observed during the regular wave tests. It is interesting to find that this non-linear snatching behaviour disappears when the wave frequency is at the platform heave/pitch natural frequencies and show up again at other wave frequencies. This non-linear snatching behaviour could be very harmful to the mooring lines and wind turbines life, as it can lead to the sharply increase of mooring tension up to 10,000 kN. The factors can affect this non-linear snatching behaviour, such as the mooring configurations, pre-tensions of the mooring system, nonlinear heave/pitch coupling stiffness of the spar, and the tools to predict it would be worth for a future study.

In the irregular wave tests, for both spar-only and spar with realistic mooring lines, two main peak spectrums have been observed in the platform heave and pitch motions – one is at the peak wave frequency and the other one is at their natural frequencies. For spar with realistic mooring lines, the surge motion also show a peak spectrum at the pitch natural frequencies, which shows the coupling of the two motions (as founded in the platform RMS). For the mooring line motions, along both X-axis and Z-axis, the main peak spectrum is at the peak wave frequency, and the other peak occurs at about 0.025 Hz for motion along X-axis and 0.023 Hz in Z-axis, which could indicate the mooring line motion natural frequencies. For mooring line tensions, the main peak spectrum is still found at the peak wave frequency, while the other peak spectrum is at a quite low frequency (about 0.002 Hz). This corresponds

to the frequency observed in the heave motion in Sea State 3 and means there should exist some non-linear dynamic behaviour at this small frequency which could usefully be investigated with further studies.

Acknowledgement

This study is supported by the "Engineering Future Studentships", Faculty of Engineering at the University of Strathclyde. Special thanks to the staff at the KHL for their kind help and professional instructions for experiments.

References

Ahn, H.-J. & Shin, H. 2019. Model test and numerical simulation of OC3 spar type floating offshore wind turbine. International Journal of Naval Architecture and Ocean Engineering, 11**,** 1-10.

Chakrabarti, S. K. 1994. Offshore structure modeling, World Scientific.

Duan, F., Hu, Z., Liu, G. & Wang, J. 2016a. Experimental comparisons of dynamic properties of floating wind turbine systems based on two different rotor concepts. Applied Ocean Research, 58**,** 266-280.

Duan, F., Hu, Z. & Niedzwecki, J. 2016b. Model test investigation of a spar floating wind turbine. Marine Structures, 49**,** 76-96.

Duan, F., Hu, Z. & Wang, J. Model tests of a spar-type floating wind turbine under wind/wave loads. International Conference on Offshore Mechanics and Arctic Engineering, 2015. American Society of Mechanical Engineers, V009T09A044.

Equinor 2019. How-Hywind-works, available at https://www.equinor.com/en/what-we-do/hywind-where-the-wind-takes-us/hywind-up-close-and-personal.html.

Hsu, W.-t., Thiagarajan, K. P. & Manuel, L. 2017. Extreme mooring tensions due to snap loads on a floating offshore wind turbine system. Marine Structures, 55**,** 182-199.

Ishida, S., Kokubun, K., Nimura, T., Utsunomiya, T., Sato, I. & Yoshida, S. At-sea experiment of a hybrid spar type offshore wind turbine. International Conference on Offshore Mechanics and Arctic Engineering, 2013. American Society of Mechanical Engineers, V008T09A035.

Jonkman, J. 2010. Definition of the Floating System for Phase IV of OC3. National Renewable Energy Lab.(NREL), Golden, CO (United States).

Landau, H. 1967. Sampling, data transmission, and the Nyquist rate. Proceedings of the IEEE, 55**,** 1701-1706.

Proskovics, R. 2015. Dynamic response of spar-type offshore floating wind turbines. University of Strathclyde.

Ramachandran, G., Robertson, A., Jonkman, J. & Masciola, M. D. 2013. Investigation of response amplitude operators for floating offshore wind turbines. National Renewable Energy Lab.(NREL), Golden, CO (United States).

Rolo, L. 2014. Design, testing and validation of a scale model semisubmersible offshore wind turbine under regular/irregular waves and wind loads. MSc University of Strathclyde.

Ruzzo, C., Fiamma, V., Collu, M., Failla, G., Nava, V. & Arena, F. 2018. On intermediate-scale open-sea experiments on floating offshore structures: Feasibility and application on a spar support for offshore wind turbines. Marine Structures, 61**,** 220-237.

Santos-Herrán, M. 2016. Model Design, Testing and Validation of Three Scaled Spar Type Offshore Floating Wind Turbines under Wave Loads. MSc, University of Strathclyde.

Shin, H. Model test of the OC3-Hywind floating offshore wind turbine. The Twenty-first International Offshore and Polar Engineering Conference, 2011. International Society of Offshore and Polar Engineers.

Skaare, B., Hanson, T. D., Nielsen, F. G., Yttervik, R., Hansen, A. M., Thomsen, K. & Larsen, T. J. Integrated dynamic analysis of floating offshore wind turbines. European wind energy conference and exhibition, 2007. Citeseer, 7-10.

Stansberg, C., Contento, G., Hong, S. W., Irani, M., Ishida, S., Mercier, R., Wang, Y., Wolfram, J., Chaplin, J. & Kriebel, D. 2002. The specialist committee on waves final report and recommendations to the 23rd ITTC. Proceedings of the 23rd ITTC, 2**,** 505-551.

Tecni-cable 2016. Stainless Steel Wire Rope - Fittings - Tools - TECNI, available at http://www.tecni-cable.co.uk/Products/US-Mil-Spec-Cable-7x7-Stainless-Mil-DTL-83420-Composition-B.

Tomasicchio, G. R., D'Alessandro, F., Avossa, A. M., Riefolo, L., Musci, E., Ricciardelli, F. & Vicinanza, D. 2018. Experimental modelling of the dynamic behaviour of a spar buoy wind turbine. Renewable Energy, 127**,** 412-432.

Utsunomiya, T., Matsukuma, H., Minoura, S., Ko, K., Hamamura, H., Kobayashi, O., Sato, I., Nomoto, Y. & Yasui, K. 2013a. At sea experiment of a hybrid spar for floating offshore wind turbine using 1/10-scale model. Journal of offshore mechanics and Arctic engineering, 135.

Utsunomiya, T., Sato, I., Kobayashi, O., Shiraishi, T. & Harada, T. Design and installation of a hybrid-spar floating wind turbine platform. International Conference on Offshore Mechanics and Arctic Engineering, 2015. American Society of Mechanical Engineers, V009T09A063.

Utsunomiya, T., Sato, I., Yoshida, S., Ookubo, H. & Ishida, S. Dynamic response analysis of a floating offshore wind turbine during severe typhoon event. International Conference on Offshore Mechanics and Arctic Engineering, 2013b. American Society of Mechanical Engineers, V008T09A032.

Utsunomiya, T., Sato, T., Matsukuma, H. & Yago, K. Experimental validation for motion of a spar-type floating offshore wind turbine using 1/22.5 scale model. International Conference on Offshore Mechanics and Arctic Engineering, 2009. 951-959.

Utsunomiya, T., Yoshida, S., Kiyoki, S., Sato, I. & Ishida, S. Dynamic response of a spar-type floating wind turbine at power generation. International Conference on Offshore Mechanics and Arctic Engineering, 2014. American Society of Mechanical Engineers, V007T05A027.

Yu, M., Hu, Z.-q. & Xiao, L.-f. 2015. Wind-wave induced dynamic response analysis for motions and mooring loads of a spar-type offshore floating wind turbine. Journal of Hydrodynamics, Ser. B, 26**,** 865-874.

Zürcher, K. 2016. Waterjet testing techniques for powering performance estimation using a single catamaran demihull. University of Tasmania.

Experimental investigation on ~~D~~dynamic responses of a spar-type offshore floating wind turbine and its mooring system behaviour~~, Part I: Experiment~~

Xue Xu[*], *Sandy Day*

Department of Naval Architecture, Ocean and Marine Engineering, Henry Dyer Building, University of Strathclyde, 100 Montrose Street, Glasgow, G4 0LZ, UK

[*]*corresponding author;* e-mail: xue.xu@strath.ac.uk

ABSTRACT

This study investigated the dynamic behaviour of a spar-type OFWT analysed under various wave loads by conducting an experiment campaign. Both the characteristic of the spar platform itself and the spar with realistic moorings have been investigated. A particular focus of the study was the motions of the mooring lines, which were measured at a series of discrete points along one line using an underwater motion capture system, in parallel with tension measurement at the anchor points. The main objective of this study is to provide experimental measured data to validate numerical software on the research of mooring line motions.

A free decay test has been carried out to confirm the spar platform motions natural frequencies and damping characteristics. The platform was then subjected to a range of regular and irregular waves to obtain the motion characteristics of the platform and the mooring lines. For the mooring line motions, which has rarely been discussed in published research, a non-linear snatching phenomenon has been observed at the tank for some wave frequencies. This non-linear behaviour shows that snatching leads to the high instantaneous mooring line tensions and platform accelerations could cause the failure of the mooring lines in the real structure.

***Keywords*:** offshore floating wind turbines, spar platform, mooring motion, tank tests

1 Introduction

With the burning of fossil fuel such as coal, natural gas and oil, a huge amount of greenhouse gas has been emitted to the environment and has caused severe pollution problems. Also, the fossil fuel is not sustainable. Thus, developing clean and renewable energy is becoming an urgent priority; one of the potential resources for large-scale renewables is wind energy. People mainly use two types of wind turbines – onshore and offshore, to harvest the wind energy while offshore wind resources allow more reliable generation of electricity. According to the water depth of the offshore environment, two types of foundation systems for offshore wind turbines have been proposed -- fixed foundations and floating platforms with mooring systems. For water depth between 20 to 50 m, fixed foundations would be the preferred choice due to the lesser cost. However, for sites further away from the coast where the wind resources are greater than near shore, the water depth can be up to hundreds of metres on sites and floating systems must be used.

The spar platform is a ballast-stabilized substructure for OFWTs. It normally consists of a spar buoy and catenary mooring lines. The long cylindrical spar platform achieves stability by using ballast to lower the centre of mass far below the centre of buoyancy, which creates righting moment and high inertial resistance in pitch (Proskovics, 2015). It is one favoured solution for deep water sites because of its simplicity in design, modelling and commercialization (Shin, 2011). Thus, in this study, a spar type OFWT model which is known as the OC3-Hywind installed with the NREL 5 MW benchmark wind turbine, as proposed by Jason Jonkman based on the Statoil Hywind model (Jonkman, 2010), will be employed.

The earliest tank test of a 5 MW spar type OFWT (the Hywind model) was conducted by Skaare et al. (2007), at a linear scale of 1:47 using Froude scaling. Both the irregular waves and wave loads were investigated, but the focus was on the comparison with a numerical software code (SIMO/REFLEX) and the platform dynamic characteristic was not presented. This, however, still provides a reference scaling ratio model tests on the Hywind model. Utsunomiya et al. (2009) have conducted an experiment for a spar-type floating platform with 60 m draft and a 2MW wind turbine under both regular/ irregular waves and steady wind load (scale factor 1:22.5). The experimental results were compared with their numerical simulations to verify the numerical codes (mainly based on Morison's Equation). Reasonable agreement was achieved but the damping force evaluations needed further improvement. They then developed a 2 MW wind turbine with 70 m draft spar platform and a 1:10 model has been made, to conduct at-sea experiment, where the wind speed/ direction, tidal height, wave height, motion of the spar platform, mooring tension and strains in the tower/spar platform have been measured. Their platform is designed as a hybrid structure, where the upper part is constructed of steel and the lower part is pre-stressed concrete. This provides a good preliminary concept model for further design of offshore wind turbines (Utsunomiya et al., 2013a). This hybrid-spar had also survived during Typhoon Sanba, where the average wind speed at the hub height was 48.3 m/s, which verifies the safety of the structure (Ishida et al., 2013). The author also developed numerical tools to compare the simulation results with the at-sea measurement. Their dynamic mass-spring model for mooring lines show better agreement with the experimental measured values than the quasi-static catenary mooring model. The standard deviations of yaw responses were overestimated by the numerical tools but the mean values agreed well (Utsunomiya et al., 2013b). In the at-sea experiment, the group used a 100 kW wind turbine on top of the hybrid-spar. The platform responses were investigated when the turbine was operating, where they found the mean pitch responses was not very large, but the standard deviation of the roll/pitch responses was significant (Utsunomiya et al., 2014). In 2015, they published the design methodology for hybrid spar which includes the environmental design conditions, design load cases, dynamic and fatigue analysis; the installation procedure was also presented, where they consider the spar as a simple one-dimensional structure. However, they also pointed out that further studies are needed to reduce the cost for commercial application (Utsunomiya et al., 2015).

The most recent open-sea experiments on a spar type OFWT is conducted by Ruzzo et al. (2018), and they used a 1:30 scale model of the OC3-Hywind. The experiments site is located in the sea front of Reggio Calabria (Italy). The intermediate-scale, open-sea experiment can help to overcome some limitations of small-scale models, such as the limitation of experiment durations and the scale effects. However, the open-sea wave frequencies may not able to cover the complete frequency range of the platform motions, but, in their studies, the roll/heave/pitch motions can be captured.

The research group in the University of Ulsan have also done experiment studies on the OC3-Hywind model, with scaling factor 1:128. In 2011, Shin conducted a model tests to investigate the OC3-Hywind platform motion characteristics (Shin, 2011). They then developed three new spar platforms with the same mass and volume of the OC3-Hywind but different body shapes and carried out the model tests still with the scale 1:128. Both the wave and wind (with operating turbine) were tested, and the platform motion RAOs and maximum motion were presented. By adding the ring cylinders on the spar platform, they found that the added mass and damping has increased which resulted in an increase of the motion period and decrease in platform motion amplitude. However, their rotor was scaled with the Froude method, which means the aerodynamic characteristics may not be captured accurately and thus the platform responses presented may not be precisely represented. The 1:128 OC3-Hywind tank test model has also been used to validate their in-house code and an open-source numerical software – FAST v8. The platform six degrees of freedom and the mooring tensions for one mooring line were presented under both regular and irregular wave with wind load. They suggested that for a coupled wind and wave tank test for floating wind turbines, when Froude scaling method were used, the blade geometry should be designed for a low Reynolds number environment. In sea state 7 (Tp=13.6, Hs=9.14), a strong nonlinearity in surge have been noticed in experiment (Ahn and Shin, 2019). The tank tests of Shin's group had inspired this study, and most of the wave profile in their papers have been included in this study.

The research group in Shanghai Jiaotong University - Duan et al. (2015) have investigated the isolated wind/wave effects and the integrated wave-wind effects on the OC3-Hywind floating systems by conducting the model test (scale factor 1:50). They then (Duan et al., 2016a) conducted a model test on the OC3-Hywind spar type floating platform, using two different rotor systems under both wind and wave load conditions to investigate the floating system response behaviours. The gyroscopic effects from the rotor rotation resulted in yaw decays and strong coupling effect between surge and pitch, and the heave motions were quite independent. In addition, they found that the wind load could reduce platform motions at natural frequencies. The mooring tensions were also measured. Duan et al. (2016b) have conducted another model test for the OC3-Hywind model to check the floating system dynamic responses. The calibration tests included the characterized stiffness of the delta type mooring system and free decay responses. It is found that the wind loads have obvious influence on surge, heave and pitch motions of the spar type floating wind turbine. Similarly, to their previous study, the mooring tensions measured from the experiment were found to be affected by either the wave or wind-wave excited surge/pitch and heave coupling and it was found that the wind loads can have a clear influence on the dynamic responses of the mooring system. It is also found that the aerodynamic loads can somewhat reduce the floating system peak response amplitudes, which could be beneficial for extending the fatigue life of the mooring system.

Tomasicchio et al. (2018) have used a Froude scaled model to conduct tank tests of an OFWT. They presented a very detailed literature review about the experiment on OFWT, and they have pointed out the major difficulties on conducting wave-basin experiments of OFWTs. They had also investigated the hydrodynamic and dynamic behaviour of the platform and the interactions with the mooring system.

It is seen that many experiments have been conducted by researchers in the past decades to investigate the characteristics of spar type OFWT platforms and the scaling ratio ranged

from 1:128 up to 1:10, while the largest model of the OC3-Hywind platform is at 1:30 scale. Most of the studies are focused on the platform motions or the mooring tensions, but there has been little research on the detailed mooring line motion dynamics. The mooring line motion, is coupled with platform motion, and thus can also show the coupling effect with the operating turbines, so it is very important to understand the mooring line motion behaviour. Consequently, in this study, the motions of one of the mooring lines will be investigated in the tank tests. In this paper, the detailed experiment set-up to measure the platform dynamic responses, mooring motions & tensions are presented, and key experiment results will be discussed.

2 Experiment Design

To investigate the OFWT spar platform and its mooring systems hydrodynamics behaviour thoroughly, it is necessary to carry out experimental measurements. This section will give the details in the preparation stage of the experiment been carried out at the Kelvin Hydrodynamics Laboratory (KHL). A brief introduction of the KHL facilities are presented first. The layout of the tank for both spar-only and spar with realistic mooring lines are given. The design and limitations of the experiment are discussed. The parameters scaling, such as the scaling methodology and the scaled model dimensions are given. The set-up of the instrument been used in the experiment are presented in detail.

2.1 Kelvin Hydrodynamics Laboratory

The Kelvin Hydrodynamics Laboratory (KHL), at the University of Strathclyde, has dimensions of 76 m×4.6 m×2.5 m. It is equipped with a variable-water-depth computer-controlled four-flap absorbing wave maker, which can generate both regular and irregular waves over 0.5 m height (subject to the water depth), as shown in Figure 1. At the back of the tank, there has a high quality variable-water-depth sloping beach, with reflection coefficient typically less than 5% over the frequency range of interest. A state-of-the-art, real-time, non-contact infrared motion capture system has been installed in the tank to measure the motions of floating vessels and structures. For this experiment, five motion capture cameras have been installed above the tank. Two at the left side and the other three are above the tank, as shown in Figure 2. To capture the mooring line motions, three underwater cameras have also been installed in the tank.

Figure 1 Four Flap Wave Maker at KHL

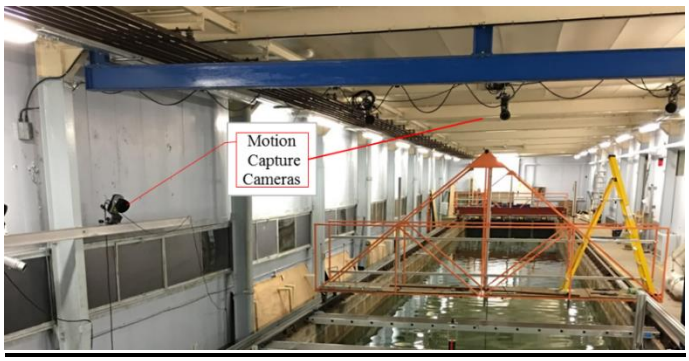

Figure 2 Structure Motion Capture Cameras at KHL

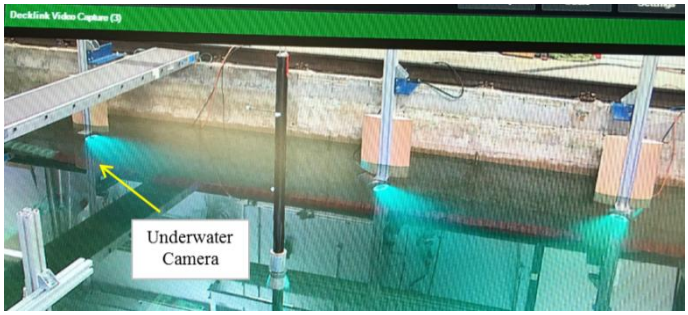

Figure 3 Underwater cameras in the tank

2.2 Brief Model Description

There are many factors that can affect the experiment outcome and need be assured before the start of an experiment, such as the water depth, the scaling factor/methods, the mooring design, the wave frequencies selected, tests running time, the sampling frequency and the effect of using the 2-D flume assumption.

The effect of wind loading is not included in the tank tests reported here, as the intention is to provide a set of baseline data for validation of numerical simulation. Since the focus of this study is on the hydrodynamic response of the spar platform and dynamic behaviour of the mooring lines, and it is expected that wind induced loads have relatively little effect on the wave frequency responses of the platform (Yu et al., 2015), it was decided to focus on the mooring line dynamics under purely hydrodynamic loading as a base case. It would be of interest in the future to carry out further tests with steady or unsteady wind loading which will add further complexity to the system dynamics.

2.2.1 Water Depth

The water depth in the tank is chosen as 2.0 m, according to the wave conditions during tests, and the wave maker capability. The beach at the back of the tank has been adjusted in height to maximise absorption over the frequency range of interest, as some long duration runs of waves will be generated during the test.

2.2.2 Scaling Methods and Factor

It is important to scale the model and environmental conditions as reliably as possible, such that the result is meaningful and helpful for real design and further research. Both Reynolds number and Froude number are important non-dimensional scaling parameters for fluids. However, Reynolds number is normally used to scale flows around models in unbounded fluids dominated by viscous effects, which is not the case in the present experiment. Froude number describes the relationship between inertial and gravitational forces. It forms the basis

of a scaling method for physical experiments in water waves in which viscous forces are of lesser importance, as maintaining Froude similarity (i.e. keeping the correct model scale Froude number) will scale the waves and the dynamic behaviour of structures correctly (Chakrabarti, 1994). Thus, Froude scaling is used to conduct the experiment campaign in this study.

For a scaling factor - λ, to satisfy both the geometric similarity and the Froude similarity, an established scaling factor table for OFWT model test is presented in Table 1.

Table 1 Established Scaling Factors for OFWT model test (Rolo, 2014)

Parameter	Unit	Scale Factor
Length (e.g. displacement, wave height and length)	L	λ
Area	L^2	λ^2
Volume	L^3	λ^3
Density	M/L^3	1
Mass	M	λ^3
Time (e.g. wave period)	T	$\lambda^{0.5}$
Frequency (e.g. rotor rotational speed)	T^{-1}	$\lambda^{-0.5}$
Velocity (e.g. wind speed)	LT^{-1}	$\lambda^{0.5}$
Acceleration	LT^{-2}	1
Force	MLT^{-2}	λ^3
Moment (e.g. rotor torque)	ML^2T^{-2}	λ^4
Power	ML^2T^{-3}	$\lambda^{3.5}$
Stress	$ML^{-1}T^{-2}$	λ
Mass moment of inertia	ML^2	λ^5
Area moment of inertia	L^4	λ^4

Considering the 2.0 m water depth at the KHL, the scaling factor has been chosen as 1:74 (Santos-Herrán, 2016), which gives the spar platform model draft at 1.621 m. For the Hywind Scotland Pilot Park, the water depth on site is 105m and the draft of the spar platform is 78 m (Equinor, 2019). Its ratio between water depth and platform draft is about 0.743 and 0.810 in this study, which shows the scaling factor -- 1:74 is reasonable.

2.2.3 Mooring Design

Two sets of tests were carried out in this study. In the first the spar was moored with “soft” elastic mooring lines; in the second set of tests, realistic mooring lines were utilised. Figure 4 (a) presents the layout of the tank for spar-only tests. The soft elastic lines are used to prevent the model from drifting down wave and the stiffness is chosen to minimise the interaction of mooring lines with the system dynamics.

For spar with realistic mooring lines tests, compared with the OC3-Hywind model, the water depth in full scale has decreased from 320 m to 148 m. Although the platform draft can work well in this depth, the mooring length and anchor position need to be adjusted. This has been done by using the Principle of Similarity based on the geometry, and the static balance has been checked in numerical model before conducting experiment, which shows the current design is reasonable. For the mooring stiffness, it has been scaled (using the scaling factor) down from the OC3-Hywind mooring system. As the transverse fluid forces on the mooring lines are dominated by viscous effects, ideally the Reynolds scaling method should be used.

However, since this study focuses on the platform dynamic responses, which are dominated by Froude scaling it is accepted that the tests could not capture all aspects of the mooring responses correctly. The mooring line length, diameters and weight distribution are therefore chosen to be close to the target values based on Froude scaling.

Due to the width limitation of the tank, the mooring configuration has been slightly re-designed from the original layout. For the NREL OC3-Hywind model, the angle between each mooring line is 120°. In this tank test, to make the mooring system as similar as possible to the NREL model, Mooring Line 1, as shown in Figure 4 (b), is aligned with the wave direction, i.e., positive of X-axis but the angle between the other two mooring lines is reduced to 60°, with the lines placed symmetrically about the centreline of the tank.

2.2.4 Wave Frequencies

The wave frequencies were chosen to lie in the range from 0.253 Hz to 1.229 Hz (at model scale), which covers the predicted platform heave and pitch natural frequencies, and also covers the range over which the wave maker (and the beach absorption) work efficiently.

2.2.5 Test Running Time and Sampling Rate

For free decay tests, the test duration varies substantially with the degree of freedom, since for example the heave motion is damped much more slowly than the yaw motion. In most cases, at least 10 to 15 motion cycles have been recorded and usually 10 motion cycles were used for the natural frequency and damping ratio calculations (only about 5 cycles for yaw motion).

For regular wave tests, the recorded running time is about 120 s at tank test scale, which is enough for the platform to respond for at least 10 stable periodic motion cycles. The data used for the analysis is started when the platform motion becomes stable, as it can take about 10 s for the generated wave to reach the model. In addition, when the wave has just reached the model, it can cause some transient splash effects and the first few cycles of platform motion show transient response under regular waves.

For irregular wave tests, a 3 hour duration at full scale is typically adopted to model a full storm in offshore engineering tests as recommended by the ITTC (Stansberg et al., 2002). In the present tests, the test duration was chosen to be 1200 s at model scale – which corresponds to about 2 hr 40 mins (9600 s) in full scale, which is hence considered reasonable to capture the key phenomena associated with the sea states encountered in a real sea site.

The sampling frequency is set at 137 Hz during the tank tests, which means the highest recorded frequency which can be identified without aliasing is 68.5 Hz (the Nyquist frequency)(Landau, 1967). The choice of a prime number reduces the risk of harmonics, while the value chosen is large enough to cover all the possible wave frequencies. A further consideration is possible noise from the AC mains electricity with frequency 50 Hz in UK. Thus, if the mains noise (could from the data recording and transferring equipment) appears during the data recording process, it can be identified from the spectrum analysis and can be eliminated from the predicted response spectrum of the floating systems. In this study, mains frequency noise was not found to be an issue through all the tank tests.

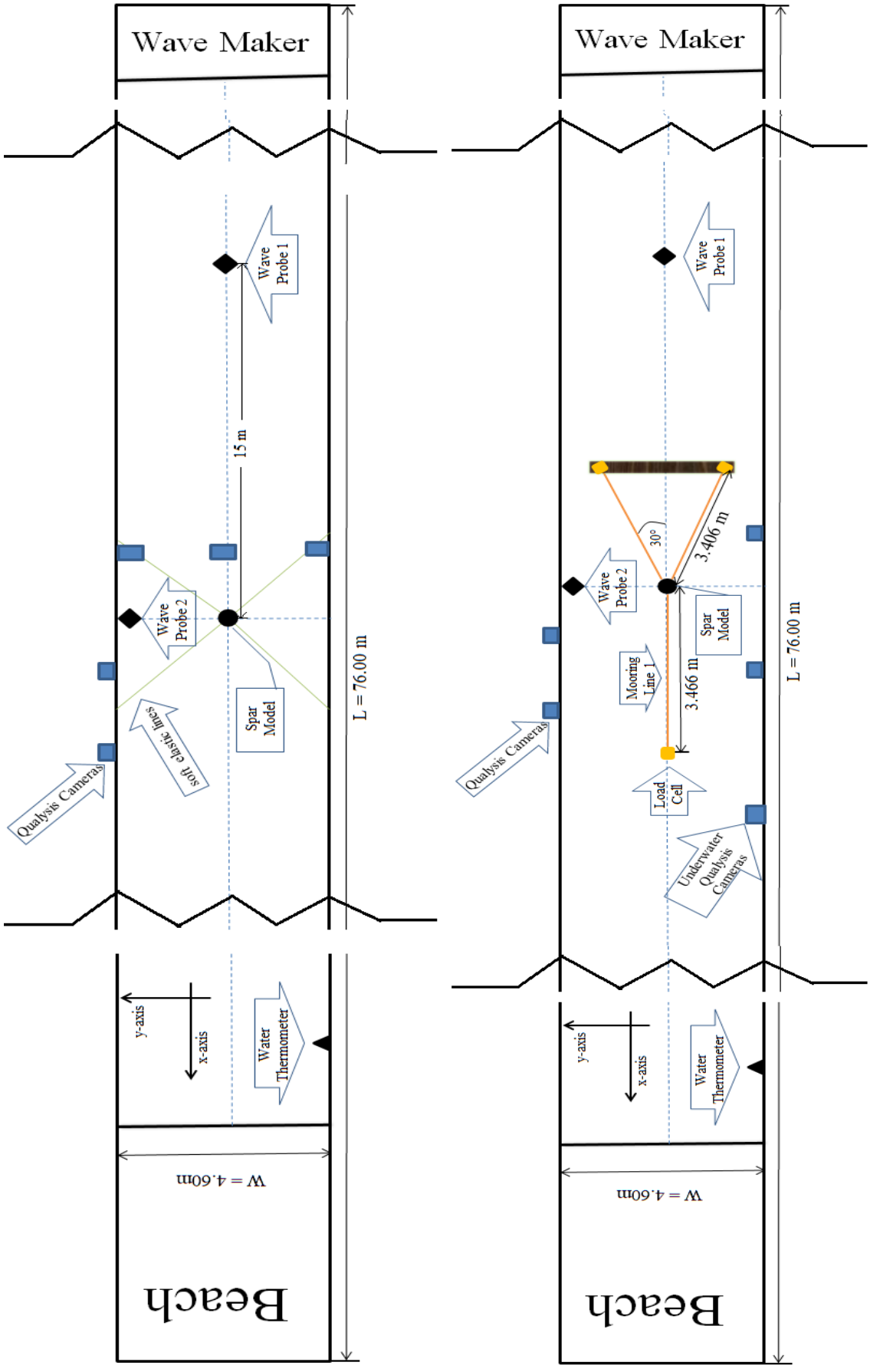

(a) Spar-only (b) Spar with realistic mooring lines

Figure 4 Tank layout

During the regular wave tests with realistic moorings, a non-linear snatching behaviour was discovered at some frequencies in the floating systems. In this phenomenon, one mooring line becomes very tight and then goes slack within a very short time period. In order to confirm that the sampling rate was adequate to capture this phenomenon, the time histories of the mooring tension data have been checked, as shown in Figure 5. There are about 160 points recorded in the 10 seconds during the period in which the snatching is happening. Examination of the curve peak in detail shows that there are about 5 points defining the peak; hence, it is unlikely any higher points have been missed. Hence, it can be seen that the sampling frequency at 137 Hz is a reasonable recording frequency capturing the featured changes in the floating system.

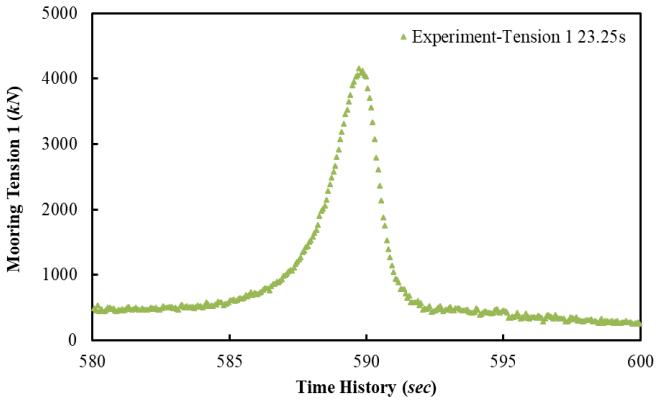

Figure 5 Recorded time steps of mooring tension in experiment

2.2.6 2-D Flume

The wave generated at KHL is considered as a long-crested, which means that there are no directional waves as in realistic open seas. However, compared with the platform motion in real sea site, the motion can be larger in the tank tests than would be the case in the real sea, as the wave energy are all in one direction, instead of spreading to other directions. The results may be seen as a limiting case of zero spreading, and will be used later to compare with the numerical simulations, where the 2-D flume assumption is also employed.

2.2.7 Blockage and Wall Effects

When conducting the tank tests, *"the model should be small enough to avoid noticeable effects of restricted water in the towing tank"(Zürcher, 2016).* Thus, the blockage and wall effects of the tank, due to the radiated and diffracted waves should be considered. The blockage means the effects of finite width due to tank walls on the flow around a body and also the wall effect on reflected waves. In this study, the blockage ratio, i.e. the ratio between the model's cross sectional area and the cross-section area of the tank is 2.24%, which is very small.

In addition, as shown in the heave free decay test figures (Figure 16 and Figure 18), no motions due to the reflections of radiated waves have been observed. Thus, the blockage and wall effects are neglected in this tank test study.

2.2.8 Brief Test Description

A spar-only model and a spar with three scaled realistic mooring lines will both be tested in free decay, a range of regular waves and four sea states. A simplified tower has been installed upon the spar platform in order to allow correct ballasting. The tank tests will involve no

wind flow. The spar model is placed at the middle of the tank both longitudinally and transversely and a wave probe has been placed centrally between the spar model and the wave maker, as shown in Figure 4.

For spar-only tests, four very soft elastic moorings were applied to the platform to keep it on station. The stiffness of the lines are chosen so that they do not affect the first order (wave-frequency) motions of the platform.

For the test of the spar with scaled realistic mooring lines, a frame was installed at the bottom of the tank to attach the load cell and the mooring lines. Through all the tests, the spar motions in six degrees of freedom were measured. The three mooring line tensions and the motions of Mooring Line 1 (which is the mooring line downstream of the wave maker aligned with the X-axis) will be recorded as well.

2.3 Tank Test Model's Pitch/Roll Inertia

Since the spar platform is a perfect axis-symmetric cylinder, the pitch and roll inertia can be assumed the same.

The model is weighed to determine the mass. Then the CG is measured by placing the model on a knife-edge, adjusting its position until the model reached a balance position and then measuring the distance from the platform base to that point, as shown in Figure 6. Finally, the whole system pitch/roll inertia about its CG is measured by conducting a Bifilar Suspension test. In this test, the model is suspended on two wires with the CG of the structure located at the mid position of the wires, as shown in Figure 7. The model is then perturbed around a vertical axis, and the natural period is measured, allowing calculation of the moment of inertia.

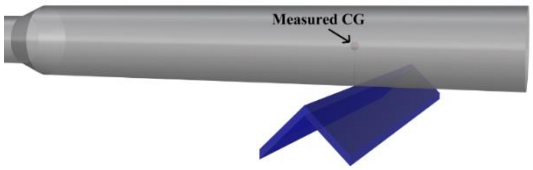

Figure 6 Measure the CG of the whole model

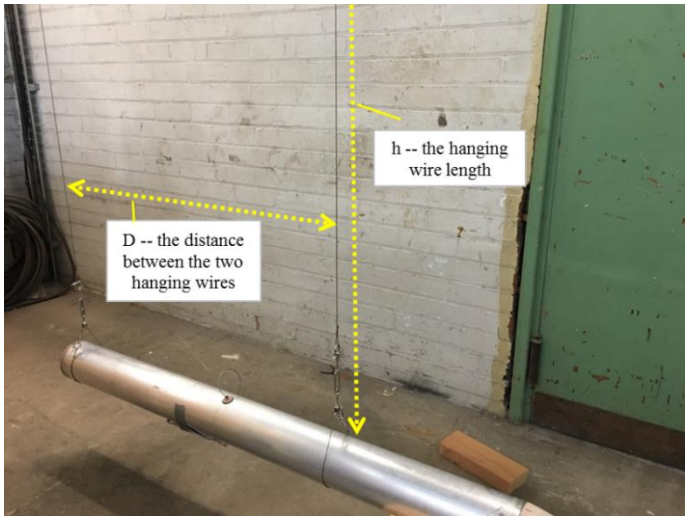

Figure 7 Conducting the Bifilar Suspension test

In this test, the measured D = 0.960 m and h = 4.816 m. Three 10 cycles of the harmonic motion are measured as t_1 = 63.030s, t_2 = 62.670s and t_3 = 62.990s. Thus the pitch/roll inertia of the whole structure will be I = 9.303 kgm^2. The pitch/roll inertia of the NREL model after scaling is I_{NREL} = 8.883 kgm^2. Thus, the difference between the NREL model and the designed tank test model of the whole structure pitch/roll inertia is less than 5%, which means the ballast arrangement of the tank test model is considered acceptable.

2.4 Equivalent Mooring Line Extensional Stiffness

The wire (Figure 8) been used in the experiment to represent realistic mooring line is the code number 603.000.018 from the TecniCable company (Tecni-Cable, 2016). Its E is 116,739 N/mm^2 (1.16739*10^{-5} N/m^2) and the diameter is 1.8mm.

$$\text{equivalent mooring line extensional stiffness} = E \times a \tag{1}$$

where a is the equivalent cross sectional area is about 55% of the whole area. I.e. a = 55%$\times$ $\pi \times (1.8/2)^2$ = 1.4 mm^2. Thus, the equivalent mooring line extensional stiffness is 163,268 N/m of the tank test model.

Figure 8 Schematic plot of the mooring line's cross sectional area

2.5 Tank Test Model Parameters

To keep the same draft with the OC3-Hywind model, the platform mass need to be re-calculated, instead of simply scaled down, to account for the use of fresh water in the tank tests rather than seawater. Then, according to Table 1, the parameters of tank test model and full scale model, compared with full scale NREL OC3-Hywind model, are shown in Table 2. It is clear that the geometric parameters of platform are well matched with the designed model (the NREL OC3-Hywind model). For the mooring lines, the diameter scaled up from the tank test model matches well with the NREL full scale model, while the equivalent mooring line weight is slightly lighter than the target value – about 8%. A significant difference between the target value and the model is noticed in the equivalent mooring line extensional stiffness, due to it is very hard to find the exact same properties of the small scale wires. However, the tank test model stiffness was adopted in the numerical model in this study, so the results from the two approaches should be comparable. Figure 9 shows the geometry scope of the tank test model.

Table 2 Tank test model properties and parameters

Final Model Properties	Tank Test Model	Full scale Model	NREL full scale model
Water Depth (*m*)	2.0	148.0	320.0
Depth to Platform Base Below SWL (Total Draft) (*m*)	1.6	120.0	120.0
Depth to Top of Taper Below SWL (*m*)	0.054	4.0	4.0
Depth to Bottom of Taper Below SWL (*m*)	0.162	12.0	12.0
Platform Diameter Above Taper (*m*)	0.088	6.5	6.5
Platform Diameter Below Taper (*m*)	0.127	9.4	9.4
Platform Mass, Including Ballast (*kg*)	18.5	7.5E+06	7.5E+06
CM Location of the Whole Structure Below SWL Along Platform Centreline (*m*)	1.1	80.7	79.9
Pitch/Roll Inertia of the Whole Structure about CG ($kg \times m^2$)	9.3	2.1E+10	2.0E+10
Number of Mooring Lines	3	3	3
Angle Between Adjacent Lines (*deg*)	0/150/210	0/150/210	120
Depth to Fairleads Below SWL (*m*)	0.9	70.1	70.0
Unstretched Mooring Line Length (*m*)	3.6	263.1	902.2
Mooring Line Diameter (*m*)	0.002	0.1	0.1
Equivalent Mooring Line Weight (see section 2.4) (*kg/m*)	0.013	71.2	77.7
Equivalent Mooring Line Extensional Stiffness (*N/m*)	1.6E+05	8.9E+08	3.8E+08
Radius to Anchors from Platform Centreline (*m*)	3.5/ 3.4	256.4/252.1	853.9
Anchor Depth (*m*)	1.9/ 1.8	139.9/135.3	316.7
Radius to Fairleads from Platform Centreline (*m*)	0.074	5.5	5.2
Tower Height (*m*)	1.2	89.5	90.0
Tower Total Mass (*kg*)	1.3	5.2E+05	6.0E+05

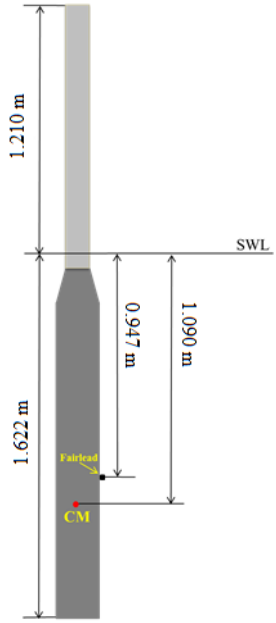

Figure 9 Tank scale model

2.6 Qualysis System and the Cameras, and the Load Cells

The platform 6 DOF motions – surge, sway, heave, roll, pitch and yaw, and the underwater mooring line motions (X, Y and Z) were recorded using a Qualysis motion capture system. The cameras (as shown in Figure 2 & Figure 3) detect the model's motion by tracking the movement of the reflective targets, which have been installed on the model. To make sure all 6 DOF motions of the platform can be captured, four reflective targets have been installed on the tower part of the model. The weight of these reflective targets has been accounted for in the tower model ballast. Figure 10 presents the arrangement of these reflective targets on the tower. For the underwater mooring line motion capturing, seven reflective targets were used, as shown in Figure 11. The density of each reflection target is 991.260 kg/m^3, which is very near the fresh water density, so they are considered neutrally buoyant and the flow effect been generated by these reflection targets have been neglected in this research. The first reflective target – named as Rear in the Qualysis software, has been installed on the load cell for Mooring Line 1 (as shown in Figure 12). This rear reflective target is being used as a reference point, since it is "anchored" and should not move during all the tests, which can help in generating a reference point for the Qualysis system. Another reflective target has been attached on the spar platform at the fairlead position of Mooring Line 1; this target's motion allows comparison with the platform's motion measured from the above-water system to double check if the underwater camera system is correctly synchronised with the above water system. The other five reflective targets are attached along Mooring Line 1. Details of these targets position on Mooring Line 1 are presented in Table 3. The uneven arrangement of the reflection targets can help to reduce the possibility of mis-identification of the targets by the Qualysis system.

The three mooring line tensions are measured by underwater load cells. These three load cells were placed at the anchor points on the bottom of the tank, rather than at the fairlead position. The maximum tension at the anchor points will typically be less than at the fairlead; however determining the maximum tension was not the focus in the context of the present study. Locating load cells on the model leads to concerns regarding the interference with the flow around the model, the effect of the cabling on the platform dynamics, and the instantaneous angles of the devices as the platform moves; so it was considered that the

effect of these issues could be reduced by measuring the tensions far from the model on the tank floor. The load cells measure loads from 0 to 100 N very accurately, which lies in the range of the expected measured mooring tensions. The calibration results show that the error is less than 1%. The height of the load cells has been considered as this will affect the mooring line anchorage height and position, details of the anchor depth have been shown in Table 2. The depth of the anchors are slightly different between the rear anchor and the other two, due to the different methods used to locate the anchors. This difference is only around 3% and it is considered reasonable to ignore this effect.

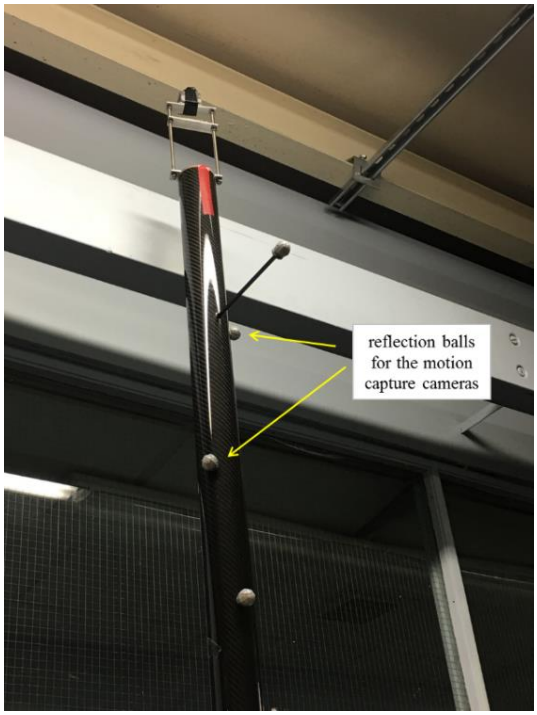

Figure 10 Qualysis reflection balls arrangement on the tower model

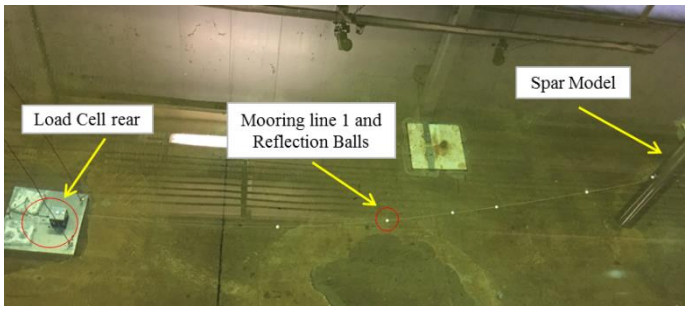

Figure 11 Mooring line with underwater reflection balls in the tank

Table 3 Reflection balls position on the Mooring Line 1

Arc Length	Model Scale	Full Scale
Reflection Ball Number	(*mm*)	(*m*)
1	2321.150	172.007
2	1638.460	121.417
3	1228.850	91.063
4	955.770	70.827
5	409.620	30.354
Spar (at fairlead)	0	0

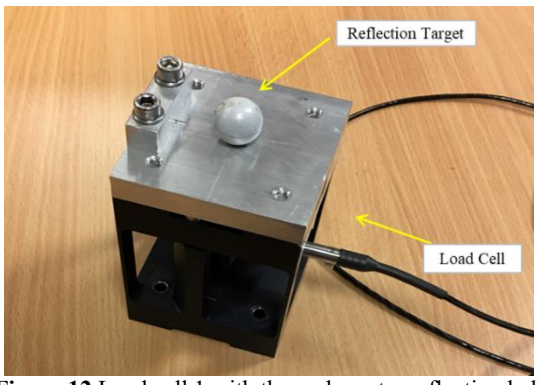

Figure 12 Load cell 1 with the underwater reflection ball

2.7 Wave Probes

Two wave probes are being applied in the tank to measure the wave passing the model. One resistance-type probe was installed upstream of the model – to measure the (regular) wave height passing through the model without any diffraction effects from the model. A second ultrasonic probe is installed adjacent to the model and near the wall of the tank to allow the phase of motions relative to the wave surface to be established. The irregular waves used were calibrated prior to model installation by measured the water surface elevation at the model position using the same wavemaker time history, and adjusting the significant wave height to meet the target values The wave height of the regular waves is 2.52m at full scale; frequencies ranged from 0.029 Hz to 0.143 Hz. This range was chosen to covers the natural frequencies of the platform DOFs, apart from surge, which is too small to be checked at model scale. The irregular wave parameters are shown in Table 4; it can be seen that the measured significant wave heights are matching quite well with the target significant wave heights in each sea state (Shin, 2011), which shows satisfactory calibration of the sea states.

Figure 13 and Figure 14 show calibrated results for Sea State 1. The fitted curve shows that it is generally fits the Rayleigh distribution, although there are some unexpected points at the peak. The wave spectrum shows close match between the measured wave from Wave Probe 1 (located where the model was installed) and the calculated target wave spectrum. The target wave spectrum is calculated by using the JONSWAP equation and the shape parameter is 3.3.

Table 4 Wave parameters for the four sea states

	Target Full Scale		Target Tank Scale		Measured Tank Scale	
Sea State	Tp (s)	Hs (m)	Tp (s)	Hs (m)	Tp (s)	Hs (m)
1	9.700	3.660	1.128	0.050	1.093	0.050
2	11.300	5.490	1.314	0.074	1.302	0.075
3	13.600	9.140	1.581	0.124	1.569	0.124
4	17.000	15.240	1.976	0.206	1.883	0.205

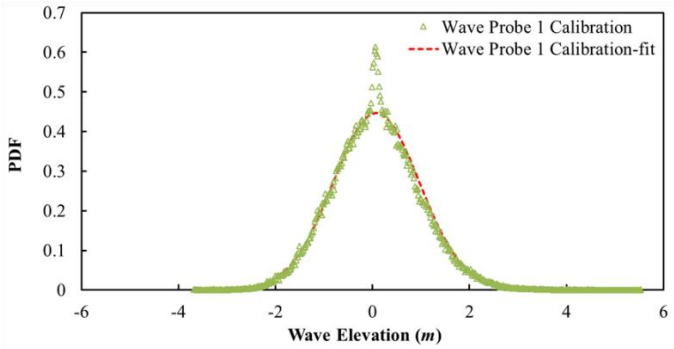

Figure 13 Wave amplitude distribution, measured by Wave Probe 1 for Sea State 1 (full scale)

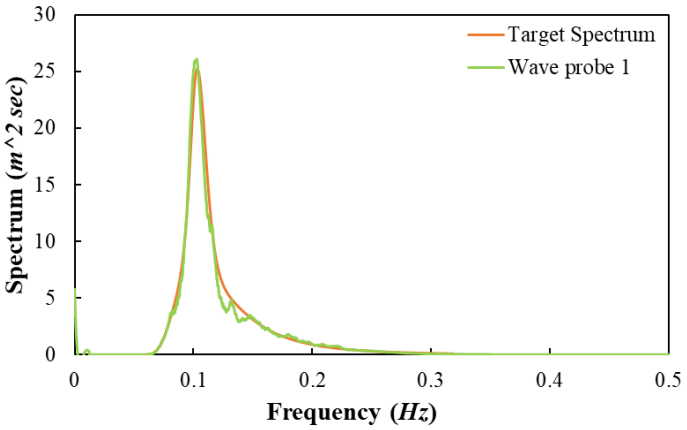

Figure 14 Wave spectrum, measured by Wave Probe 1 compared with the target wave spectrum, for Sea State 1 (full scale)

2.8 Mooring Set-up

Before the tank test start, the mooring's pre-tension of the three mooring lines have been measured, as shown in Table 5. As shown in the table, the tension on Mooring Line 2 and 3 are slightly different. This is assumed to be caused by the small magnitude of the forces and small inaccuracies in locating the model in the tank. It was found to be very hard to adjust the position of the anchor frame on the bottom of the tank extremely precisely, and the measured load on the transducers were found to be very sensitive to small movements. Thus, the pre-tension shown in Table 5 were the best results achievable at the tank.

Table 5 Pre-tensions of the three mooring lines

	Experiment test scale (*N*)	Experiment full scale (*kN*)
Tension 1	0.938	380.041
Tension 2	0.655	265.405
Tension 3	0.732	296.567

To ensure that the platform was not leaking and to double check that the anchor position does not change during the tests, a repeatable static check was conducted both before and after all wave tests. When the water surface and the model are still, three masses – 100g, 200g, 300g were added on top of the model tower. The platform positions and mooring tensions were then recorded during this process to check how the tension changes. During this process, the X-position of the model (along the tank) changes due to the asymmetry of the mooring system. The still-water platform Z-position does not change between the start and the end of experiment campaign, which confirms that the model did not take on any water. During the free decay tests, the regular wave tests, and the first three irregular wave

tests, the still-water X position did not change between the value before and after each test. However, after the last irregular wave tests – Sea State 4, it was discovered that the platform X-position has changed by about 2.4 mm (0.178 m in full scale) which indicates that the anchor position might have changed during the test. After checking all the tank test data for the anchor position, the results show that the anchor position for Mooring Line 1 changed by about 50 mm (3.7 m in full scale) in the very last tank test-which was Sea State 4 (the largest sea-state). However, it was confirmed that for all the free decay tests, regular waves and Sea State 1 to 3, the anchor position did not change and therefore the test results obtained were unaffected by this. It may be assumed that the anchor position changed during Sea State 4 due to the greater loads caused by the larger waves and this group of data is not used in this study.

The absolute value of three mooring tensions showed a difference between the results before and after the tank tests. This is assumed to be due to the amplifier zero value drifting during the tank tests. However, the tension values were seen to reduce linearly with the same gradient before and after the tests. This means that the dynamic changes in mooring tensions in the measured time histories, for example, due to wave loads or platform motions, are still correct. Thus, the recorded data may be corrected with an offset value representing the estimated drift. The baseline tension values are taken from the case measured with no added mass before the experiment started, which was recorded just after the load cell/amplifier system had been calibrated and the model been put into the tank, and the mooring anchors adjusted to match the target values as closely as possible. As the amplifiers may be expected to drift slightly during the tank tests, the zero offset values may be variable. However, if the anchors have not moved, and the model draft has not changed, it is reasonable to assume that the tension will not in fact have varied. Thus, before running each test, when the model is still and balanced, the tensions were modified with an offset value to adjust the measured pre-tension in each test match with the values in Table 5. By adopting this process, the modified data will represent the real tensions on each mooring line. The same process was also conducted when dealing with the mooring tensions in irregular waves.

3 Results and Discussions

3.1 Free Decay Tests

As the main parameters which can affect the platform's dynamic behaviour, the natural frequencies and damping ratios can be obtained by analysis of the free decay test.

3.1.1 Spar-only

As the spar model is a perfect symmetrical cylinder, the pitch and roll, and the surge and sway will be the same. In addition, although there has no realistic scaled mooring line for the spar-only test, four elastic mooring lines have been used to prevent the model drifting away, which are sufficiently soft to make sure that the motion response for the heave and pitch were not affected by the presence of the lines. The sway is not considered as the wave propagates only in one direction – along the X-axis. Therefore, only the surge, heave, pitch and yaw data will be analysed.

It is typically noticed that in the tank test, the damping ratio is more variable than the natural frequencies among each mode of the free decay test, so the free decay tests were repeated 10 times for surge, heave and pitch, and 5 times for yaw. For each mode of motion in each

free decay test, 5-10 cycles are selected. Data is analysed by fitting the response of a linearised spring-mass-damper system to the time histories of the motion as shown in Eq (2):

$$F(t) = A \times e^{-\zeta * \omega_n * t} \times cos\left(\sqrt{1-\zeta^2} \times \omega_n \times t - \varphi\right) + B \qquad (2)$$

where *F(t)* is fitted value after calculation – ideally this should be the same as the experimental data; t is the time history; A is the amplitude of the fitted function; ζ is the damping ratio; ω_n is the undamped natural frequency; φ is the phase angle and B is the offset.

In the case without realistic moorings, the free decay test in surge and yaw is carried out to confirm that the natural frequency is sufficiently far from the values for heave and pitch that the heave and pitch are unaffected by the moorings. Since the soft moorings lead to a very low natural frequency, the surge decays in a small number of cycles; hence only two cycles were selected. Figure 15 shows an example of the surge free decay and its fit curve. The small variations are assumed to relate to the coupling effect from the pitch motions. It can be seen that the surge natural frequencies are far away from both heave and pitch natural frequencies, which suggests that the four station-keeping lines will not affect the heave/pitch natural frequencies.

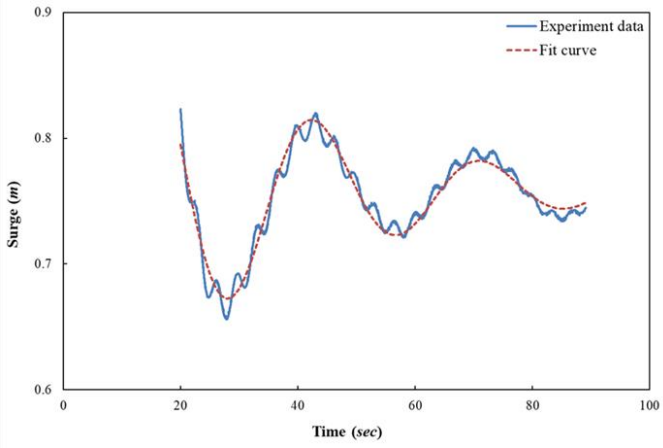

Figure 15 Surge free decay in experiment, spar-only

Figure 16 and Figure 17 show the heave and pitch free decay with the fitting curves, respectively.

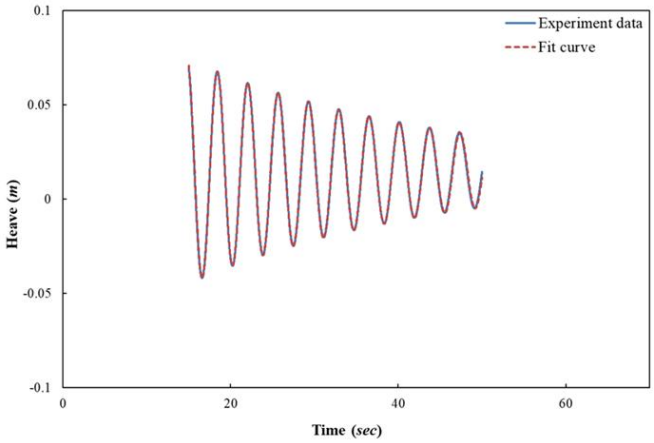

Figure 16 Heave free decay in experiment, spar-only

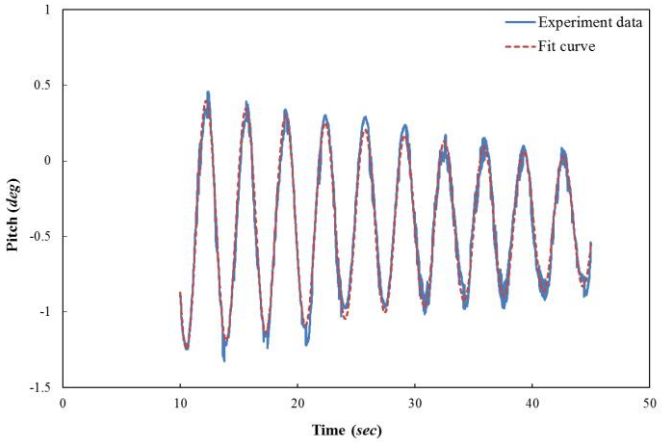

Figure 17 Pitch free decay in experiment, spar-only

Table 6 presents the mean value of measured natural frequencies of the spar-only and the NREL OC3-Hywind model. The pitch and heave natural frequency are matching very well with the NREL model.

Table 7 presents the mean value and the standard deviation (STD) of the damping ratio for heave and pitch. The difference between each of the tests are below 2%. The small value of the STD shows that the damping although may change from each test but it is still stable.

Table 6 Natural frequencies for spar-only compared with the NREL OC3-Hywind (Ramachandran et al., 2013)

	Experiment Scale	Full Scale	NREL
Pitch Frequency (Hz)	0.292	0.034	0.034
Heave Frequency (Hz)	0.275	0.032	0.032

Table 7 Mean value and STD of damping ratio, for spar-only

	Mean Damping Ratio	STD
Heave	0.014	0.004
Pitch	0.023	0.013

3.1.2 Spar with Realistic Mooring Lines

Similar with the process described in Section 3.1.1, Table 8 and Table 9 show the natural frequencies and damping ratios for the spar with realistic mooring lines, compared with the NREL OC3-Hywind model. It can be seen that only the yaw natural frequency does not match with the NREL model. This is assumed to be due to the slightly different mooring configuration from the NREL results and in particular the lack of the delta connection (which can restrict the yaw motion of the spar platform) (Jonkman, 2010) in the present experiment. Compared with the spar-only tank tests, the pitch and heave natural frequencies did not change significantly, but the surge and yaw motion's natural frequencies have increased as expected. The standard deviations of the damping ratio are all very small, and the damping behaviour are much more repeatable than the spar-only tests, especially in surge and yaw and thus the tank tests results would be considered acceptable.

It is noticed that the pitch damping ratio estimated from these tests appeared to reduce from 0.023 to 0.007 when the spar with realistic mooring lines. This result is counter-intuitive, as it can be expected that adding the mooring lines should increase damping. This test was investigated in some depth. A study of the time histories of the motions suggested that while the fit to the data appeared good, the simple approach adopted for conducting the free decay tests in pitch was flawed once the moorings were present. The free decay tests were

conducted both with and without moorings by displacing and then releasing the tower. For the tests without moorings, the resulting motion was close to pure pitch; however, with the realistic moorings present, the restoring force from the moorings contributed to a coupled oscillatory pitch-surge response, which had not been present in tests without the moorings. This combination of response had the result of reducing the apparent rate of decay of the pitch motion in this test. Ideally, a pure angular displacement in pitch would be imposed so that no surge resulted; however, this could be hard to achieve in practice. As discussed later, tests in waves show that the introduction of the realistic mooring lines does reduce the pitch motions compared to the spar only case, reinforcing the conclusion that the pitch damping coefficient estimated from these free decay tests with the mooring lines is not valid.

Table 8 Natural frequencies for spar with realistic mooring lines compared with NREL OC3-Hywind (Ramachandran et al., 2013)

Platform DOFs	Experiment Scale	Full Scale	NREL
Pitch Frequency (*Hz*)	0.292	0.034	0.034
Heave Frequency (*Hz*)	0.275	0.032	0.032
Yaw Frequency (*Hz*)	0.292	0.034	0.121
Surge Frequency (*Hz*)	0.069	0.008	0.008
Roll Frequency (*Hz*)	0.292	0.034	0.034

Table 9 Estimated Mean value and STD of damping ratio for spar with realistic mooring (*Note: this value is regarded as unreliable for reasons discussed in text)

	Mean Damping Ratio	STD
Heave	0.028	0.004
Pitch	0.007*	0.001
Surge	0.017	0.009
Yaw	0.084	0.003
Roll	0.011	0.001

Figure 18 shows the fairlead motion (after removing the offset between the two recording points) compared with the platform heave when conducting the heave free decay test. This shows that the two results match perfectly and thus demonstrates that the underwater Qualysis system data matches the data from the above water system.

For the surge free decay test with the realistic moorings (see Figure 19), the natural frequency is predicted well by the linearized Fit Function, but the plot shows some non-linear damping behaviour only been observed in the surge decays. The rate of decay of the measured data is greater than that for the fitted data, which is typically the case when non-linear viscous damping is affecting the motions. It can thus be concluded that viscous damping has more effect in surge than the other degrees of freedom.

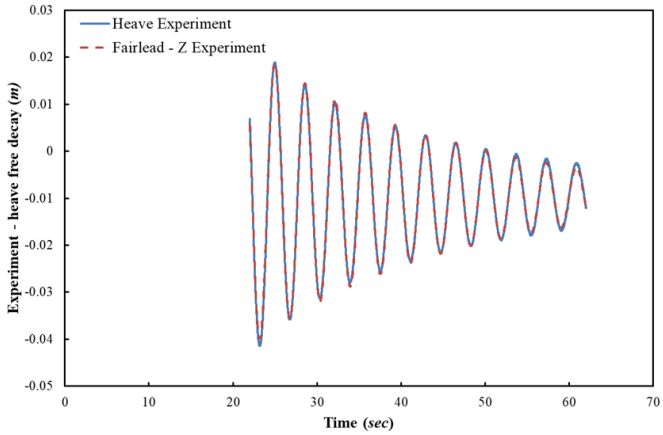

Figure 18 Fairlead-Z and platform heave free decay motion in experiment, spar with realistic mooring lines

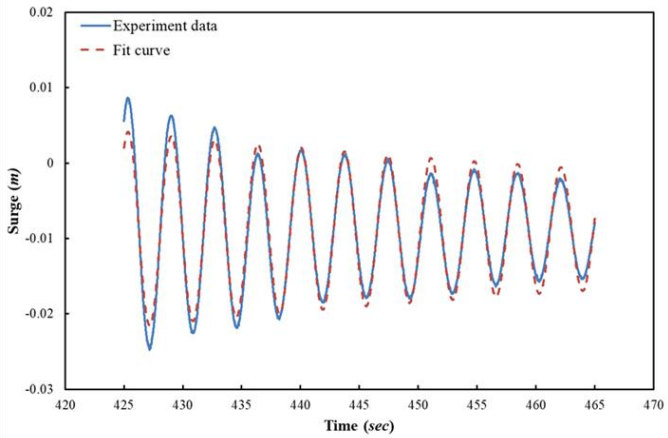

Figure 19 Surge free decay in experiment, spar with realistic mooring lines

3.2 Regular Waves

3.2.1 Repeatability Check

To make sure that the tank test results are reliable, it is necessary to repeat a test more than once. In this experiment, a wave frequency (f = 0.269 Hz for spar-only and f = 0.287 Hz for spar with realistic mooring lines, wave amplitude = 0.017m) has been selected to be applied to the spar platform model three times. In this process, other wave frequencies will be run by the wave maker between each of the repeat test, which can make sure that the results are more accurate. Table 10 presents the results for spar-only and Table 11 presents the results for spar with realistic mooring lines. It can be seen from the table that the experiment results are very stable.

Table 10 Repeatable check test results, spar-only

	Data20	Data22	Data24	MEAN
Input frequency (*Hz*)	0.269	0.269	0.269	0.269
Measured Wave Amplitude (*mm*)	15.2	15.2	15.4	15.3
Heave Amplitude (*mm*)	107.6	106.2	106.4	106.8
Pitch Amplitude (*deg*)	2.84	2.83	2.85	2.84

Table 11 Repeatable check test results, spar with realistic mooring lines

	Data019	Data023	Data025	MEAN
Input frequency (*Hz*)	0.287	0.287	0.287	0.287
Measured Wave Amplitude (*mm*)	16.7	16.7	16.8	16.7
Heave Amplitude (*mm*)	61.2	61.3	61.2	61.2
Pitch Amplitude (*deg*)	4.98	4.96	5.00	4.98
Surge Amplitude (*mm*)	76.5	76.5	77.0	76.7
Yaw Amplitude (*deg*)	1.44	1.41	1.44	1.43

3.2.2 Platform Responses

A range of regular waves has been applied to the platform (both with and without realistic mooring lines) to obtain the platform motion RAOs (response amplitude operator) – which can be used to predict the platform dynamic responses under other wave conditions. As a fully non-dimensional parameter, the definition of the RAO for surge/sway/heave is shown in Eq (3) and for roll/pitch/yaw is shown in Eq (4). The equation to calculate the maximum wave slope shown in Eq (5).

$$RAO\ \ (m/m) = \frac{motion\ amplitude}{wave\ amplitude} \tag{3}$$

$$RAO\ \ (deg/deg) = \frac{motion\ amplitude}{maximum\ wave\ slope} \tag{4}$$

$$maximum\ wave\ slope = \arctan\left(\frac{2 \times \pi \times wave\ amplitude}{wave\ length}\right) \times \frac{180°}{\pi} \tag{5}$$

3.2.2.1 Spar-only

Figure 20 and Figure 21 present the heave and pitch RAO of the spar platform itself, respectively. As shown in the figures, the heave and pitch peak responses are at 0.032 Hz and 0.034 Hz, which are well matched with the natural frequencies measured from the free decay tests. For the heave RAO, the peak value is around 8; this relatively high value is due to the absence of realistic mooring lines and their associated damping for these tests.

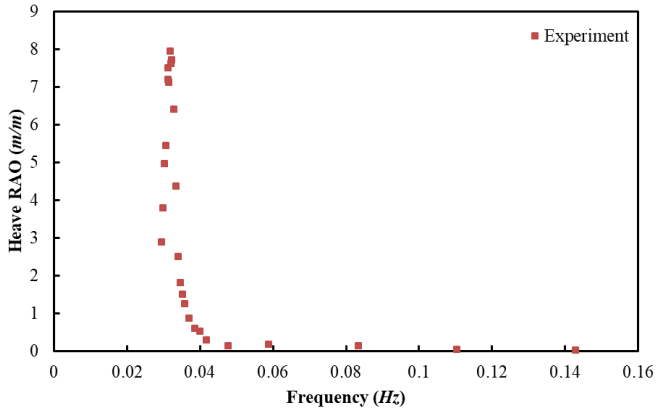

Figure 20 Heave RAO for spar-only (full scale)

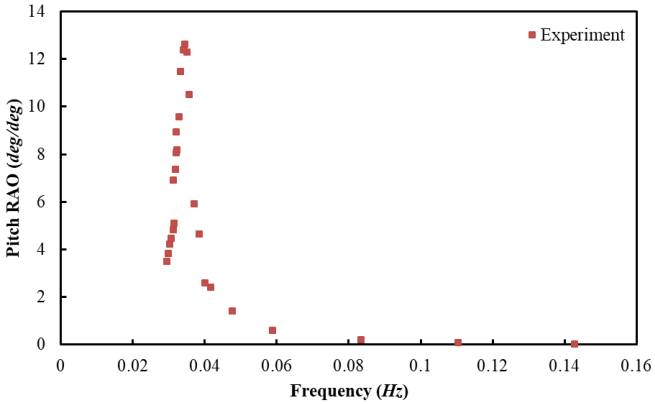

Figure 21 Pitch RAO for spar-only (full scale)

3.2.2.2 Spar with Realistic Mooring Lines RMS

Since non-linear behaviour has been observed at some wave frequencies (see details in Section 3.2.3.1), for the spar with realistic mooring lines, the motion response is not sinusoidal in some cases, and hence the root-mean-square motion (RMS) will be used to represent platform hydrodynamic responses rather than the amplitude of a sinusoidal motion

Due to the wave only propagating towards the positive X-axis and the lack of wind, no sway and roll will be expected and the yaw would be expected to be very small. Thus, only the surge, heave, and pitch RMS values will be presented here, as shown in Figure 22, Figure 23 and Figure 24. The RMS values are calculated from sections of the data when the platform is showing stable periodic motion curves in both experiment and numerical models. The equation is:

$$X_{rms} = \sqrt{\frac{x_1^2 + x_2^2 + \cdots + x_n^2}{n}} \tag{6}$$

As shown in Table 8, the full-scale surge natural frequency obtained from free decay tests is about 0.008 Hz. This is well outside the capability of the wave maker to generate waves and can happen only very rarely in real ocean environment. However, it is seen in Figure 22 that the surge RMS has a peak frequency similar to the peak frequency in pitch. This is presumed to be due to a coupling effect between surge and pitch.

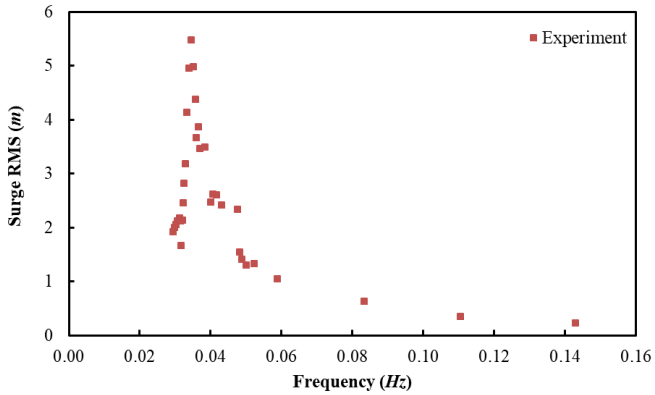

Figure 22 Surge RMS, spar with realistic mooring lines (full scale)

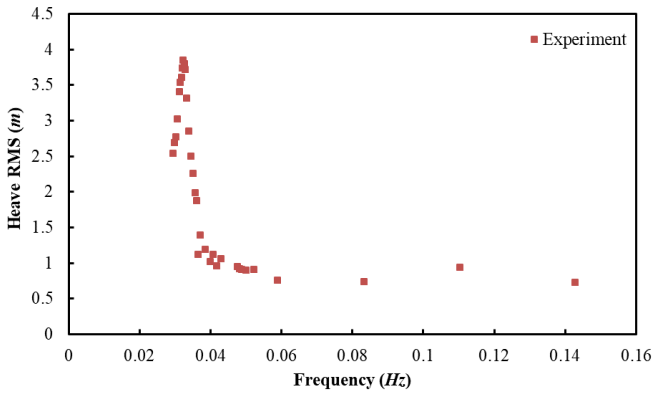

Figure 23 Heave RMS, spar with realistic mooring lines (full scale)

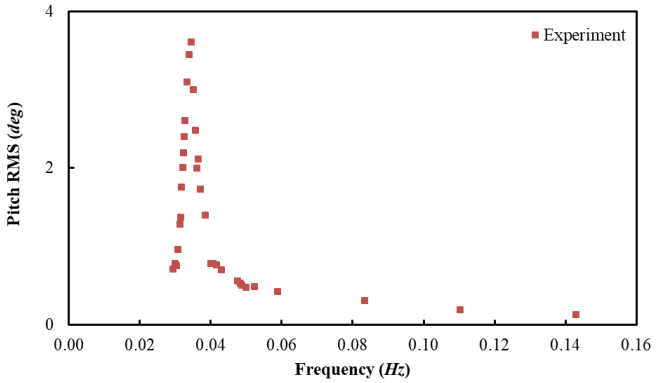

Figure 24 Pitch RMS, spar with realistic mooring lines (full scale)

It can be seen in Figure 23 that the peak heave RMS occurs at a frequency around 0.032 Hz with the RMS value close to 4. This corresponds to a heave amplitude at full-scale of 5.94m, compared to the equivalent value of 10.08m heave amplitude for the spar-only model. This reduction in amplitude is presumed to be caused by the additional damping introduced by the moorings.

The surge/pitch peak RMS occurs at around 0.034 Hz, which is similar to the spar-only tank tests. The peak RMS value of pitch is found to be 3.61 deg, which corresponds to a pitch amplitude of 5.64 deg. This can be compared with the equivalent pitch amplitude of 5.85 deg for the spar only tests, which suggests that the damping from the mooring also reduces the pitch motion. This reduction in pitch motion compared to the spar-only case reinforces the suggestion discussed in Section 3.1.2 that the pitch damping coefficient estimated from the free decay tests for the spar with realistic mooring lines is not accurate, and that the value of the pitch damping coefficient should be larger than that shown in Table 9.

3.2.3 Mooring Line Tensions and Motions

3.2.3.1 Non-linear Snatching Phenomenon

During the experiment, when monitoring the time history output curves, it is interesting to notice at some frequencies a “snatching” like behaviour is seen in which the mooring lines went slack and then suddenly went tight, yielding a substantial effect on platform motions and mooring line tension, as shown in Figure 25. Surprisingly, when the wave frequency was near the platform’s heave/pitch natural frequency, the snatching disappeared and the motion reverted back to quite sinusoidal behaviour, as shown in Figure 26, where the motion

reverts to sinusoidal when the wave frequency co-incides with the heave natural frequency. In Hsu et al. (2017)'s study, they have also found this snatching behaviour, which they names "snap" loads, on a semi-submersible OFWT. However, in their study, only the mooring tensions under extreme environmental loads were investigated.

The snatching could result due to a variety of reasons, such as the drag coefficient of the mooring lines, the mooring line weight or mooring configurations. In addition, increasing the mooring line pre-tension might be able to help to eliminate the snatching. This should be studied in detail in the future, as this non-linear motion in the platform could potentially be quite harmful for the wind turbine, due to the potential for rapid accelerations on top of the tower along the surge direction. However, there is no suggestion of strongly non-linear behaviour in surge at the tower top, as shown in Figure 27.

Figure 28 shows the tension time history in the Mooring Line 1 when the snatching happens. It can be seen that the full-scale mooring tensions can increase dramatically from about 200 kN (the pre-tension) up to more than 4,000 kN, which is very harmful to the mooring lines and could cause the mooring line to fail.

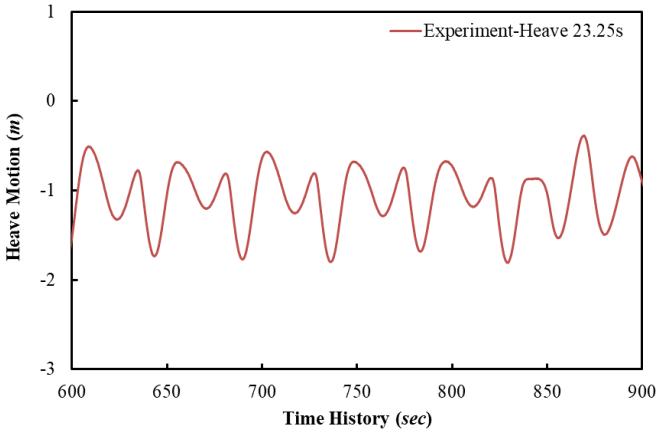

Figure 25 Non-linear heave motion in experiment, 23.25s (full scale)

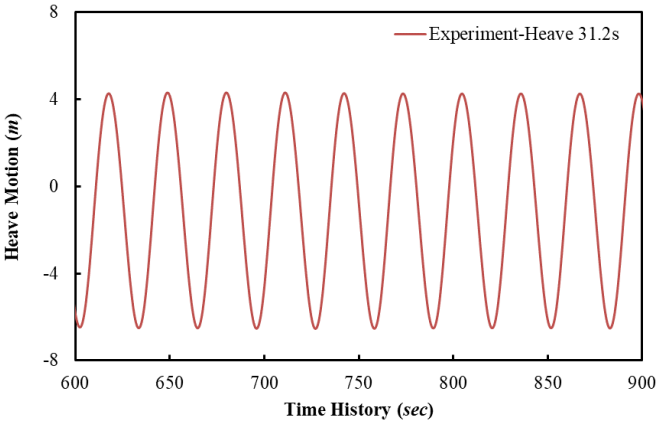

Figure 26 Heave motion in experiment, 31.20s (full scale)

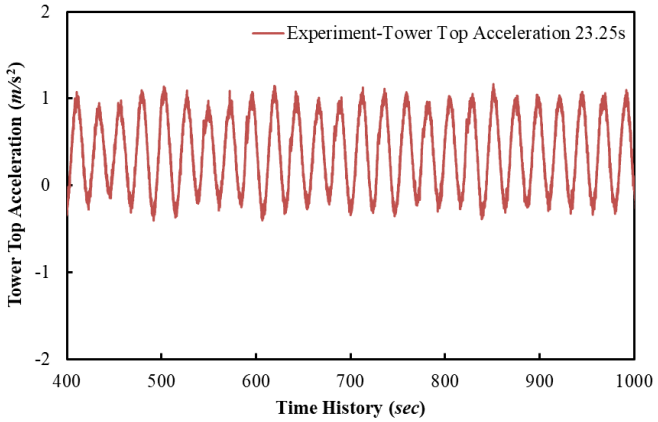

Figure 27 Tower top acceleration in experiment along X-axis, 23.25s (full scale)

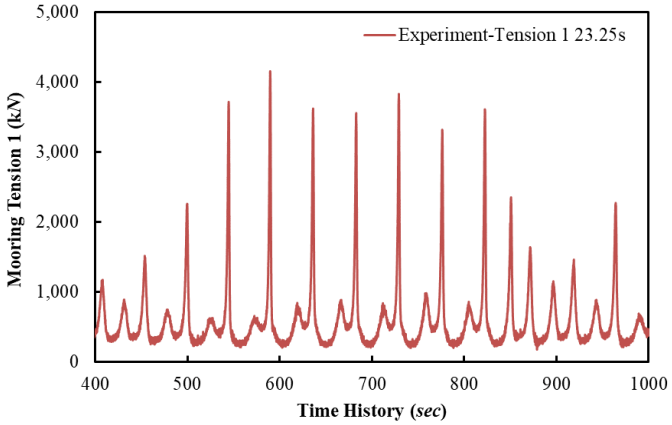

Figure 28 Mooring Tension 1 in experiment, 23.25s (full scale)

3.2.3.2 Mooring Tensions

As the snatching was seen at some regular wave frequencies, thus, as for the platform motions, it is no longer appropriate to present the results as RAOs based on the amplitudes of sinusoidal signals. Instead, the RMS mooring tension values, and the maximum and minimum tensions found will be presented. Figure 29 presents the RMS values of the three mooring line tensions with the various regular wave frequencies. It is seen that the average tension in the experiment could reach up to nearly 1,400 kN on Mooring Line 1 and 1,100 kN on Mooring Line 2 and 3. The small difference between Mooring Line 2 and 3 is due to the adjustment of the anchor frames, as mentioned in Section 2.8.

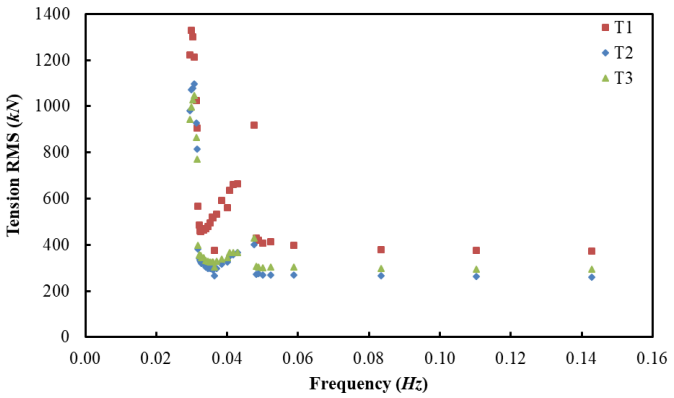

Figure 29 RMS of the mooring tensions (full scale)

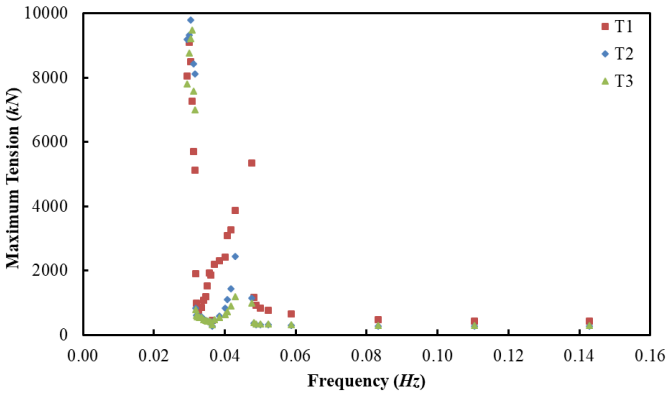

Figure 30 Maximum mooring tensions (full scale)

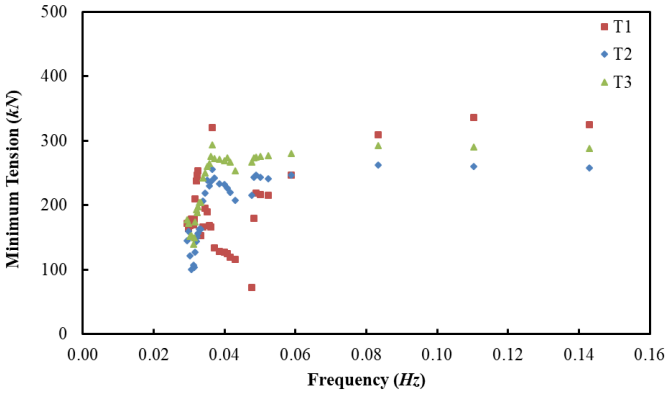

Figure 31 Minimum mooring tensions (full scale)

Figure 30 and Figure 31 present the maximum and the minimum values on each mooring line. For the maximum mooring tensions, it can be seen that the maximum mooring tensions could reach up to 10,000 kN. The suddenly sharp increase in mooring tensions during the snatching clearly has the potential to be very dangerous for the structure and could cause failure in the mooring lines. For the minimum mooring tensions, it is seen that when the snatching happens and the mooring line are close to becoming slack, the minimum tension could be as low as 100 kN for Mooring Line 2 and 3, and about 60 kN for Mooring Line 1.

3.2.3.3 Mooring Motions

The motion of Mooring Line 1 (along with the X-axis) has been recorded by the underwater cameras. The position of the seven reflective targets on Mooring Line 1 is shown in Table 3. In this section, the Mooring Line 1 RMS motion amplitudes along the X-axis and Z-axis (surge and heave) are presented. As the wave only propagates towards the positive X-axis, motions in the y-direction can be ignored. Due to the limit of the length, only the data for the representative Points 1, & 4 and the fairlead are presented, as shown from Figure 32 to Figure 34. The RMS amplitude is calculated in terms of the motion amplitude of each point relative to its initial static position. The experiment results have been converted into full scale before plotting. Along the Z-axis, a peak frequency can be seen which co-incides with the heave natural frequency, while Figure 34(b) shows that the platform fairlead motion, measured by the underwater Qualysis gives almost the same results as the platform heave RMS, measured by the above-water Qualysis system.

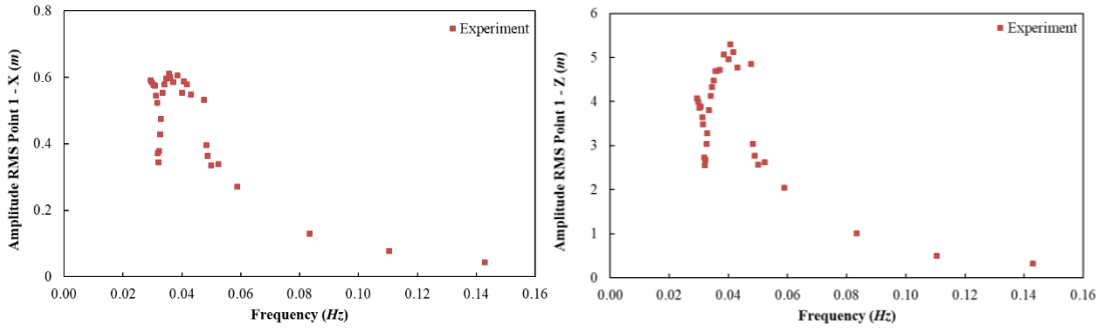

(a) X- axis (b) Z-axis

Figure 32 Amplitude RMS for Point-1 (full scale)

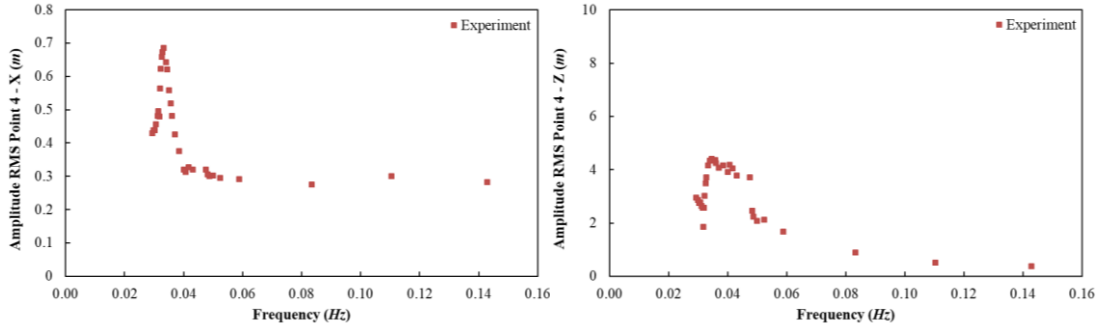

(a) X- axis (b) Z-axis

Figure 33 Amplitude RMS for Point-4 (full scale)

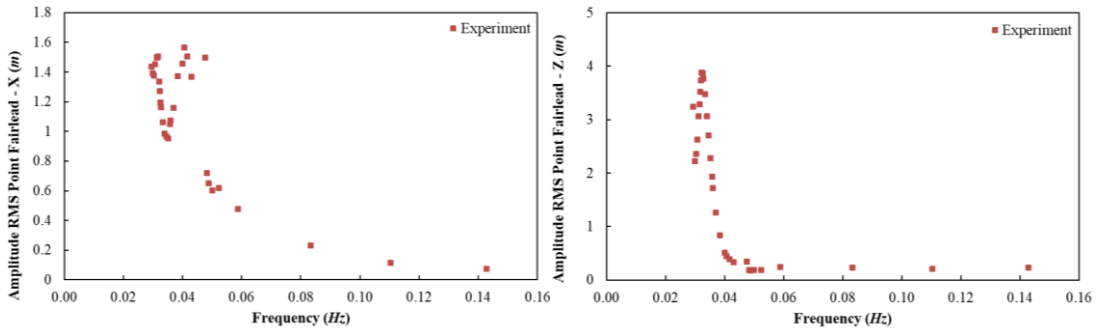

(a) X- axis (b) Z-axis

Figure 34 Amplitude RMS for point at the spar Fairlead position (full scale)

3.2.4 Linearity Test

Linearity tests have been conducted for both heave and pitch, at their peak RAO frequencies. The purpose of the linearity test is to check how linear is the experimental results. A range of wave amplitude from 0.004 m to 0.018 m has been applied to the spar model. The wave frequencies are at the peak RAO frequency of heave and pitch, respectively. With the linear increasing of the wave amplitude, at the set wave frequency, the resulted platform RAO is expected to decrease which is due to the increasing of viscous damping. Figure 35 and Figure 36. present the heave/pitch linearity tank test results for spar-only. Since the snatching has disappeared when the wave frequency nears the platform heave/pitch motion natural frequency, as discussed in Section 3.2.3.1. Thus, the platform heave/pitch time history show a sinusoidal curve in this part and the RAO can be found in a meaningful manner. Figure 37 and Figure 38presents the heave/pitch linearity tank test results of the spar with realistic mooring lines, both of the heave and pitch RAO decreasing with the increasing wave height, as expected.

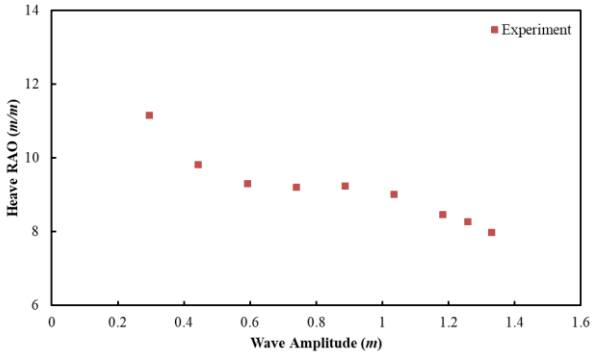

Figure 35 Heave linearity test, spar-only (full scale)

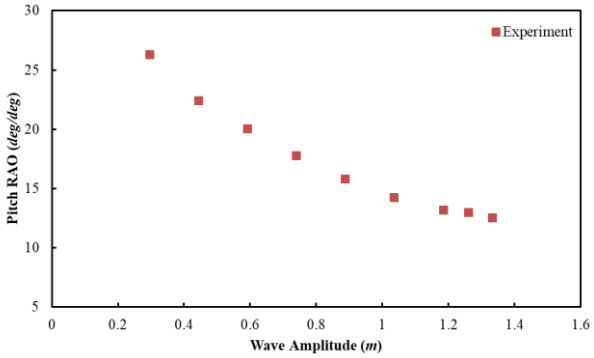

Figure 36 Pitch linearity test, spar-only (full scale)

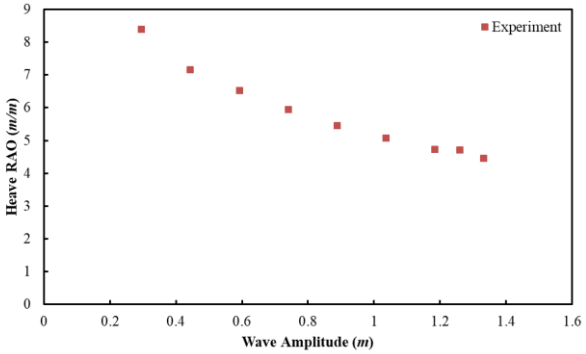

Figure 37 Heave linearity test, spar with realistic mooring lines (full scale)

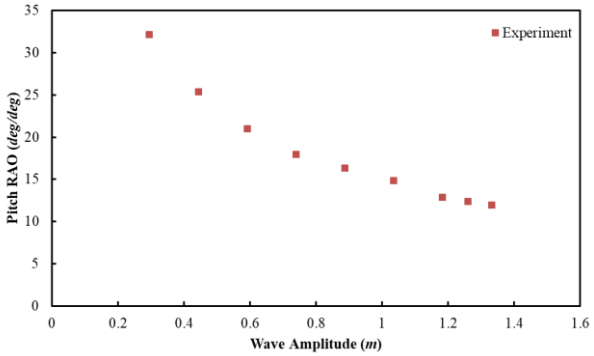

Figure 38 Pitch linearity test, spar with realistic mooring lines (full scale)

3.3 Irregular Waves

3.3.1 Platform Motions Probability Density Function (PDF) and Spectrum

The platform responses (both with and without mooring lines) under the four sea states (Table 4) are been tested. Selected sea state results are presented here.

3.3.1.1 Spar-Only

Due to the lack of realistic moorings, only the heave and pitch motion's PDF and motion spectrum are presented. The experimental measured data have been calculated into full scale before calculating its PDF and spectrum. For experimental heave spectrum, as presented in Figure 40, the first and major peak is happening at its natural frequency and the other peak is at the peak wave frequency – around 0.070 Hz. For the pitch motion spectrum, the major peak is at the peak wave frequency, while a very small peak is seen at the pitch natural frequency. Figure 39 and Figure 41 show the heave and pitch motion amplitude are mainly within 1m and 2°, in Sea State 3.

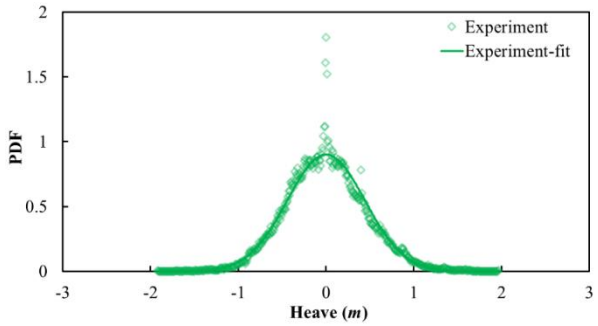

Figure 39 Heave motion amplitude PDF for Sea State 3, spar-only (full scale)

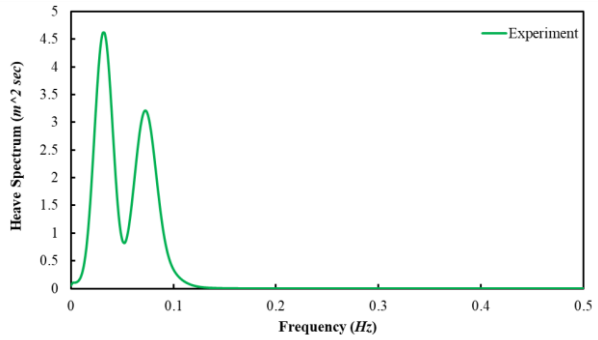

Figure 40 Heave motion spectrum for Sea State 3, spar-only (full scale)

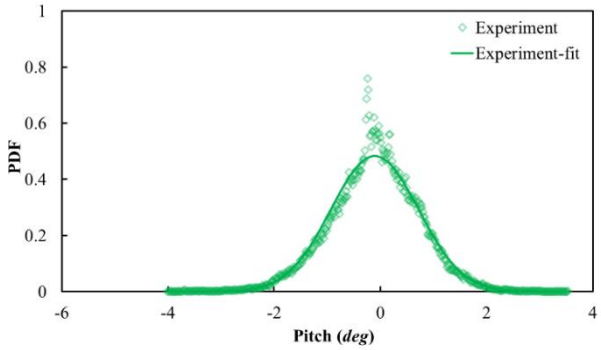

Figure 41 Pitch motion amplitude PDF for Sea State 3, spar-only (full scale)

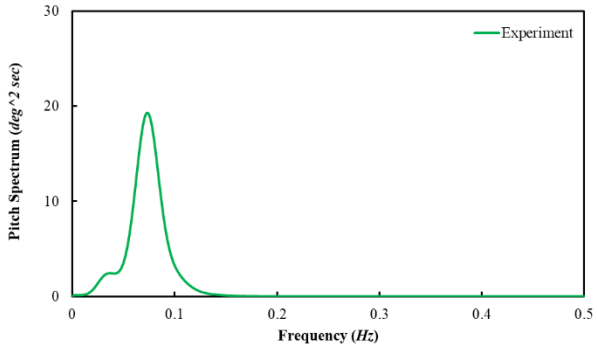

Figure 42 Pitch motion spectrum for Sea State 3, spar-only (full scale)

3.3.1.2 Spar with Realistic Mooring Lines

The heave, pitch and surge motion's PDF and spectrum from Sea State 2 are shown from Figure 43 to Figure 48. The experimental measured data have been calculated into full scale before calculating its PDF and spectrum.

Figure 43 shows the heave motion amplitude probability density function (PDF) are mainly within 0.5 m. When looking at the heave motion spectrum, in Figure 44, one peak has been found at the wave spectrum peak frequency (about 0.089 Hz) while another one is seen at the heave motion natural frequency (about 0.032 Hz). Figure 45 shows the pitch amplitude mainly lies below 1°. For the pitch motion spectrum, as shown in Figure 46, the two peaks occur around the peak wave frequency, and the pitch natural frequency (around 0.034 Hz). As mentioned in Section 3.2.2.2, the pitch motions do not appear to be substantially affected by the presence of the mooring line, so the mooring system seems cannot affect the pitch motion behaviour. In surge motion PDF, it is seen that the surge motion amplitude can range from 0 to 2m, as shown in Figure 47. For the surge motion spectrum, see Figure 48, two peaks are observed – one is at the peak wave spectrum frequency and the other one is around the pitch natural frequency (0.034 Hz), which shows the prediction of the coupling effect between the surge and pitch motion.

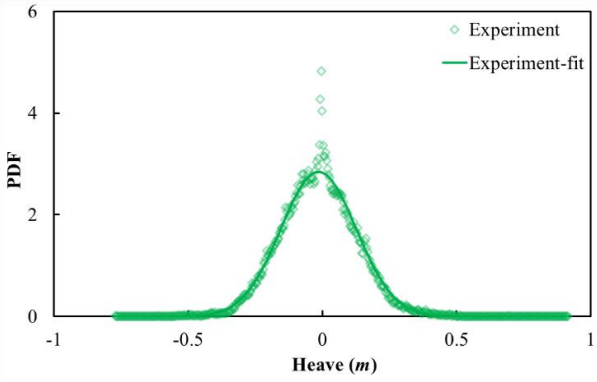

Figure 43 Heave PDF for Sea State 2, spar with realistic mooring (full scale)

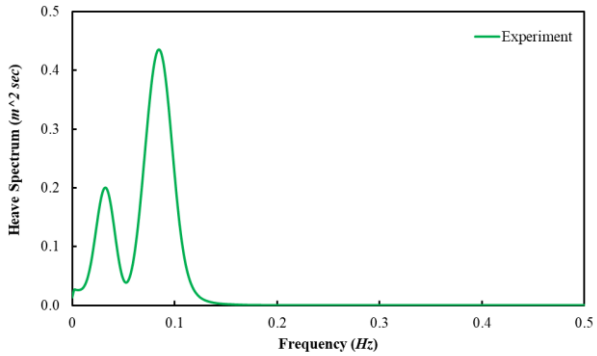

Figure 44 Heave motion spectrum for Sea State 2, spar with realistic mooring (full scale)

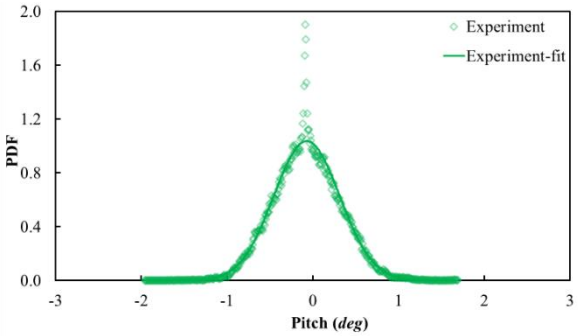

Figure 45 Pitch PDF for Sea State 2, spar with realistic mooring (full scale)

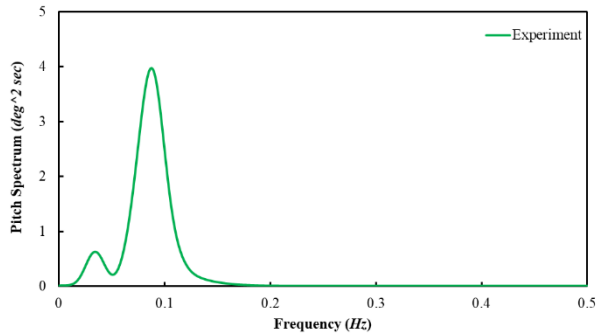

Figure 46 Pitch motion spectrum for Sea State 2, spar with realistic mooring (full scale)

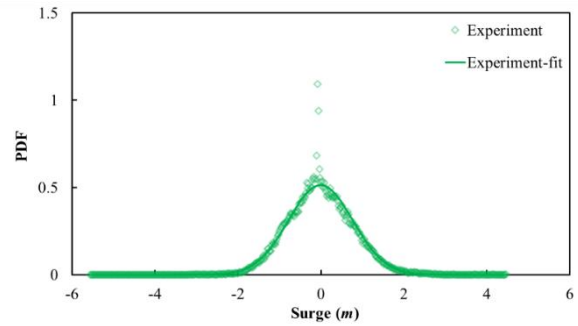

Figure 47 Surge PDF for Sea State 2, spar with realistic mooring (full scale)

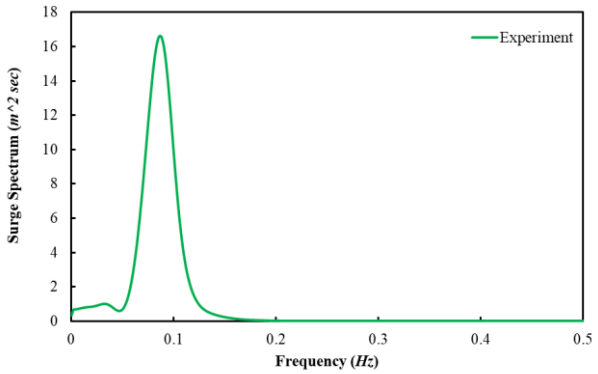

Figure 48 Surge motion spectrum for Sea State 2, spar with realistic mooring (full scale)

When checking the heave motion spectrum in Sea State 3, a very low frequency behaviour – 0.002 Hz – has been discovered, as shown in Figure 49, and this low frequency shows quite high energy. The spectrum of heave, pitch and surge motion in the heave free decay test were first checked to make sure that this small frequency is not related to any coupling effect, but no evidence of behaviour at this frequency was found. The tank test time history (scaled into full scale) in Sea State 3 and the recorded video were then examined.

The time history of the heave motion in Sea State 3 is shown in Figure 50. A few quite large motions can be seen from around 1500s to 4000s and from 5350s to 6100s; these large motions were also observed in the video, especially for the time from 5350s to 6100s.
In particular, it can be seen that the mean vertical location of the platform is depressed for an extended period from 5350 to 6100s. At the same time, large values of tension can be seen in the tension time history, which suggests that the quite large heave energy is caused by a series of large waves. Large motions can be seen in sway and yaw at the same time. This suggests that this large slowly-varying vertical motion is not due to the model taking on water. A truncated time history has been produced to exclude these large motions, and the response spectrum recalculated are shown in Figure 51, where the large energy at 0.002 Hz has disappeared. Thus, it can be concluded that the large energy apparent at 0.002 Hz is caused by the slowly varying large vertical motion of the platform in the tank. The same small frequency (0.002 Hz) can also be seen in the mooring line motions along X-axis in Sea State 3 and it is assumed that this could be related to the large heave motion as well.

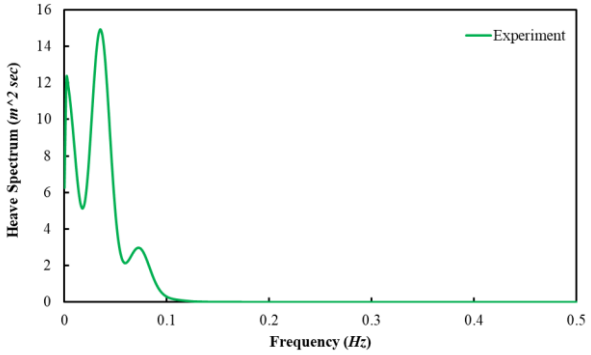

Figure 49 Heave motion spectrum for Sea State 3, spar with realistic mooring (full scale)

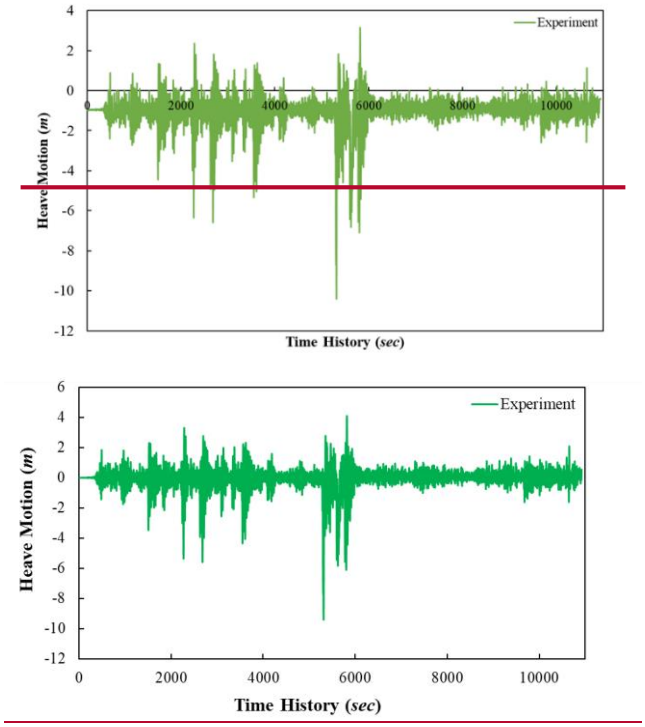

Figure 50 Heave motion time history in experiment, Sea State 3, spar with realistic mooring (full scale)

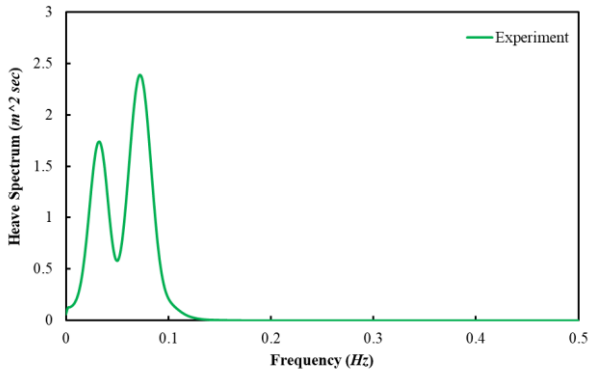

Figure 51 Heave motion spectrum from truncated time history in experiment, Sea State 3, spar with realistic mooring (full scale)

3.3.2 Mooring Line Motions and Tensions

Similar to the regular wave results presented, only three selected points' data in Sea State 2 are discussed in this part. Figure 52 to Figure 54 show the motions of Point 1 (the point furthest from the spar platform apart from the anchor), Point 4 (point near the middle of the line) and the Fairlead position motion (as a reference point compared with the platform motion), along both X-axis and Z-axis. An obvious peak has been observed at the peak wave frequency (0.089 Hz) and the other peak occurs at about 0.025 Hz for motion along X-axis and 0.023 Hz in Z-axis. These peaks could indicate the mooring line motion natural frequencies along the two directions; similar peaks are also found in the other three sea states. It seems that with the position changing from the anchor to the platform fairlead position, the mooring motions in both X-axis and Z-axis are increasing till the middle of the mooring line and then decreasing to the fairlead position in all of the four sea states. The experiment generally shows a higher peak spectrum at the peak wave frequency and a smaller peak spectrum at its natural frequencies. Comparing all the points for motion along X-axis, reveals a tendency that the motion energy gets higher for the points near the platform, and weaker

in the middle floating part of the mooring. Near the anchor position, the motion energy is still higher than the floating part but smaller than points near the platform, which could indicate the damping effect is the main factor in the middle parts. The motion along Z-axis shows an opposite behaviour than with the X-axis. At the fairlead position, it can be seen that the motion along the Z-axis matches perfectly with the platform heave spectrum which gives re-assurance that the underwater and above-water motion capture systems are working correctly. In contrast, the X-axis, motion at the fairlead position shows smaller energy than platform surge motion, but the curve shape is quite similar. This difference is believed to be due to the effect of platform pitch on the X-axis motion of the centre of gravity of the platform.

The three mooring line tension spectrum from Sea State 2 are shown in Figure 55. The tension spectrum of Mooring Line 1 shows two peaks – the main peak occurs at around 0.089 Hz, which is the peak wave frequency, while the other one occurs at around 0.025 Hz – which is similar to the mooring line motion spectrum along X-axis, which indicates that the mooring line motion can indicate its tension behaviour. For the mooring tension in Mooring Lines 2 and 3, as shown in Figure 55(b), the experimental spectrum exhibits two peaks – one is still at the peak wave frequency, and the major one is at a quite low frequency, about 0.002 Hz, which corresponds to the frequency observed in the heave motion in Sea State 3. This indicates there should exist some non-linear dynamic behaviour or the effect from difference frequency waves at this small frequency, which could usefully be investigated with further studies.

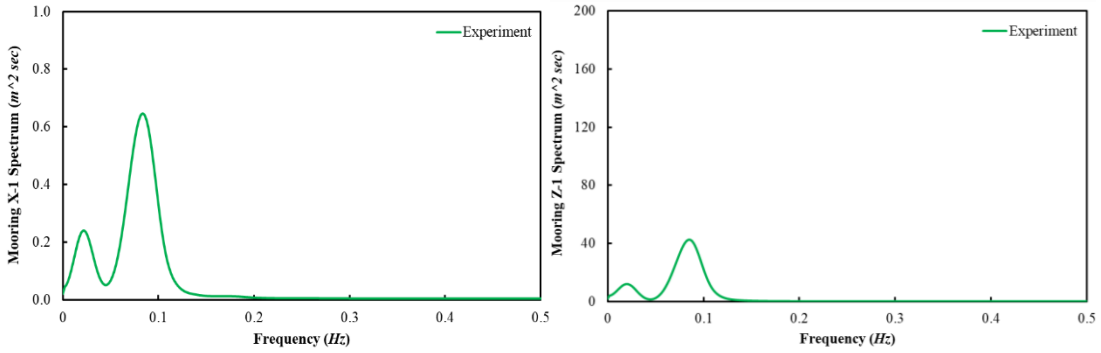

(a) X- axis (b) Z-axis

Figure 52 Point-1 motion spectrum, on Mooring Line 1 in Sea State 2 (full scale)

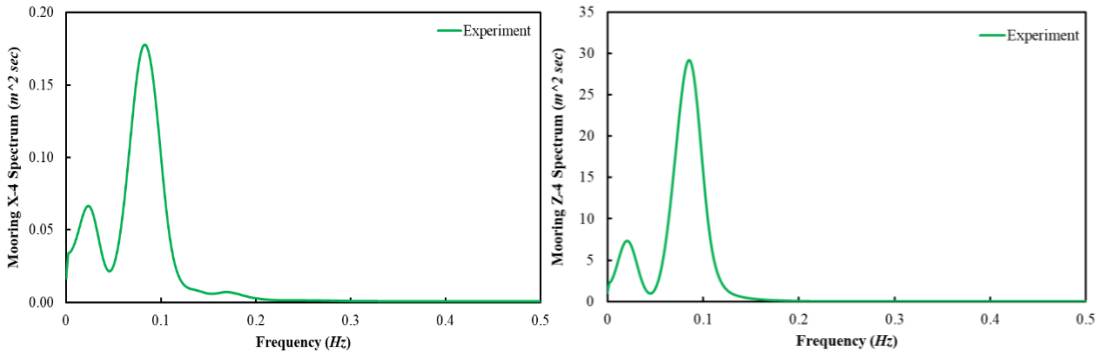

(a) X- axis (b) Z-axis

Figure 53 Point-4 motion spectrum, on Mooring Line 1 in Sea State 2 (full scale)

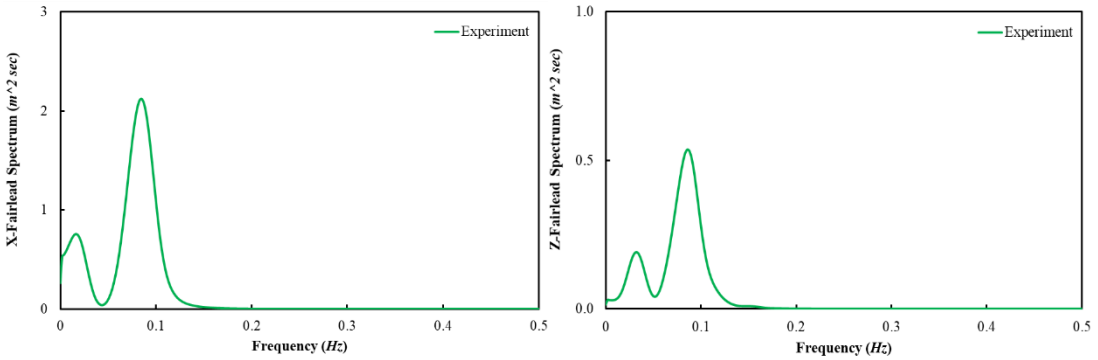

(a) X- axis (b) Z-axis

Figure 54 Fairlead motion spectrum, on Mooring Line 1 in Sea State 2 (full scale)

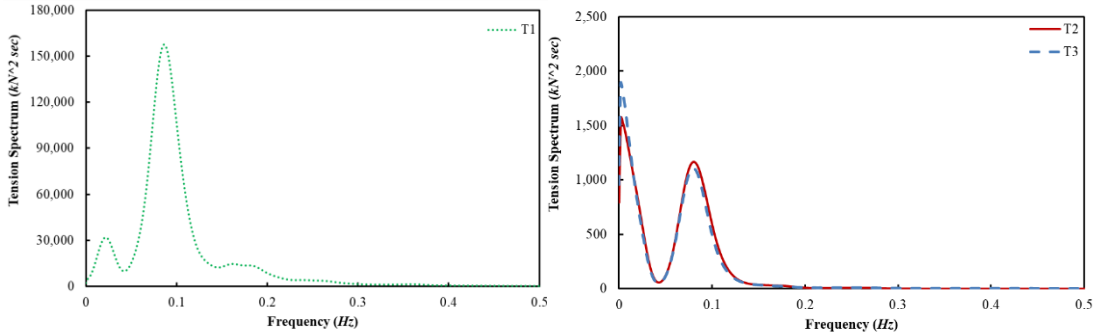

(a) Mooring Line 1 Tension (b) Mooring Line 2/3 Tension

Figure 55 Mooring tension spectrums, Sea State 2 (full scale)

4 Conclusion

This study conducted the tank test for a spar type OFWT (both with and without realistic mooring lines). Detailed process of experiment set-up and the limitations of the experiment have been discussed and they are all felt to be acceptable in this study scope. The platform 6 DOF motions and the mooring line tensions/motions were captured by the Qualysis camera both above the tank and under the water line of the tank. The mooring line tensions are measured by high accuracy underwater load cells.

The spar platform (both with and without realistic mooring lines) natural frequencies are obtained through the free decay tests. The heave, pitch and surge (spar with realistic mooring lines) natural frequencies can match perfectly with the NREL OC3-Hywind model, while the yaw cannot match due to different mooring configurations and the lack of the delta connection. The damping ratios have also been obtained which can be used to set-up numerical models for future study.

The spar platform RAO (spar-only) and RMS (spar with realistic mooring lines) are obtained through the regular wave tests, which show the peak responses for heave and pitch are matching perfectly with the results from free decay tests. The coupling motion between surge and pitch have been observed. A non-linear snatching phenomenon has been observed during the regular wave tests. It is interesting to find that this non-linear snatching behaviour disappears when the wave frequency is at the platform heave/pitch natural frequencies and show up again at other wave frequencies. This non-linear snatching behaviour could be very harmful to the mooring lines and wind turbines life, as it can lead to the sharply increase of mooring tension up to 10,000 kN. The factors can affect this non-linear snatching behaviour, such as the mooring configurations, pre-tensions of the mooring system, nonlinear

heave/pitch coupling stiffness of the spar, and the tools to predict it would be worth for a future study.

In the irregular wave tests, for both spar-only and spar with realistic mooring lines, two main peak spectrums have been observed in the platform heave and pitch motions – one is at the peak wave frequency and the other one is at their natural frequencies. For spar with realistic mooring lines, the surge motion also show a peak spectrum at the pitch natural frequencies, which shows the coupling of the two motions (as founded in the platform RMS). For the mooring line motions, along both X-axis and Z-axis, the main peak spectrum is at the peak wave frequency, and the other peak occurs at about 0.025 Hz for motion along X-axis and 0.023 Hz in Z-axis, which could indicate the mooring line motion natural frequencies. For mooring line tensions, the main peak spectrum is still found at the peak wave frequency, while the other peak spectrum is at a quite low frequency (about 0.002 Hz). This corresponds to the frequency observed in the heave motion in Sea State 3 and means there should exist some non-linear dynamic behaviour at this small frequency which could usefully be investigated with further studies.

Acknowledgement

This study is supported by the "Engineering Future Studentships", Faculty of Engineering at the University of Strathclyde. Special thanks to the staff at the KHL for their kind help and professional instructions for experiments.

References

Ahn, H.-J. & Shin, H. 2019. Model test and numerical simulation of OC3 spar type floating offshore wind turbine. International Journal of Naval Architecture and Ocean Engineering, 11**,** 1-10.

Chakrabarti, S. K. 1994. Offshore structure modeling, World Scientific.

Duan, F., Hu, Z., Liu, G. & Wang, J. 2016a. Experimental comparisons of dynamic properties of floating wind turbine systems based on two different rotor concepts. Applied Ocean Research, 58**,** 266-280.

Duan, F., Hu, Z. & Niedzwecki, J. 2016b. Model test investigation of a spar floating wind turbine. Marine Structures, 49**,** 76-96.

Duan, F., Hu, Z. & Wang, J. Model tests of a spar-type floating wind turbine under wind/wave loads. International Conference on Offshore Mechanics and Arctic Engineering, 2015. American Society of Mechanical Engineers, V009T09A044.

Equinor 2019. How-Hywind-works, available at https://www.equinor.com/en/what-we-do/hywind-where-the-wind-takes-us/hywind-up-close-and-personal.html.

Hsu, W.-t., Thiagarajan, K. P. & Manuel, L. 2017. Extreme mooring tensions due to snap loads on a floating offshore wind turbine system. Marine Structures, 55**,** 182-199.

Ishida, S., Kokubun, K., Nimura, T., Utsunomiya, T., Sato, I. & Yoshida, S. At-sea experiment of a hybrid spar type offshore wind turbine. International Conference on Offshore Mechanics and Arctic Engineering, 2013. American Society of Mechanical Engineers, V008T09A035.

Jonkman, J. 2010. Definition of the Floating System for Phase IV of OC3. National Renewable Energy Lab.(NREL), Golden, CO (United States).

Landau, H. 1967. Sampling, data transmission, and the Nyquist rate. Proceedings of the IEEE, 55**,** 1701-1706.

Proskovics, R. 2015. Dynamic response of spar-type offshore floating wind turbines. University of Strathclyde.

Ramachandran, G., Robertson, A., Jonkman, J. & Masciola, M. D. 2013. Investigation of response amplitude operators for floating offshore wind turbines. National Renewable Energy Lab.(NREL), Golden, CO (United States).

Rolo, L. 2014. Design, testing and validation of a scale model semisubmersible offshore wind turbine under regular/irregular waves and wind loads. MSc University of Strathclyde.

Ruzzo, C., Fiamma, V., Collu, M., Failla, G., Nava, V. & Arena, F. 2018. On intermediate-scale open-sea experiments on floating offshore structures: Feasibility and application on a spar support for offshore wind turbines. Marine Structures, 61**,** 220-237.

Santos-Herrán, M. 2016. Model Design, Testing and Validation of Three Scaled Spar Type Offshore Floating Wind Turbines under Wave Loads. MSc, University of Strathclyde.

Shin, H. Model test of the OC3-Hywind floating offshore wind turbine. The Twenty-first International Offshore and Polar Engineering Conference, 2011. International Society of Offshore and Polar Engineers.

Skaare, B., Hanson, T. D., Nielsen, F. G., Yttervik, R., Hansen, A. M., Thomsen, K. & Larsen, T. J. Integrated dynamic analysis of floating offshore wind turbines. European wind energy conference and exhibition, 2007. Citeseer, 7-10.

Stansberg, C., Contento, G., Hong, S. W., Irani, M., Ishida, S., Mercier, R., Wang, Y., Wolfram, J., Chaplin, J. & Kriebel, D. 2002. The specialist committee on waves final report and recommendations to the 23rd ITTC. Proceedings of the 23rd ITTC, 2**,** 505-551.

Tecni-cable 2016. Stainless Steel Wire Rope - Fittings - Tools - TECNI, available at http://www.tecni-cable.co.uk/Products/US-Mil-Spec-Cable-7x7-Stainless-Mil-DTL-83420-Composition-B.

Tomasicchio, G. R., D'Alessandro, F., Avossa, A. M., Riefolo, L., Musci, E., Ricciardelli, F. & Vicinanza, D. 2018. Experimental modelling of the dynamic behaviour of a spar buoy wind turbine. Renewable Energy, 127**,** 412-432.

Utsunomiya, T., Matsukuma, H., Minoura, S., Ko, K., Hamamura, H., Kobayashi, O., Sato, I., Nomoto, Y. & Yasui, K. 2013a. At sea experiment of a hybrid spar for floating offshore wind turbine using 1/10-scale model. Journal of offshore mechanics and Arctic engineering, 135.

Utsunomiya, T., Sato, I., Kobayashi, O., Shiraishi, T. & Harada, T. Design and installation of a hybrid-spar floating wind turbine platform. International Conference on Offshore Mechanics and Arctic Engineering, 2015. American Society of Mechanical Engineers, V009T09A063.

Utsunomiya, T., Sato, I., Yoshida, S., Ookubo, H. & Ishida, S. Dynamic response analysis of a floating offshore wind turbine during severe typhoon event. International Conference on Offshore Mechanics and Arctic Engineering, 2013b. American Society of Mechanical Engineers, V008T09A032.

Utsunomiya, T., Sato, T., Matsukuma, H. & Yago, K. Experimental validation for motion of a spar-type floating offshore wind turbine using 1/22.5 scale model. International Conference on Offshore Mechanics and Arctic Engineering, 2009. 951-959.

Utsunomiya, T., Yoshida, S., Kiyoki, S., Sato, I. & Ishida, S. Dynamic response of a spar-type floating wind turbine at power generation. International Conference on Offshore Mechanics and Arctic Engineering, 2014. American Society of Mechanical Engineers, V007T05A027.

Yu, M., Hu, Z.-q. & Xiao, L.-f. 2015. Wind-wave induced dynamic response analysis for motions and mooring loads of a spar-type offshore floating wind turbine. Journal of Hydrodynamics, Ser. B, 26**,** 865-874.

Zürcher, K. 2016. Waterjet testing techniques for powering performance estimation using a single catamaran demihull. University of Tasmania.